

Application of Self-Labeling Proteins in Single-Molecule

FRET Studies



Zur Erlangung des akademischen Grades eines
DOKTORS DER NATURWISSENSCHAFTEN

(Dr. rer. nat.)

Fakultät für Chemie und Biowissenschaften
Karlsruher Institut für Technologie (KIT) - Universitätsbereich

Genehmigte

DISSERTATION

von

Naghmeh Azadfar, M.Sc. Biol

aus

Gonbad Kavous, Iran

Dekan:

Prof. Dr. Willem M. Klopper

Referent:

Prof. Dr. Gerd Ulrich Nienhaus

Korreferent:

Prof. Dr. Martin Bastmeyer

Tag der mündlichen Prüfung

14.12.2016

Declaration

“I hereby affirm that I have written this thesis independently and without use of resources other than those quoted. Cited and copied work is marked as such.”

Contents

1	Introduction	1
1.1	Protein Labelling Methods for Single-Molecules Studies	1
1.2	Self-Labeling Proteins	3
1.2.1	SNAP- and CLIP-Tags	3
1.2.2	<i>In vitro</i> and <i>in vivo</i> Applications of SNAP- and CLIP-tag Technology	7
1.3	Model Protein Systems	8
1.4	Nbp2-SH3 Domain for Protein-Protein Interaction Study	9
1.5	Peptide Model Experiments	10
1.5.1	15 aa Peptide	10
1.5.2	Poly-L-proline: FRET ruler	10
1.6	CaM Protein	12
1.7	Thesis Outline	15
2	Background	17
2.1	Fluorescence	17
2.2	FRET– Förster Resonance Energy Transfer	19
2.2.1	Theoretical Calculation of the FRET efficiency	19
2.2.2	Single-Molecule FRET and its Applications	21
2.2.3	Burst Detection and Analysis	23
2.2.4	Burst Wise FRET Calculation	24
2.2.5	Calculating γ -factor via the Stoichiometry Map	25
2.3	Fluorescence Lifetime Imaging Microscopy-Based FRET (FLIM- FRET)	28
2.3.1	FLIM setup	28
2.3.2	Fluorescent Lifetime Determination	29
2.3.3	FLIM-FRET Measurements	31
2.4	Fluorescence Anisotropy	32
2.4.1	Time-Resolved Anisotropy	32
2.4.2	Anisotropy Measurements	33

3	Materials and Methods	35
3.1	Polyproline constructs	35
3.1.1	Preparation of the S-PP-C Plasmid for Expression in Yeast cells	37
3.2	15 Amino Acid Construct and 15 Amino Acid (15 aa) Peptide . . .	37
3.3	CaM Construct	37
3.3.1	Preparation of the S-CaM-C Plasmid for Bacterial Expression	37
3.3.2	Preparation of the S-CaM-C Plasmid for Yeast Cell Expression	39
3.4	Nbp2 Constructs	40
3.5	Expression and Purification of Recombinant Proteins	40
3.5.1	Bacterial Cell Transformation	43
3.5.2	Yeast Cell Transformation	43
3.6	Yeast Cell Labelling	44
3.6.1	Fixed Cell Labelling	44
3.6.2	Live Cell Labelling	45
3.7	Labelling Proteins <i>in vitro</i>	45
3.8	Ensemble Fluorescence Measurements	46
3.8.1	Single-Molecule Detection with Confocal Microscopy	46
4	Results and Discussion	51
4.1	Protein Peptide Interaction Study	51
4.1.1	Bulk FRET Measurements to Study Nbp2-SH3 Domain-Peptide Interactions	52
4.2	Single-Molecule FRET Studies	58
4.2.1	Single-Molecule FRET Study of the 15-aa Construct	58
4.2.2	Rotational Freedom	60
4.2.3	Distance Characterisation	61
4.2.4	Average FRET value Measurements	62
4.2.5	Single-Molecule FRET Study of Polyproline	64
4.3	Conformation Characterization by the Single-Molecule-FRET Method	68
4.3.1	Affinity Binding Study of Ca ²⁺ Ions to the CaM Construct .	69
4.3.2	Single-Molecule FRET investigation of the CaM Construct .	71
4.4	Fluorescence Lifetime and FLIM-FRET Imaging Studies	74
4.4.1	Fluorescence Lifetime Study of PP Constructs <i>in vitro</i> . . .	75
4.4.2	FLIM-FRET Imaging of PP Constructs Inside Fixed Yeast Cells	76
4.4.3	Fluorescence Lifetime Study of CaM Construct <i>in vitro</i> . .	77
4.4.4	FLIM-FRET Imaging of CaM Constructs In Living Yeast Cells	80
	Summary	83

Acronyms	87
Bibliography	89
Appendix	99
Acknowledgements	127
List of Publications	129
List of Posters	131

List of Figures

1.1	Methods for fluorescent labelling of proteins.	2
1.2	Dimension of SNAP-tag protein (PDB code: 3KZZ).	4
1.3	Reaction between SNAP-tag and its substrate.	5
1.4	SNAP-tag structure (PDB code: 3KZZ).	5
1.5	CLIP-tag reaction with its substrate.	6
1.6	SNAP-tag and CLIP-tag sequence comparison.	6
1.7	Semisynthetic fluorescent sensor proteins based on the SNAP-tag.	7
1.8	The class I and class II consensus motifs and the SH3 domain structure.	10
1.9	Conversion mechanism for Pro13 from PPI to PPII.	12
1.10	Hierarchical structure of CaM.	13
1.11	The calcium binding site in CaM.	14
1.12	Illustration of Ca ²⁺ -free (a) and Ca ²⁺ -loaded (b) CaM.	14
1.13	Solution structure of a CaM-M13 peptide complex in different views (PDB entry 2BBM).	15
2.1	Jablonski diagram.	18
2.2	The value of κ^2 depends on the emission dipole of the donor and the absorption dipole of the acceptor molecule.	20
2.3	Fluorescence traces of the CaM construct in Tris buffer pH 7.4, recorded with a bin size of 100 μ s.	26
2.4	Screen shot of the stoichiometry map and FRET histogram from the burst analysis program.	27
2.5	Two-dimensional FRET efficiency-stoichiometry histogram.	27
2.6	Schematic representation of the excitation and detection paths.	30
2.7	The fluorescence lifetime decay fitting process.	30
2.8	Absorbance and emission spectra of the SNAP-Cell 430 dye.	31
2.9	Fluorescence Polarisation diagram.	33
3.1	Cartoon representation of the SNAP-PP-CLIP construct	35

3.2	Linearisation of the Nbp2 vector and amplified SNAP-6PP-CLIP gene.	36
3.3	Restriction enzyme screening of the 6PP construct.	38
3.4	Restriction enzyme screening for the S-PP-C gene in the pRS313-MET3 vector.	39
3.5	Cartoon representations of the 15 aa construct and the 15 aa peptide.	40
3.6	S-CaM-C expression vector preparation.	41
3.7	S-CaM-C yeast cell expression vector preparation.	42
3.8	Schematic representations of full-length Nbp2, the Nbp2-SH3 domain and peptides.	43
3.9	Construction of the confocal microscope.	47
3.10	Absorption and emission spectra of the A546 and DY647 dyes.	48
3.11	Schematic of the sample holder.	49
4.1	Structure of Nbp2-SH3 domain and Nbp2-SH3-Ste20 complex	52
4.2	Bulk fluorescence measurements of Nbp2-SH3 with Pbs2 peptide.	54
4.3	Bulk fluorescence measurements of Nbp2-SH3 with Ste20 peptide.	55
4.4	Bulk fluorescence measurements of full length Nbp2 with Ste20 peptide.	56
4.5	Study of the interaction between Nbp2-SH3 domain and peptides without SNAP-tags.	57
4.6	Tracking of the fluorescence intensity at 673 nm every two minutes during one hour.	58
4.7	Representative smFRET histograms of the directly labelled random 15 amino acids peptide (A546-15aa-A647) and the random 15 amino acids peptide labelled by SNAP-/CLIP-tag (S-15aa-C) both show a single high FRET peak.	59
4.8	VV(t) and VH(t) polarized decays of free SNAP-Surface Alexa Fluor 546 and Alexa Fluor 546 conjugated to the SNAP-tag.	60
4.9	Anisotropy decays curve calculated in OriginPro from VV(t) and VH(t) for A546 and labelled SNAP-tag with A546 fluorophore, assuming $G = 1$	61
4.10	Cartoon of S-xPP-C construct designs (x = 6, 12, 20, and 24)	62
4.11	Absorbance spectra of labelled PP constructs.	63
4.12	Fluorescence spectra of PP constructs.	63
4.13	smFRET histogram of PP constructs for different lengths of PP constructs.	65
4.14	<i>cis-trans</i> isomerization of polyproline oligomers.	66
4.15	$\langle E_{FRET} \rangle$ (black squares) and corresponding errors of the Gaussian fit from smFRET histograms (Figure 4.13) for the S-xPP-C constructs.	68

4.16	Bulk fluorescence measurements of CaM construct.	70
4.17	smFRET measurements of the CaM construct in 25 mM Tris, 100 mM KCl, pH 7.5.	73
4.18	Comparison of smFRET results obtained with the CaM construct (labelled with TMR-Star-DY647 dye pair) and directly labelled CaM protein by Kim <i>et al.</i> [78]	74
4.19	Fluorescence lifetime decays of the PP constructs.	75
4.20	FLIM-FRET analysis of PP constructs in yeast cells.	78
4.21	Fluorescence lifetime measurements of the CaM construct.	79
4.22	FLIM-FRET analysis of CaM constructs in yeast cells.	81
A.1	PCR program.	102
A.2	PCR-Master Mix.	102
A.3	Absorbance spectrum of labeled CaM construct.	106
A.4	Extinction coefficient determination of the 15 aa peptide.	107
A.5	Absorbance (a) and fluorescence spectra (b) of the labeled 15-aa construct labeled with A546 and DY647.	107
A.6	The synthesized and labeled 15-aa peptide	108
A.7	Gaussian fitting parameter. Gaussian fitting equation is $y = y_0 + \frac{A}{w\sqrt{\frac{\pi}{2}}} e^{-2\frac{(x-x_c)^2}{w^2}}$	109
A.8	CaM construct in 25 mM Tris, 300 mM NaCl, pH 7.5 buffer.	109
A.9	CaM construct in 25 mM Tris, 300 mM NaCl, pH 7.5 buffer in addition of 10 mM EGTA.	110
A.10	CaM construct in 25 mM Tris, 300 mM NaCl, pH 7.5 buffer in addition of 1 mM calcium.	112
A.11	CaM construct in 25 mM Tris, 300 mM NaCl, pH 7.5 buffer in addition of 1 mM calcium and 10 μ M M13 peptide.	113
A.12	CaM construct in 25 mM Tris, 100 mM KCl, pH 7.5 buffer in addition of 10 mM EGTA.	114
A.13	CaM construct in 25 mM Tris, 100 mM KCl, pH 7.5 buffer in addition of 1 mM calcium.	116
A.14	CaM construct in 25 mM Tris, 100 mM KCl, pH 7.5 buffer in addition of 1 mM calcium and 10 μ M M13 peptide.	117
A.15	6PP construct in 20 mM Tris-HCl, 300 mM NaCl, pH 7.4 buffer.	120
A.16	12PP construct in 20 mM Tris-HCl, 300 mM NaCl, pH 7.4 buffer.	121
A.17	20PP construct in 20 mM Tris-HCl, 300 mM NaCl, pH 7.4 buffer.	122
A.18	24PP construct in 20 mM Tris-HCl, 300 mM NaCl, pH 7.4 buffer.	123

List of Tables

4.1	Comparison of Nbp2-SH3 binding affinities	54
4.2	Extracted lifetimes from fitting the lifetime decays of the PP constructs and calculated FRET efficiencies for the second lifetime based on equation 2.19. All lifetime decays were deconvoluted from IRF.	76
4.3	Average lifetimes of PP constructs in yeast cells.	77
4.4	Calculated lifetimes and FRET efficiencies from fitted lifetime decays for different conditions.	80
4.5	Average lifetimes of CaM construct in yeast cells.	81
A.1	The protocol of buffers and solutions.	99
A.2	List of primers.	100
A.3	Spectral characterization of dyes.	104
A.4	Correction factors of dyes at 280 and 571 nm.	105
A.5	Calculated labeling efficiencies for each constructs.	105
A.6	Goodness of Fit for Gaussian fitting results of FRET histograms for CaM construct in 25 mM Tris, 300 mM NaCl, pH 7.5 buffer.	109
A.7	Gaussian fitting results of FRET histograms for CaM construct in 25 mM Tris, 300 mM NaCl, pH 7.5 buffer.	110
A.8	Goodness of Fit for Gaussian fitting results of FRET histograms for CaM construct in 25 mM Tris, 300 mM NaCl, pH 7.5 buffer in addition of 10 mM EGTA.	111
A.9	Gaussian fitting results of FRET histograms for CaM construct in 25 mM Tris, 300 mM NaCl, pH 7.5 buffer in addition of 10 mM EGTA.	111
A.10	Goodness of Fit for Gaussian fitting results of FRET histograms for CaM construct in 25 mM Tris, 300 mM NaCl, pH 7.5 buffer in addition of 1 mM calcium.	112
A.11	Gaussian fitting results of FRET histograms for CaM construct in 25 mM Tris, 300 mM NaCl, pH 7.5 buffer in addition of 1 mM calcium.	112

A.12 Goodness of Fit for Gaussian fitting results of FRET histograms for CaM construct in 25 mM Tris, 300 mM NaCl, pH 7.5 buffer in addition of 1 mM calcium and 10 μ M M13 peptide.	113
A.13 Gaussian fitting results of FRET histograms for CaM construct in 25 mM Tris, 300 mM NaCl, pH 7.5 buffer in addition of 1 mM calcium and 10 μ M M13 peptide.	114
A.14 Goodness of Fit for Gaussian fitting results of FRET histograms for CaM construct in 25 mM Tris, 100 mM KCl, pH 7.5 buffer in addition of 10 mM EGTA.	115
A.15 Gaussian fitting results of FRET histograms for CaM construct in 25 mM Tris, 100 mM KCl, pH 7.5 buffer in addition of 10 mM EGTA.	115
A.16 Goodness of Fit for Gaussian fitting results of FRET histograms for CaM construct in 25 mM Tris, 100 mM KCl, pH 7.5 buffer in addition of 1 mM calcium.	116
A.17 Gaussian fitting results of FRET histograms for CaM construct in 25 mM Tris, 100 mM KCl, pH 7.5 buffer in addition of 1 mM calcium.	116
A.18 Goodness of Fit for Gaussian fitting results of FRET histograms for CaM construct in 25 mM Tris, 100 mM KCl, pH 7.5 buffer in addition of 1 mM calcium and 10 μ M M13 peptide.	117
A.19 Gaussian fitting results of FRET histograms for CaM construct in 25 mM Tris, 100 mM KCl, pH 7.5 buffer in addition of 1 mM calcium and 10 μ M M13 peptide.	118
A.20 FRET positions and mean values of FRET peaks in various conditions.	119
A.21 FRET positions and its mean values of directly labeled CaM protein by Kim <i>et al.</i> [78].	119
A.22 Goodness of Fit for Gaussian fitting results of FRET histograms for 6PP construct in 20 mM Tris-HCl, 300 mM NaCl, pH 7.4 buffer. . .	120
A.23 Gaussian fitting results of FRET histograms for 6PP construct in 20 mM Tris-HCl, 300 mM NaCl, pH 7.4 buffer.	120
A.24 Goodness of Fit for Gaussian fitting results of FRET histograms for 12PP construct in 20 mM Tris-HCl, 300 mM NaCl, pH 7.4 buffer. .	121
A.25 Gaussian fitting results of FRET histograms for 12PP construct in 20 mM Tris-HCl, 300 mM NaCl, pH 7.4 buffer.	121
A.26 Goodness of Fit for Gaussian fitting results of FRET histograms for 20PP construct in 20 mM Tris-HCl, 300 mM NaCl, pH 7.4 buffer. .	122
A.27 Gaussian fitting results of FRET histograms for 20PP construct in 20 mM Tris-HCl, 300 mM NaCl, pH 7.4 buffer.	123
A.28 Goodness of Fit for Gaussian fitting results of FRET histograms for 6PP construct in 24 mM Tris-HCl, 300 mM NaCl, pH 7.4 buffer. . .	124

A.29 Gaussian fitting results of FRET histograms for 6PP construct in 24 mM Tris-HCl, 300 mM NaCl, pH 7.4 buffer.	124
A.30 FRET positions and mean values of PP constructs in 20 mM Tris-HCl, 300 mM NaCl, pH 7.4 buffer.	124
A.31 FRET positions of directly labeled 20 polyproline oligomer [74]. . .	125
A.32 Summary of fit results of polarized decays from free SNAP-Surface Alexa Fluor 546 and Alexa Fluor 546 conjugated to the SNAP-tag.	125

Chapter 1

Introduction

1.1 Protein Labelling Methods for Single-Molecules Studies

Proteins are fundamental building blocks of all biological systems. Owing to their ability to interact, proteins perform vital functions in an organism at cellular and systemic levels. Deciphering the nature of protein-protein interactions (PPI) and subsequent protein conformational changes is crucial for understanding various biological processes including programmed cell death and gene regulation [1, 2]. Traditional spectroscopy and microscopy techniques do not provide details about the dynamics of these interactions. New developments in light microscopy and advances in highly stable and customizable genetically encoded fluorescent proteins provide ideal tools to obtain spatial and temporal distribution of PPI in living cells. We focus our attention on a technique with high spatial and temporal resolution: Förster resonance energy transfer (FRET), sometimes also called fluorescence resonance energy transfer.

FRET is a process of radiationless transfer of energy in a fluorescent system from a donor (D) in an excited electronic state to a nearby acceptor (A) at a distance of up to 100 Å [3]. PPI and protein conformational change are prerequisites for protein regulation, and typically occur at distances similar to those required for FRET. A careful selection and development of appropriate fluorophores, coupled with advances in laser technology, enables us to use FRET to study these dynamic biological processes.

There are two different types of fluorophores for labelling proteins *in vitro* and *in vivo*, these are, fluorescent proteins and organic dyes (Figure 1.1). Due to insufficient photostability, fluorescent proteins generally cannot be used for single-molecule FRET (smFRET) measurements. Organic dyes, while comparatively stable, are too unwieldy to target precisely. We sought to develop a simpler and more efficient strategy to label proteins suitable for smFRET measurements, com-

binning the targeting fidelity of protein tags with the photostability of organic dyes. Unlike fluorescent proteins, organic dyes cannot generally be used for intracellular labelling due to non-specific binding. A careful selection of the tagging method can improve specificity of binding and enable intracellular labelling. We utilize a strategy that combines genetic targeting with photostable organic dyes. An example of this strategy are the self-labelling SNAP- and CLIP-tags. These tags are of particular interest for our purposes of smFRET in this thesis (Figure 1.1) [4, 5].

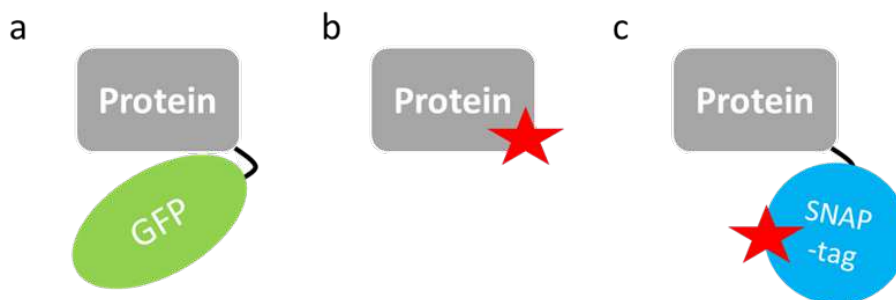


Figure 1.1: a) Genetic fusion to a fluorescent protein. b) Direct labelling of cysteine or lysine residues using organic dyes. c) Chemical tag strategy using the SNAP-tag. Gray: a protein; Green: Green Fluorescent Protein (GFP protein); Red star: organic dye; Blue: SNAP-tag protein.

SNAP- and CLIP-tags are genetically encoded chemical tags derived from a DNA repair protein [5]. These tags can be genetically fused to the protein of interest and can be covalently and specifically labeled with a small molecule such as fluorophores. This approach combines the simplicity of fusion protein expression with the diversity of chemically synthesized probes. These tags are unique in the fact that they can be coupled to appropriate substrates without an additional catalyst. As a result there is no restriction on using such tags for *in vitro* and *in vivo* measurements. This allows for a direct comparison of these tag systems in different environments. SNAP- and CLIP-tags have been previously used as fusion partners to label proteins of interest for cellular imaging and in super-resolution microscopy [5, 6]. The combined advantage of genetic targeting, photostability and versatility of organic dyes makes SNAP- and CLIP-tags a promising technique for smFRET measurements, however, a systematic evaluation of this labelling strategy has been lacking.

In this thesis, the SNAP-tag/CLIP-tag labelling strategy for smFRET application has been systematically investigated using model peptide and protein systems. We use this labelling strategy to explore various parameters underlying protein conformational changes, such as the length and flexibility. We discuss our

results in the context of previously published smFRET measurements with traditional labelling systems to evaluate the relative utility of SNAP- and CLIP-tag constructs.

1.2 Self-Labeling Proteins

In recent years, a number of so-called, self-labelling proteins, such as Halo-Tag [7], β -lactamase-tag [8], TMP-tag [9] and SNAP-tag [10], have been engineered from enzymes as alternative protein labelling strategies [11]. Self-labelling proteins can achieve specific conjugation with a ligand of interest (e.g. fluorophore). They can also be applied inside the cell by using cell permeable dyes. High speed, specificity, and a wide variety of available substrates are the many advantages of these self-labelling proteins. One of the weakness of these self-labelling proteins is their large size of about 20 KDa [11].

1.2.1 SNAP- and CLIP-Tags

One of the most widely used self-labeling protein is the SNAP-tag (Figure 1.2), which was used for our investigation to specifically label particular proteins of interest *in vitro* and *in vivo*. The SNAP-tag, is based on an engineered variant of O^6 -alkylguanine-DNA-alkyltransferase (hAGT), a DNA repair protein, which directly corrects repair alkylation damage of DNA as a ubiquitous protein. In that repair process, the alkyl group transfers from the damaged nucleotide to the cysteine amino acid in the active site. In 2003, Keppler *et. al* [12] studied the hAGT protein as a protein-tag. They attached various BG derivatives to the active site of the hAGT protein. Currently, the SNAP-tag is a commercially available version of the hAGT protein with various BG-derivatives including BG-NH₂, BG-GLA-NHS, BG-PEG-NH₂, SNAP-Cell TMR-Star, and SNAP-Surface 488 (SNAP-tag, New England Biolabs) [5, 13].

By evolution of hAGT protein to the SNAP-tag, the reactivity and stability of the protein increased in an irreversible reaction, whereas hAGT protein rapidly degrade after transferring of alkyl group. A key alpha helix in the structure of hAGT protein play an important role during alkyl transfer process and its degradation [10]. In the structure of the SNAP-tag, the alkyl group of the BG substrate reacts with Cys145 in the SNAP-tag and forms a thioester bond (Figure 1.3). The reporter group such as Biotin, fluorophores, and NH₂ attached to the Benzyl moiety, which binds covalently to the SNAP-tag and the guanine group release after attachment of benzyl group to the Cys145 in the SNAP-tag [10]. In advance, a fast labeling version of the SNAP-tag as SNAP_f developed with tenfold reactivity to BG derivatives. The SNAP-tag fused to the protein of interest can be labeled

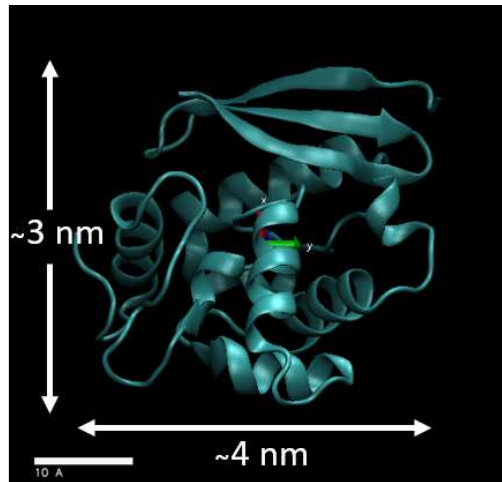


Figure 1.2: Dimension of SNAP-tag protein (PDB code: 3KZZ). Three-dimensional structure of the SNAP-tag has approximately 3 by 4 nanometers in dimension (x: ~ 3 nm; Y: ~ 4 nm; Z: ~ 4 nm). The scale bar is 10 Å.

with various organic dyes *in vitro* or *in vivo* for biotechnological applications [12].

The SNAP-tag has three tryptophan amino acids (Trp65, Trp100, and Trp167) around the dye attachment site (Cys145). The distances between Cys145 and each tryptophan vary from 9 to 17 Å (Cys145-Trp65: 16.56 Å; Cys145-Trp100: 13.67 Å; Cys145-Trp167: 9.33 Å). Typically, Photon-induced Electron Transfer (PET) can occur at distances ≤ 10 Å between Trp and a dye [14] (Figures 1.4).

The CLIP-tag is a variant of the SNAP-tag, engineered to have a specificity to *O*⁶-benzylcytosine (BC) derivatives instead of BG (Figures 1.5) [15]. Eight SNAP-tag amino acids were mutated to generate the CLIP-tag (M60I, Y114E, A121V, K131N, S135D, L153S, G157P, E159L; Figure 1.6). Substrate binding with a wide variety of functional groups on the CLIP-tag works in essentially the same way as that of the SNAP-tag. The principle aim in creating the CLIP-tag was dual colour labelling concurrent to SNAP-tag labelling *in vitro* and inside cells [16].

The reactivity study of BG and BC derivatives toward SNAP- and CLIP-tag showed the 1000 fold more efficiency of BG than BC to the SNAP-tag. A rate constant of $25 \pm 5 \text{ M}^{-1}\text{s}^{-1}$ obtained for BC toward SNAP-tag while $2.8 \times 10^4 \text{ M}^{-1}\text{s}^{-1}$ found for BG reacting with the SNAP-tag. So, both protein tags can be specifically and simultaneously labeled in the same sample solution or one cell on different localized proteins [5]. Recently, substrate improvement for better fluorescence labeling, higher the signal-to-noise ratio, and higher cell permeability indicated as a powerful tool for cell imaging applications [17].

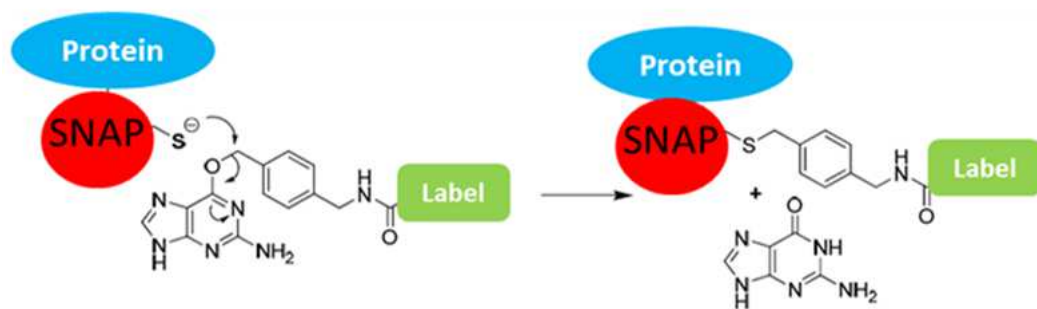


Figure 1.3: Reaction between SNAP-tag and its substrate. The reactive cysteine of the SNAP-tag is covalently bound to the benzyl group of the substrate (BG).

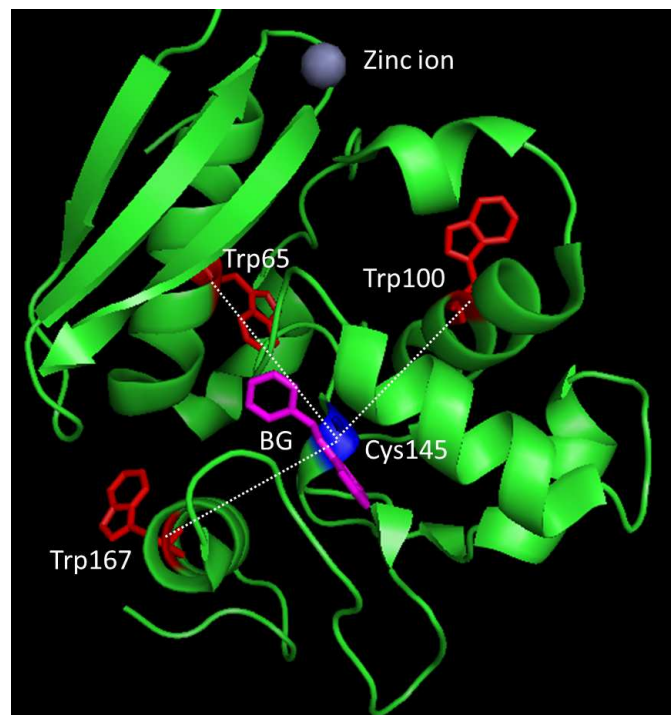


Figure 1.4: SNAP-tag structure (PDB code: 3KZZ). Cys145 amino acid shows in blue and tryptophan amino acids in red. The SNAP-tag bound to its substrate benzylguanidine (BG). The dash line shows the distance between Cys145 and each tryptophan amino acid.

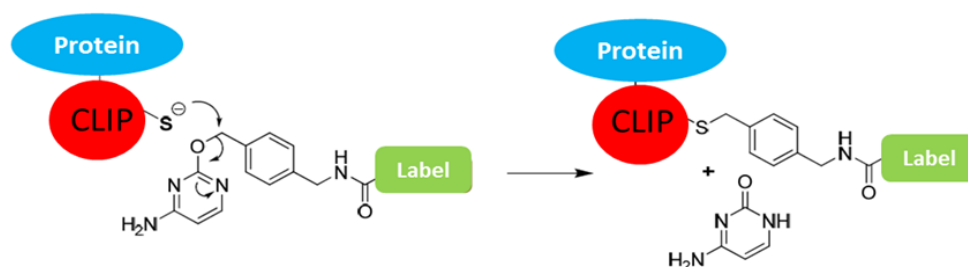


Figure 1.5: CLIP-tag reaction with its substrate. The reactive cysteine of the CLIP-tag binds to the benzyl group of the Benzyl Cytosine (BC) substrate. The cytosine group is released after covalent attachment of the CLIP-tag to the BC substrate.

	1			40
SNAP-tag	MDKDCEMKRT	TLDSPLGKLE	LSGCEQGLHE	IIFLGKGTSA
CLIP-tag	MDKDCEMKRT	TLDSPLGKLE	LSGCEQGLHE	IIFLGKGTSA
	41			80
SNAP-tag	ADAVEVPAPA	AVLGGPEPLM	QATAWLNAYF	HQPEAIEEFP
CLIP-tag	ADAVEVPAPA	AVLGGPEPLI	QATAWLNAYF	HQPEAIEEFP
	81			120
SNAP-tag	VPALHHPVFQ	QESFTRQVLW	KLLKVVKFGE	VISYSHLAAL
CLIP-tag	VPALHHPVFQ	QESFTRQVLW	KLLKVVKFGE	VISESHLAAL
	121			160
SNAP-tag	AGNPAATAAV	KTALSGNPVP	ILIPCHRVVQ	GDLVVG ^Y YEG
CLIP-tag	VGNPAATAAV	NTALDGNPVP	ILIPCHRVVQ	GDS ^D VGPY ^L LG
	161			182
SNAP-tag	GLAVKEWLLA	HEGHRLGKPG	LG	
CLIP-tag	GLAVKEWLLA	HEGHRLGKPG	LG	

Figure 1.6: SNAP-tag and CLIP-tag sequence comparison. Amino acids in green represent differences in the sequence. The CLIP-tag was derived from the SNAP-tag via 8 point mutations.

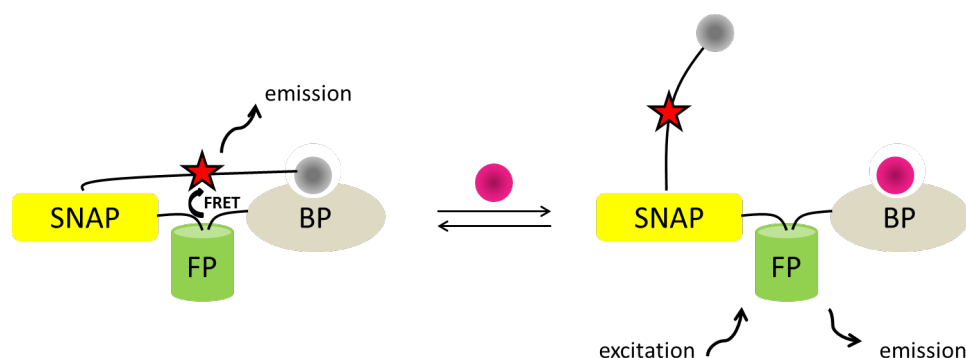


Figure 1.7: Semisynthetic fluorescent sensor proteins based on the SNAP-tag. The synthetic part is covalently bound to the SNAP tag, which contains a fluorophore and a ligand (gray ball). FP: fluorescent protein, BP: binding protein, pink sphere: an analyte, star: fluorophore.

1.2.2 *In vitro* and *in vivo* Applications of SNAP- and CLIP-tag Technology

Tag-based labelling technology has been used for specific labelling of fusion proteins with photostable fluorophores with high quantum yield. Among the site-specific tag-based labelling methods, SNAP-tag technology has been utilized for various applications to perform cellular imaging and study protein-protein interactions. One example of a SNAP-tag application is to produce BG-BG dimers, which were used to measure protein spatial proximity [18]. In another experiment, Maurel *et al.* [19] studied dimerization and oligomerization of GPCR (G Protein Coupled Receptor) receptors with SNAP-tag technology, utilizing time-resolved FRET both *in vitro* and *in vivo*. In 2009, Brun *et al.* [20] developed a fluorescent biosensor protein by fusing the SNAP-tag to a fluorescent protein (FP) and a binding protein (BP). The absence or presence of an external ligand switches the conformation of the biosensor between closed and open forms, leading to a change in the FRET efficiency via a change of the distance between the FP and the label on the SNAP-tag as illustrated in Figure 1.7.

The SNAP-tag also finds application in intracellular studies. Examples of cellular applications include simultaneous dual protein labelling inside live cells [21], protein localization and *cis* location [22], pulse-chase experiments [5], receptor internalization [23], and endocytosis and recycling studies [24]. Cellular labelling using the SNAP- and CLIP-tag systems has several advantages: 1) these tags can be fused to any protein of interest for labelling with fluorescent or non-fluorescent SNAP- or CLIP-tag substrates [10]; 2) the fusion construct allows for specific la-

bellings inside living cells [5]; 3) a low background can be achieved due to high specificity [10]; 4) substrates are non-toxic for living cells [5]; and 5) the fusion tag and the substrate bind covalently, avoiding potential problems of weak non-covalent binding via antibody such as leaching or drift. Self-labelling protein tags have additional advantages over fluorescent proteins such as Green Fluorescent Protein (GFP). As mentioned earlier, the tags can bind to photostable fluorophores that have high quantum yield. Proteins of interest fused to SNAP- or CLIP-tags can be labelled by permeable dyes on the membrane or inside living cells. Various dyes with high photostability, such as Atto dyes, Alexa Fluor dyes (AF), and red-shifted dyes, can be prepared as membrane permeable dyes with BG and BC (available from BioLabs Company, Frankfurt am Main, Germany) [25]. Therefore, it is possible to choose between several fluorophores for measurements in living cells.

1.3 Model Protein Systems

SNAP- and CLIP- tag system have several advantages over conventional fluorophore tagging. Despite evidence of previous application of these tags *in vitro* and inside cells, a careful understanding of its mechanism is still lacking. The fluorophore itself in this system is reasonably small and extremely photostable, but since the tag as a whole is large; further studies would be required to understand its utility in smFRET.

To test the applicability of self-labelling proteins such as the SNAP- and CLIP-tags in smFRET studies, we utilized three different model protein systems: A 15 amino acid peptide, polyproline (PP) linkers, and calmodulin (CaM) protein were fused between the SNAP- and CLIP-tags. SNAP- and CLIP-tags were simultaneously labelled with donor and acceptor dyes, respectively. smFRET measurements were all performed on double-labelled constructs, and the FRET efficiency between donor and acceptor dyes was measured. Moreover, we performed fluorescence lifetime measurements of the PP and CaM constructs *in vitro* and *in vivo*.

In this thesis we describe an investigation of conformational fluctuations, measured by FRET between two tags separated by well-known constructs. The distance between two tags was systematically varied with PP linkers to study the effect on FRET, and the FRET signals of single CaM molecule were measured in the presence or absence of calcium ions. This investigation of distance sensitivity between SNAP- and CLIP-tags will inform future protein-protein interaction studies that require more efficient FRET pairs.

1.4 Nbp2-SH3 Domain for Protein-Protein Interaction Study

Src Homology 3 domains (SH3) are eukaryotic protein domains, which have often been found in signal-transduction pathways. For example, the enzyme tyrosine kinase has a tyrosine kinase domain, a SH2 domain and a SH3 domain. SH3 domain interacts with other catalytic domains to activate tyrosine kinase [26]. SH3 domain can also interact with non-catalytic domains to play a role in signaling pathways as adaptors (e.g. Grb, Crk and Nck) [27]. Additionally, the SH3 domain can be found in regulatory proteins (GTPase activating protein and guanine nucleotide exchanger factor) [28], endocytic proteins (endophilins and amphiphilins) and cytoskeletal proteins (myosins and spectrins) [29].

The SH3 domain has approximately 60 residues organized in five β -sheets, which are linked by a distal loop, a 310 helix, an RT loop and an N-Src loop. There are various SH3 domains with different sequences in the N-Src and distal loops, with differences in the overall folding [29, 30, 31].

The SH3 domain recognizes a polyproline helix II (PPII) containing the PxxP motif, which is a proline rich part of a protein. There are two categories of PxxP motifs: class I (+x Ψ Px Ψ P) and class II (Ψ Px Ψ Px+). Ψ is a hydrophobic residue and + is an Arg or Lys amino acid. Ψ P and P Ψ residues interact inside the grooves on the surface of the SH3 domain containing Phe8/Tyr8, Phe10/Tyr10, Trp36, Pro51 and Phe54/Tyr54 amino acids [32]. In 2004, Fernandez-Ballester et al. [33] highlighted the importance of the SH3 domain structural basis to select class I and II ligands. They observed that the presence of certain residues around the conserved Trp36 determines the type of peptide binding. Often, SH3 domains bind to both classes (I and II), which means the binding preferences are different and poorly understood [33].

The binding position of the peptide (N-terminal of class I and C-terminal of class II ligands) on the surface of the SH3 domain is located between the RT and N-Src loops, the residues are not conserved in these areas (Figure 1.8). Therefore, the SH3 domain can interact with peptides via a combination of the core motif and the extended region [34].

The yeast cell is a good model to study protein-protein interactions, because it has 27 SH3 domains and it is easy to find their interactions and networks. Moreover, the sequence and target binding diversity for yeast SH3 domains can be employed as indicator for other large communities of SH3 domain in other organisms. It is also an easy system to manipulate the genome, which makes it a versatile model for the study of SH3 binding properties [34, 35, 36]. In this work, the interactions between a yeast SH3 domain, the Nbp2 SH3 domain, with various peptides such as Bck1, Pbs2, Cla4 and Ste20 were examined to evaluate the usability of the SNAP/CLIP-tag constructs.

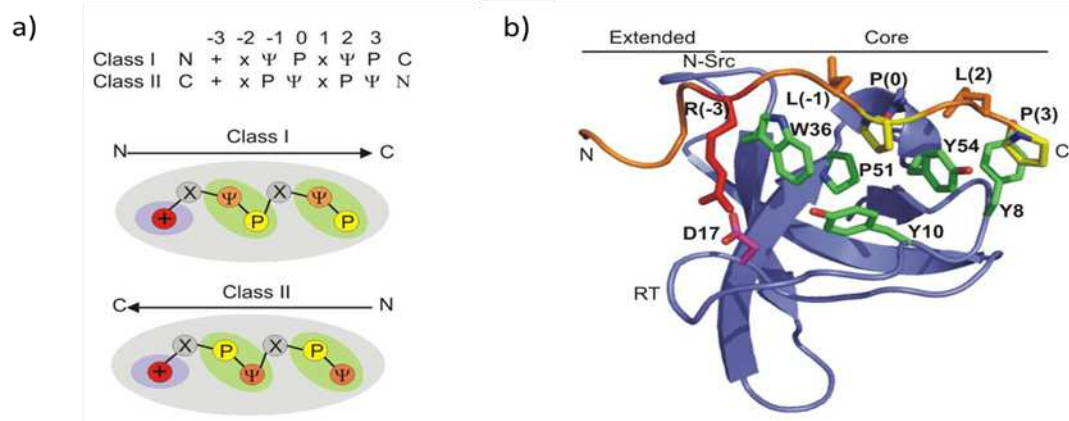


Figure 1.8: The class I and class II consensus motifs and the SH3 domain structure. a) The class I and class II consensus motifs. The hydrophobic pockets are shown in green and the negatively charged pocket is in purple. b) The SH3 domain structure of Src tyrosine kinase with the class I ligand VSL12 (PDB code: 1QWF). Conserved residues and proline are in stick form with the same color as in (a). The picture is copied from reference [34].

1.5 Peptide Model Experiments

1.5.1 15 aa Peptide

To quantify the effect of the tag size on the smFRET measurements, we used a short peptide with 15 residues (sequence: GRLEVLFGQPKAFLE) fused between the SNAP- and CLIP-tags. In addition, a similar 15 amino acid peptide (sequence: GRLEVLFGQPRAFLC) was synthesized and directly labelled with Alexa Fluor 546 and Alexa Fluor 647 (Peps4LS GmbH, Heidelberg). The purpose of this study was to address the issue of the relatively large size of SNAP- and CLIP-tags and the effect this has on smFRET measurements. In doing so, we compare smFRET measurements of SNAP- and CLIP-tag system with that of a directly labelled sequence.

1.5.2 Poly-L-proline: FRET ruler

Proline is the only amino acid in which the side chain is cyclized to the backbone and, therefore, restricts the conformational degrees of freedom. A polyproline peptide forms a helical secondary structure (the alpha helix) with no internal hydrogen bonding. The alpha helix has two different forms: configuration I (left-handed) and configuration II (right-handed). In form I, the peptide bond between

neighbouring residues is in the *cis* conformation and backbone dihedral angles of $(\phi, \psi, \omega) = (-75^\circ, 160^\circ, 180^\circ)$. Form II has the *cis* conformation and backbone dihedral angles of $(\phi, \psi, \omega) = (-75^\circ, 145^\circ, 180^\circ)$. The PPI helix is compact with a helical pitch of 5.6 Å/turn and 3.3 residues/turn. In comparison, the PPII helix is extended with a helical pitch of 9.3 Å /turn and 3.0 residues/turn. The PPI and PPII helix mostly form in organic solvents (such as n-propanol) and aqueous solution. PPI helices are rare in biological contexts, whereas PPII helices can be found in both unfolded polypeptides and folded proteins; PPII helices play important roles in cell motility biological, signal transduction, immune responses and transcription [37, 38].

The PPII helix is the dominant element of secondary structure in unfolded proteins and contributes to the energetics of protein folding. Polyproline conformation and stability of a PPI or PPII helix can be affected by stereoelectronic effects [38]. PPII can also be strongly influenced by microenvironments or interfacial effects and it is highly context dependent [16]. A recent study revealed the existence of stable subpopulations in polyproline during the transition process from PPI to PPII in aqueous solution. The stable sub-populations are representative of the different conformations of polyproline peptides [39]. The transition from PPI to PPII starts from the N-terminus and then moves to the centre of the peptide chain after the first few transitions (Figure 1.9) [39]. In addition, several post-translational modifications (PTMs) such as 4R hydroxylation and glycosylation significantly increase the thermal stability of PPII due to the interaction between hydroxyl and glycosyl groups and water molecules, in a complementary fashion to stereoelectronic effects [40].

These linkers are relatively rigid and much data is available from previous studies for comparison. Stryer and Haugland [41] were the first to demonstrate the application of a polyproline oligomer as a FRET ruler at distances of 10 Å – 60 Å. In their study, they labelled the polyproline peptide with α -naphthyl and dansyl as donor and acceptor dyes at the C- and N-terminal ends, respectively. They used 1 to 12 proline amino acids in oligomers with dye-to-dye distances between 12 Å and 46 Å. Stryer and Haugland assumed that the polyproline oligomer is rigid, then estimated distances based on this assumption. They observed that, the efficiency of energy transfer was a function of distance. Later, in 1967, Schimmel *et al.* [37] also found the polyproline oligomer to be a rigid linker.

The predicted distances which, they explained by incomplete orientational averaging of the large dyes and chain bending, respectively. Furthermore, Best and colleagues [42] studied *cis* and *trans* conformations of polyproline peptides by smFRET and lifetime measurements, in which they determined the length of a 20 polyproline oligomer to be 9-13 nm. They demonstrated that about 30% of the 20 polyproline oligomer contains an internal *cis* conformation according to smFRET

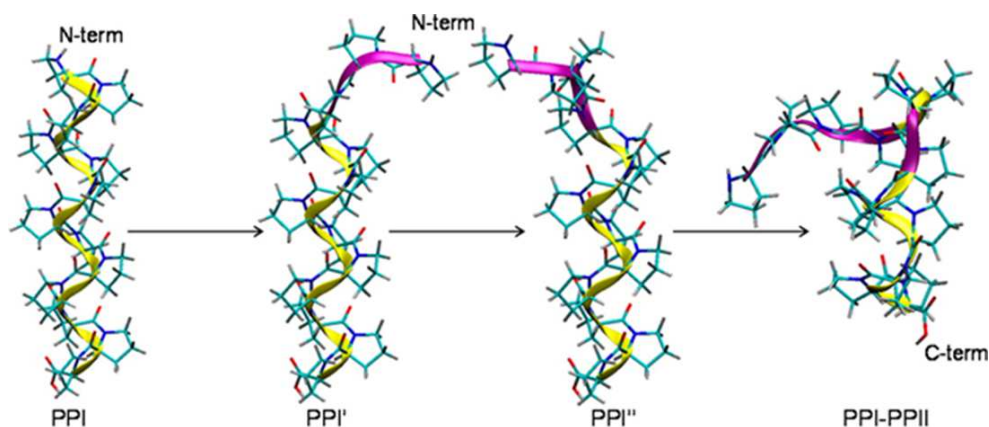


Figure 1.9: Conversion mechanism for Pro13 from PPI to PPII. The *cis* and *trans* residues are shown as yellow and purple ribbons, respectively. Image copied from Ref. [39].

and NMR results. In summary, the polyproline peptide is a semi-flexible FRET ruler.

1.6 CaM Protein

Finally, we used a model protein with a large conformational fluctuation to test the SNAP-tag/CLIP-tag system. CaM is one of the most studied Ca^{2+} -binding proteins (CaBPs) and a great model system for smFRET investigation, because it goes through a large conformational change upon binding calcium ions. The folded conformation can be further stabilized by adding binding factors, such as M13. The system is well-suited to our systematic investigation of smFRET, as it has been studied by many other techniques.

CaM has four helix-loop-helix (HLH) structural motifs arranged in a so-called EF-hand motif that coordinates Ca^{2+} binding in the C- and N-terminal domains (Figure 1.10 & 1.11). In the EF-hands, the Ca^{2+} binds to seven oxygen atoms in a pentagonal bipyramidal arrangement (six oxygen ligands from the protein and one from a water molecule in the surrounding solution) [43].

The conformations of the EF-hand motifs in each domain change independently upon Ca^{2+} binding, however, the domains act in concert to activate signalling pathways. Cooperative binding is very important for the function of CaM inside cells [43]. Various biophysical techniques, described in brief below, have been utilized to characterize the conformational changes induced by Ca^{2+} . Calcium binding increases the stability and the thermal denaturation midpoint of CaM

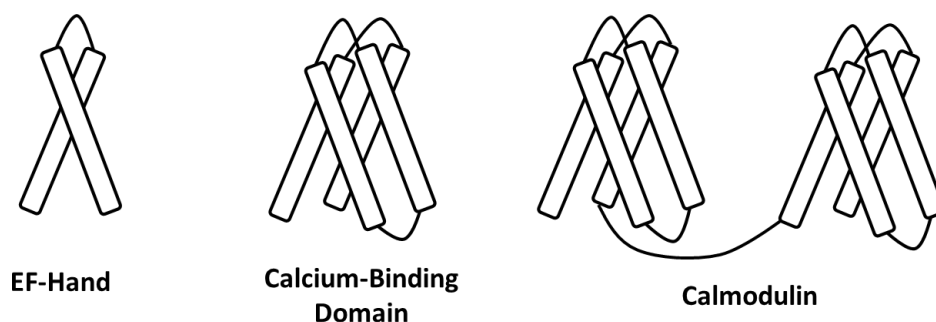


Figure 1.10: Hierarchical structure of CaM. Each Helix-Loop-Helix motif is an EF-Hand Ca^{2+} -binding motif. Each globular domain consists of two EF-Hand motifs, and two domains comprise the CaM protein.

[44].

CaM undergoes conformational changes upon addition of a small amount of calcium [43], and the binding affinity of calcium at each binding site is high ($10^{-6} M^{-1}$). In 1985, Babu [18] reported an X-ray crystal structure of CaM at 1.7 Å resolution. The structure resembles a dumb-bell shape containing two globular domains with dimensions of about 25 x 25 x 20 Å and ≈ 65 Å length (Figure 1.12) [43].

In conjunction with a microfluidic mixer to facilitate rapid and uniform mixing, multiphoton microscopy was used to examine fast Ca^{2+} -induced transitions of acrylodan-labeled calmodulin [19]. The kinetic rates of the conformational changes in two homologous globular domains differ by more than an order of magnitude. The transition time constants were ≈ 20 ms for the N-terminal and ≈ 490 μs for the C-terminal domains of the protein [19]. A combination of molecular dynamics simulations and nuclear magnetic resonance (NMR) was used to clarify the coordination of Ca^{2+} during conformational transitions between closed and open states. The authors found that a Ca^{2+} ion is coordinated by a single oxygen of the bidentate ligand E140, triggering a concerted movement of the two EF-hands that ultimately exposes the target binding site [45]. Another study investigated the importance of solvation energetics in conformational changes of the Ca^{2+} -sensing EF-hand domains, probed by mutating N-terminal nonpolar residues in calmodulin. The authors found altered conformational changes as a result of the mutated residues, generating a corresponding difference in Ca^{2+} binding affinity (Figure 1.12) [46].

A central helix separates the two globular domains of CaM, and the conformation of that helix has been controversially discussed (Figure 1.12). It is an unstable

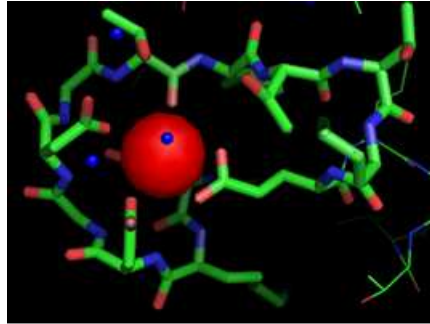


Figure 1.11: The calcium binding site in CaM. Here is the first calcium binding site in CaM showing the pentagonal bipyramidal ligation of calcium. The calcium in the middle of the site (red circle) binds to oxygen atoms from the Asparagine (ASP), Threonine (THR) and Glutamic acid (GLU) amino acids and water molecules (blue circle).(PDB code: 1CLL).

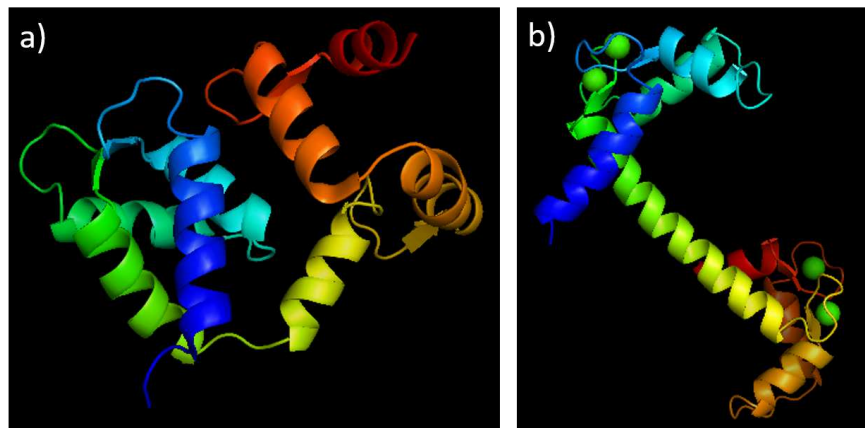


Figure 1.12: Illustration of Ca^{2+} -free (a) and Ca^{2+} -loaded (b) CaM. Here is the crystal structures of Ca^{2+} -free (PDB entry 1QX5) and Ca^{2+} -loaded (PDB entry 1CLL) CaM.

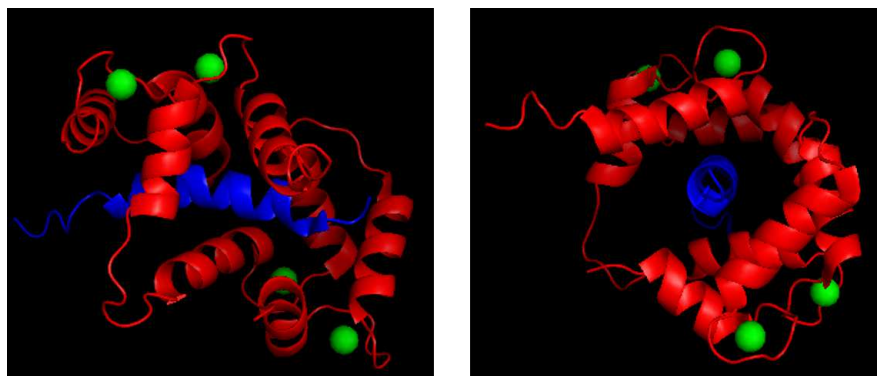


Figure 1.13: Solution structure of a CaM-M13 peptide complex in different views (PDB entry 2BBM). CaM protein (in red) interacted with M13 peptide (in blue) and calcium ions (in green), which changed its conformation to the closed form.

helix, because it is highly exposed to solvents. The alpha helical linker acts as a "flexible tether" between two domains. Conformational studies of peptide binding to CaM show that the central helix serves as a pivot to allow the domains to move around the peptide [43].

In 1992, Ikura *et al.* [47] used NMR to investigate the structure of an M13 peptide bound to CaM (Figure 1.13), and found the M13 peptide to reside as an alpha helical structure inside the CaM protein. M13 is an amphipathic synthetic peptide from the skeletal muscle myosin light chain kinase (skMLCK, residues 577-602). Trp4 and Phe17 are the two main hydrophobic amino acids in CaM, which anchor the peptide to the protein. A later study by Meador *et al.* [48] showed that the Trp5 and Leu18 amino acids of the M13 peptide have a role in anchoring the peptide. In this thesis, we compare the conformational dynamics of M13-bound CaM, evident in smFRET, to the established literature.

The extensive literature describing CaM structural dynamics from a variety of investigative modes provides the backdrop for our comparisons of CaM as a smFRET sensor. This allowed us to consider our smFRET signals using a system with well-described conformational dynamics.

1.7 Thesis Outline

We discussed SNAP- and CLIP-tags as viable labelling strategy for *in vitro* and *in vivo* environments and their applications. At the end of this chapter, the model protein systems used in various fluorescence measurements are briefly discussed. Chapter 2 introduces relevant background including FRET, fluorescence lifetime,

and time-resolved anisotropy methods.

The third chapter describes the details of the experimental methods employed for genetic engineering, protein expression and purification. Analytical methods such as absorption spectroscopy, fluorescence spectroscopy measurements are subsequently explained.

The fourth chapter presents the experimental results and evaluates them in context with currently published works. In the first part of this chapter, the interaction between Nbp2-SH3 and peptides was investigated using bulk FRET measurements. In the second part of the chapter, the smFRET method to determine differences between constructs comprised of a 15 amino acid (15 aa) polypeptide, a polyproline (PP) polypeptide, and calmodulin is described. The distances between donor and acceptor, FRET peak broadening and conformational changes in an *in vitro* study was also investigated. The final part of the results section, the distance between SNAP- and CLIP-tags and protein conformational changes are discussed for the PP and CaM constructs by fluorescence- lifetime techniques *in vitro* and *in vivo*.

The appendix contains lists of buffers and solutions, primers, construct sequences, dye properties, the applied fitting functions, smFRET histograms, and absorbance spectra of labelled constructs.

Chapter 2

Background

2.1 Fluorescence

A molecule that absorbs light and subsequently emits light at a longer wavelength does so by a process called fluorescence. The time interval between the absorption of a photon, excitation of an electron from, and emission of a new photon is on the order of nanoseconds [3]. Fluorescence provides biologist with an elegant tool to study static and dynamic processes with minimum external intervention. The spectral properties of fluorescent molecules depend on the chemical structure of the molecule and its surrounding environment [3].

The process of absorption and emission of light can be visualized by a Jablonski diagram (Figure 2.1). The diagram depicts the electronic ground state (S_0), the first two excited singlet electronic states (S_1 and S_2) and the first excited triplet state (T_1). In each electronic state, there are several vibrational substates (gray lines). Arrows indicate transitions between the different levels. Upon absorbing a photon, the fluorophore is excited from the electronic ground state to an excited electronic state within 10^{-15} s. It will then lose energy by vibrational relaxation and internal conversion (IC) without emitting a photon and reach the ground vibrational level of S_1 .

In a process called fluorescence, the excited molecule can subsequently relax back down to the electronic ground state S_0 by emitting a photon to lose its energy. The emitted photon has less energy than the absorbed photon. The difference between these energies is termed the Stokes shift [3]. The Stokes shift is a result of vibrational relaxation or dissipation as well as reorganization and relaxation of the surrounding solvent molecules [3].

High fluorescence quantum yield is one of the factors for determining fluorophore utility. Quantum yield is a measure of fluorescence efficiency, describing the ratio of the number of emitted photons to the number of absorbed photons.

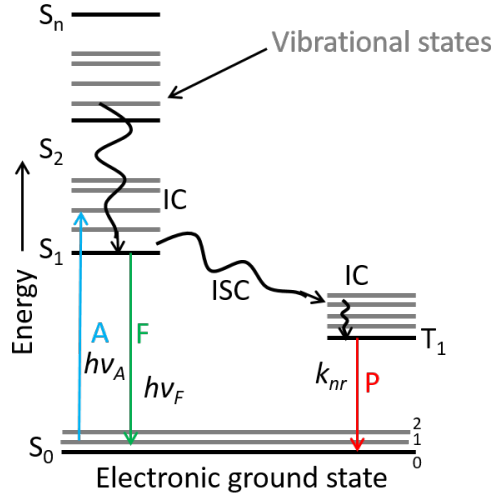


Figure 2.1: Jablonski diagram. A = absorption, F = fluorescence, P = phosphorescence, S_0 = electronic ground state, $S_1 \dots S_n$ = excited singlet states, T_1 = excited triplet state, IC = internal conversion, ISC = intersystem crossing, $h\nu_A$ = the absorbed energy, $h\nu_F$ = the emitted energy, k_{nr} = the rate for the competing non-radiative route.

The rate constant k_{nr} describe nonradiative processes that depopulate the excited state [3].

The time spent by a photon in the excited state before returning to the ground state is the fluorescence lifetime (τ), which is a characteristic property of a fluorophore.

$$\tau = \frac{1}{k_r + k_{nr}}, \quad (2.1)$$

where k_r is the radiative (emission) pathway with a rate of k_r , and usually the inverse of k_r is the intrinsic or radiative lifetime.

Minimizing the quenching effect in fluorescently labelled proteins is of particular interest, due to the desirability of bright fluorophores with a high quantum yield. Three amino acids in the structure of protein (Tryptophan (Trp), Tyrosine (Tyr) and Phenylalanine (Phe) are largely responsible for quenching fluorophores in proteins. Quenching is caused by photo-induced electron transfer (PET), which is an excited state electron transfer process. In this process, an excited electron is transferred from the donor to the acceptor. This results in ion formation and finally to charge separation, whereby the covalent bond between the ionized reactants is broken [3]. The following sections will describe the theoretical and

experimental assays for FRET and advancement thereof. We would also briefly look at fluorescence anisotropy measurement.

2.2 FRET– Förster Resonance Energy Transfer

2.2.1 Theoretical Calculation of the FRET efficiency

FRET is an electrodynamic phenomenon or a physical process, which arises through by means of intermolecular long-range dipole–dipole coupling between donor and acceptor. Transfer of energy occurs between an excited donor and a nearby acceptor in a ground state with a probability E , termed FRET efficiency. The strength of coupling is strongly dependent on the distance, R , between donor and acceptor molecules ($E \propto R^{-6}$). The energy transfer occurs at a range of 1 to 10 nm distance with a measurable efficiency, which correlates to micromolecular dimensions.

To explain the mechanism of FRET, we imagine a system with two fluorophores one as a donor and another one as an acceptor. If the emission spectrum of the donor has an overlap with the absorption spectrum of the acceptor, the resonance will occur through weak coupling with the rate of k_T . Then, the donor molecule is quenched and the acceptor molecule is excited and can subsequently emit a photon with its own quantum yield. The number of quanta that are transferred from the donor to the acceptor can be quantitatively measured as the FRET efficiency E .

$$E = \frac{\text{no. of quanta transferred D} \rightarrow \text{A}}{\text{no. of quanta absorbed by Donor}} \quad (2.2)$$

The rate k_T and the efficiency E of the energy transfer based on the Förster theory can be written as

$$k_T = \text{const } k_F J n^{-4} R^{-6} \kappa^2 \quad (2.3)$$

and

$$E = \frac{k_T}{k_T + k_F + k_D}, \quad (2.4)$$

Where R is the distance between the donor and the acceptor molecules and κ^2 is an orientation factor. Other parameters are n as a refractive index and J as a spectral overlap integral. k_F is the rate constant of fluorescence emission of the donor and k_D is the sum of the rate constants of all other de-excitation processes of the donor.

The spectral overlap, J , which is proportional to the overlap in the emission spectrum of the donor and the absorption spectrum of the acceptor is given by

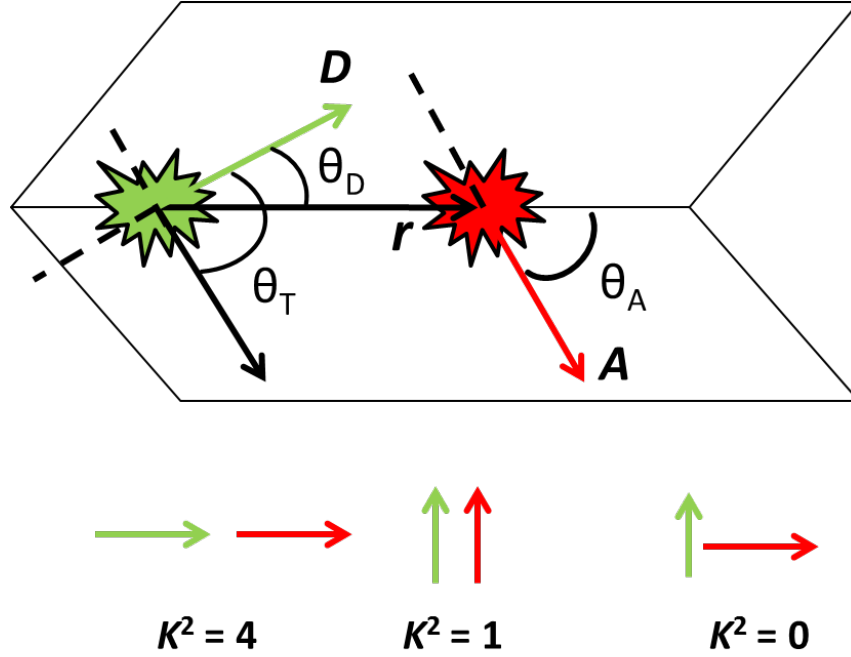


Figure 2.2: The value of κ^2 depends on the emission dipole of the donor and the absorption dipole of the acceptor molecule. \mathbf{D} : donor emission dipole; \mathbf{A} : acceptor absorption dipole. \mathbf{r} is the vector connecting the donor and the acceptor fluorophores.

$$J = \frac{\int F_D(\lambda)\epsilon_A(\lambda)\lambda^4 d\lambda}{\int F_D(\lambda)d\lambda} [M^{-1}cm^{-1}nm^4], \quad (2.5)$$

where $F_D(\lambda)$ is the fluorescence intensity of the donor at wavelength λ and $\epsilon_A(\lambda)$ is the molar extinction coefficient of the acceptor at wavelength λ . In order for energy to transfer between the two fluorophores, an overlap between emission spectrum of the donor and absorption spectrum of the acceptor is required.

The influence of the orientation of the donor's emission dipole relative to the acceptor's absorption dipole can be described by the orientation factor (κ^2). It is given by:

$$\kappa^2 = (\cos \theta_T - 3 \cos \theta_D \cdot \cos \theta_A)^2 \quad (2.6)$$

θ_T is the angle between the emission transition dipole of the donor and the absorption transition dipole of the acceptor. θ_D and θ_A are the angles between those dipoles and the vector connecting the donor and the acceptor, respectively.

Depending on the angle between the two dipoles, κ^2 varies from 0 to 4. When transition dipoles are parallel, the value of κ^2 corresponds to 1, while parallel and collinear dipoles result in a value of 4 (Figure 2.2). If both fluorophores have a certain degree of rapid rotational freedom, κ^2 is taken equal to 2/3 assuming the averaging over all possible donor and acceptor orientations on the timescale of the donor lifetime [3].

To determine the FRET efficiency E experimentally, the donor dye is excited and fluorescence emissions from the donor (I_D) and the acceptor (I_A) are collected individually. E is then calculated as follows: [3].

$$E = \frac{I_A}{\gamma I_D + I_A} \quad (2.7)$$

γ is a correction factor that depends on the detection instrumental efficiencies of the donor and the acceptor channels and the quantum yields of the dyes. The change in distance between the donor and the acceptor can be monitored by the FRET approach. E is a dimensionless number, $0 \leq E \leq 1$, and is related to the inter-dye distance (R) by the well-known Förster formula [49].

$$E = \frac{1}{1 + \left(\frac{R}{R_0}\right)^6} \quad (2.8)$$

From equations 2.3, 2.4, and 2.8 it follows that

$$k_T = \frac{1}{\tau} \left(\frac{R_0}{R}\right)^6, \quad (2.9)$$

where τ is the lifetime of the donor in the absence of an acceptor dye and R_0 is the so called Förster distance, the distance between the donor and the acceptor with a transfer efficiency of 50%.

$$R_0 = 0.211(n^{-4}\varphi_D J(\lambda)\kappa^2)^{\frac{1}{6}}, \quad (2.10)$$

where φ_D is the quantum yield of the donor in the absence of acceptor. A sufficiently high quantum yield of the donor, large absorption coefficient of the acceptor, and adequate overlap of the donor emission and acceptor excitation spectra are all necessary to effectively observe distances in the 1 to 10 nm range.

2.2.2 Single-Molecule FRET and its Applications

The FRET value between donor and acceptor of a labelled protein of interest can be measured by ensemble and/or single-molecule methods to detect changes in the conformation of the protein. A single protein can be dually labelled with two fluorophores or two different types of proteins may be labelled with a donor and an

acceptor dye each. In ensemble measurements, only the average FRET efficiency value of a large number of molecules can be obtained. Especially for biomolecules with multiple conformational states, the interpretation of ensemble FRET data, is complicated. Substates and subpopulations normally cannot be resolved. In stark contrast to ensemble measurements, single-molecule measurements allow detection of subpopulations and their distributions. For single-molecule FRET, the biomolecule solution is diluted to picomolar concentrations, ensuring the presence of only one molecule per excitation/detection volume. To increase the signal-to-noise ratio, the observation volume is decreased as much as possible, to minimize background fluorescence. Bright and photostable fluorophores are typically especially important for single molecule FRET. In smFRET experiments on immobilized molecules, even temporal fluctuations of the FRET efficiency of a single molecule can be observed in real-time, unlike in ensemble FRET measurements, in which dynamic fluctuations are lost to averaging [21].

Before designing a smFRET measurement, one has to consider the limitations of the smFRET technique. Labeling of the protein with a photostable and bright fluorophore is necessary. Typical labels are organic dyes and fluorescent protein.

Organic dyes are sufficiently photostable and bright for smFRET measurement, but their binding is limited to specific chemical groups on the proteins. The placement of amino acids with such groups often requires intensive sequence mutation, often with unpredictable effects on protein function. The advantage of fluorescent proteins is that they can be endogenously expressed and are easily targeted as a result. Their use is restricted in smFRET due to insufficient photostability and their large size, which is capable of disturbing the function of a protein of interest.

smFRET measurement ideally requires small, water-soluble, and non-aggregating donor and acceptor dyes that are characterized by a high extinction coefficient ($\epsilon > 50,000 \text{ M}^{-1}\text{cm}^{-1}$ at the excitation wavelength), a high quantum yield (> 0.1), high photostability, and low propensity for blinking. Typically, organic dyes functionalized with amine- (NHS ester) or thiol-reactive (maleimide) groups are used to conjugate to lysine and cysteine residues on the protein of interest, respectively. However, when a protein has multiple cysteine residues, unwanted cysteine residues need to be substituted by mutagenesis techniques, which are often time-consuming and may affect the protein's native function.

Genetic tags are an alternative fluorophore labeling strategy. GFP is one of the most commonly used genetic tags that can be fused to a protein of interest. While labeling efficiency is excellent, the low photostability and inability to suppress blinking behavior are problematic for smFRET measurements. Another example of a genetic tag is the calmodulin binding (CBP), which has been used for some smFRET studies [22]. The CBP peptide is small (4 kDa) and forms a non-covalent bond with its protein partner. Another genetic tag utilizing cova-

lently bond dyes is the tetra-cysteine tag (-CCXXCC-). Biarsenical dyes such as biarsenical fluorescein (FLAsH) covalently conjugate to the tag *in vitro* and *in vivo*. Recently, the fluorescein-derivative of FLAsH has been synthesized and applied in smFRET measurements [23]. Moreover, the sortase tag [24] or self-labeling proteins such as the Halo tag (33 kDa) [50] and the SNAP-tag (18 kDa) [25, 37] have proven to be useful for cellular imaging, but none of these tags have previously been used for smFRET measurements. Other strategies for protein labeling such as aldehyde tags [38] and non-natural amino acids [16, 39] have been applied to smFRET approaches as well.

2.2.3 Burst Detection and Analysis

Typically, a sample concentration of ≈ 100 pM was used to avoid more than one molecule passing through the confocal volume concomitantly. As a molecule diffuses through the focal volume — roughly on a timescale in the order of several hundred microseconds for small biomolecules — the attached fluorophores get excited and the photons are emitted as a single “burst”. Due to the stochastic behavior of this process, the time a molecule takes to pass through the focal volume varies from molecule to molecule. Hence, the number of photons of a burst is lower from a molecule that passes through the confocal volume in a shorter time and vice-versa. Inherent shot-noise additionally contributes to the variation in the detected intensities. To filter out molecules with low signal-to-noise ratio, a photon count threshold of 50 counts has been used for further FRET efficiency analysis. In a typical measurement, the events above the threshold are few. Therefore, the sample has to be measured for more than 1 h to collect enough appropriate FRET bursts.

Under conditions of single-molecule detection, the number of time bins that contain only background signals is greater than the number of bins with real signals from donor and acceptor dyes. The main source of background signal are dark counts. Other sources of noise include scattered excitation light or external light. Some background counts cannot be avoided and a small fraction goes through the detection filters as background signals. By diluting the sample to picomolar concentration, the number of bins with real signal from the sample are much smaller than the number of bins with background photons. As a result, a photon counting histogram dominantly presents the background, which can be described by Poisson distribution. From the Poisson distribution, the average background can be calculated and a noise threshold (a value at which the Poisson distribution decreases below 0.1%) determined for both channels. The bins above the noise threshold are then analyzed further. The number of photons in each channel upon donor excitation and the number of detected photons in the acceptor channel upon direct excitation of the acceptor is further determined.

The next step is burst-size histogram visualization. As the number of photons per burst is not constant, there is a size distribution for a bursts. Only burst that contain a minimum number of photons (10 being a typical number) are selected for photons in the burst size histogram. All calculated FRET values from bursts with at least 50 photons are collected in a FRET histogram.

One of the most important factors affecting the uncertainty of FRET efficiency is the shot noise. This is an inherent and unavoidable characteristic of detection of independent photons and the nature of light emission. As the width of FRET peaks in the FRET histogram can be affected by this noise, therefore the minimum and maximum numbers of photons per burst must be determined to optimize FRET peaks. The average number of photons increases as a result of choosing a higher photon count for the threshold, resulting in a narrower FRET histogram and lower shot noise but reducing the overall number of events, hence, decreasing the statistical power of an experiment. To strike an acceptable balance between those problems, a burst containing at least 50 photons was considered the minimum photon count for FRET histogram analysis.

As a result, the FRET efficiency was calculated from the photon counts in donor and acceptor channels for each burst and all collected in a FRET histogram. Donor-only labelled molecules are unavoidable in the measured solution, therefore there is a donor-only peak at zero FRET in the FRET histogram. Any low FRET population from properly double-labelled molecule can be obscured by the donor-only population.

2.2.4 Burst Wise FRET Calculation

In 2004, Kapanidis and coworkers [51] introduced the Alternating Laser Excitation (ALEX) technique for smFRET measurements. This technique generates four distinct photon-emission streams ($F_{D_{exc}}^{A_{em}}$, $F_{A_{exc}}^{A_{em}}$, $F_{A_{exc}}^{D_{em}}$, and $F_{D_{exc}}^{D_{em}}$) for a single diffusing fluorescent molecule, where F_Y^X is a photon count corresponding to donor or acceptor excitation and donor or acceptor emission (D_{exc} or A_{exc} , and D_{em} or A_{em} , respectively). The excitation wavelength to excite either the donor or the acceptor dye is switched periodically, on a time scale significantly shorter than transit time of a molecule through the confocal volume. Excitation and light detection are synchronized to recognize if the light is detected upon donor excitation or acceptor excitation. Upon donor excitation, two photon-emission streams ($F_{D_{exc}}^{A_{em}}$ and $F_{D_{exc}}^{D_{em}}$) are recorded. During acceptor excitation, only the $F_{A_{exc}}^{A_{em}}$ photon-emission stream is collected. D-leakage (Lk) is the photon count for D-emission into A-detection channel on the basis of $F_{D_{exc}}^{D_{em}}$; A-direct excitation (Dir) is the photon count for A-emission caused by A-direct excitation at the D-excitation wavelength based on $F_{A_{exc}}^{A_{em}}$; and the photon count for A-emission particularly due to FRET called F^{FRET} . This method allows one to obtain an accurate FRET efficiency (E). A

FRET efficiency measured in this way is corrected for background, LK, and Dir as compared to a FRET efficiency measured via ensemble-FRET. After analyzing collected data, four distinct species: Donor-only molecules (D-only), Acceptor-only molecules (A-only) and molecule with both donor and acceptor dye, can be sorted in a new dimension to facilitate γ calculation [52].

With a known γ , the FRET efficiency can be obtained as [53]:

$$E = \frac{F^{FRET}}{\gamma F_{Dexc}^{Dem} + F^{FRET}} \quad (2.11)$$

$$F^{FRET} = F_{Dexc}^{Aem} - \text{LK} - \text{Dir} \quad (2.12)$$

As demonstrated in a more recent study [51], stoichiometry of each burst can be calculated independent of FRET efficiency, and is based on $D - A$ species and a known γ factor.

$$S_\gamma = \frac{\gamma F_{Dexc}^{Dem} + F^{FRET}}{\gamma F_{Dexc}^{Dem} + F^{FRET} + F_{Aexc}^{Aem}} \quad (2.13)$$

In the burst analysis program, the stoichiometry map (called an E-S map) and the FRET histogram of all observed bursts were extracted from the recorded fluorescence bursts (Figure 2.3). In Figure 2.4, the zero-FRET peak population in the E-S map (left top plot, $-0.1 \leq E \leq 0.1$ and $0.8 \leq S \leq 1$) represents the donor-only molecules. Peaks with a stoichiometry less than 0.6 represent the population with an active acceptor label, termed as FRET population. The separation between the donor-only and the FRET populations in the stoichiometry map was adjusted by changing the red laser intensity used for direct acceptor excitation. For further analysis, only events from dual-labelled molecules ($0.3 \leq S \leq 0.6$) were selected for the calculation of the FRET histogram (Figure 2.4). The plotted FRET populations were fitted with a Gaussian fit function according to equation 2.14.

$$y = Ae^{-\frac{(x-x_c)^2}{2w^2}} \quad (2.14)$$

with amplitude A , width w , and the peak center x_c . We used OriginPro 9.0 (OriginLab Co., Northampton, MA, USA) for all fittings. After fitting FRET populations, x_c and w values were assigned as FRET efficiency and width of FRET histogram, respectively.

2.2.5 Calculating γ -factor via the Stoichiometry Map

Correcting γ factor is a step to obtain accurate FRET efficiency, the ratio of donor dye's quantum yield to the detection efficiency of the acceptor dye. When the

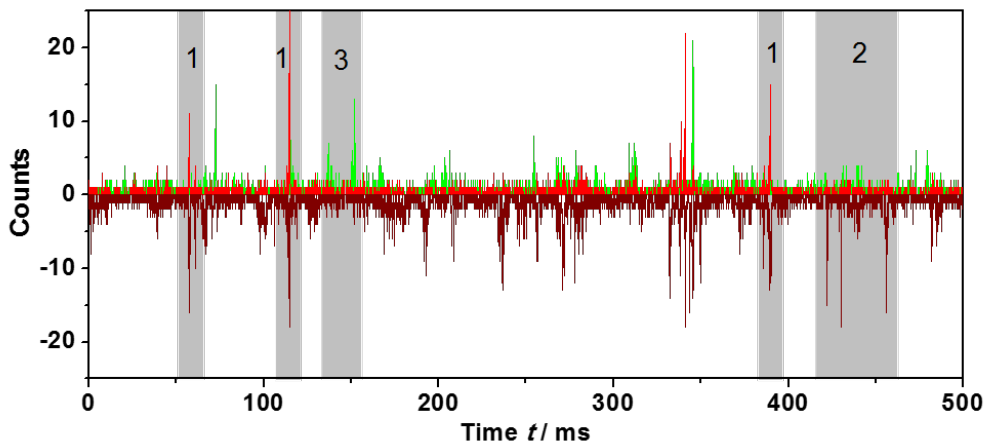


Figure 2.3: Fluorescence traces of the CaM construct in Tris buffer pH 7.4, recorded with a bin size of $100 \mu\text{s}$. Signal collected in the donor channel (light green) and the acceptor channel (light red) during excitation of the donor are plotted in the upper half of the diagram, whereas signal collected in the acceptor channel during direct excitation of the acceptor (dark red) is shown with inverted amplitude in the lower half. Peaks in interval 1 are representative of properly labeled molecules in a high FRET state. Upon donor excitation a majority of the light is emitted in the acceptor channel, while the presence of an acceptor dye is also evidenced by the acceptor signal upon direct acceptor excitation. Molecules labeled with only an acceptor dye, lead to acceptor-only bursts as in interval 2. Interval 3 shows molecules labeled with only a donor dye, which exhibit a lack of acceptor signal upon direct acceptor excitation.

stoichiometry of D-A species with low and high FRET is similar, then the γ value is equal to 1. The stoichiometry of our D-A species in stoichiometry map was different and correspondingly $\gamma \neq 1$ in our case. The γ factor can be determined from the intercept, ω , and slope, Σ , of the linear fit to a 2D stoichiometry histogram of the peak positions of two FRET subpopulations of low and high FRET efficiencies according to:

$$\gamma = \frac{(\omega - 1)}{(\omega + \Sigma - 1)} \quad (2.15)$$

The resulting γ factor can be used to re-calculate FRET efficiency (Figure 2.5) with improved accuracy.

γ factor value of ≈ 0.9 was determined for Alexa 546 and Alexa 647 dyes by Dr. Robert Rieger in 0 concentration of Guanidinium Chloride (GdmCl) [54]. We used this γ value to calculate the FRET efficiency.

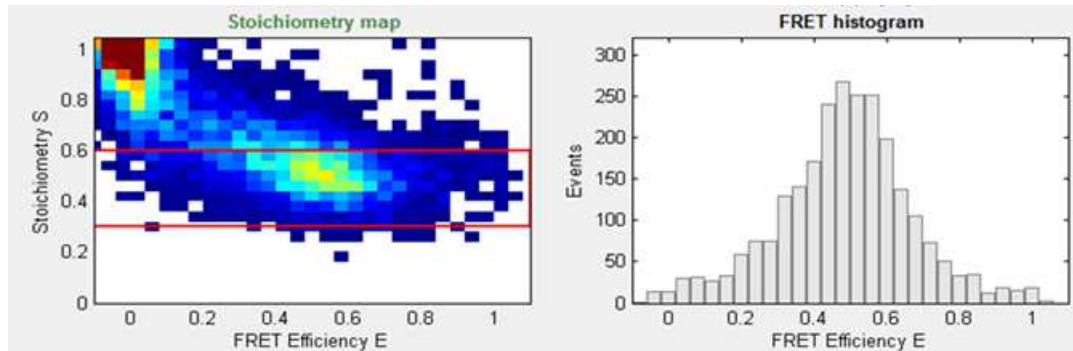


Figure 2.4: Screen shot of the stoichiometry map and FRET histogram from the burst analysis program.

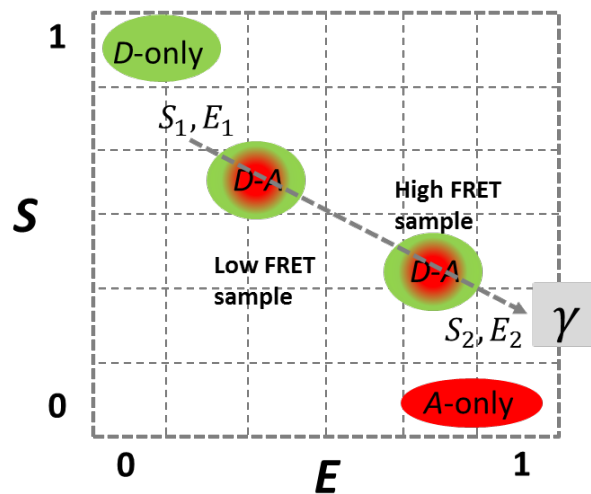


Figure 2.5: Two-dimensional FRET efficiency-stoichiometry histogram. By determining two peaks at low-FRET and a high-FRET species and fitting linearly between two peaks, the gamma factor was considered a slope. After gamma factor correction of the FRET histogram, the position of each species can be shifted.

2.3 Fluorescence Lifetime Imaging Microscopy-Based FRET (FLIM-FRET)

A fluorophore can be characterized by its fluorescence lifetime, τ . The fluorescence lifetime is defined as the average time of a fluorophore in an excited state before returning back to the ground state. In the simplest case, the fluorescence intensity decay can be described by a single exponential function with a characteristic decay time τ :

$$F(t) = F_0 e^{-\frac{t}{\tau}}, \quad (2.16)$$

Where F_0 is the intensity at time $t=0$. For more complicated decay processes, a sum of exponential decay functions with different time constants τ_i and amplitudes (F_{i0}) can be utilized:

$$F(t) = \sum_i F_{i0} e^{-\frac{t}{\tau_i}} \quad (2.17)$$

The time course from the excitation pulse up to the relaxation times of all probes to the ground state is analyzed, and the average fluorescence lifetime, $\bar{\tau}$, is determined by its integral intensity.

$$\bar{\tau} = \frac{\sum_i F_{i0} \tau_i^2}{\sum_i F_{i0} \tau_i} \quad (2.18)$$

The $\bar{\tau}$ of commonly used fluorophores is on the order of a few nanoseconds. Depending on environmental factors such as the polarity of the solvent, ions in the surrounding solution or the presence of an acceptor dye in a FRET dye pair, the fluorescence lifetime can differ. By measuring the lifetime of the donor molecule in the presence (τ_{DA}) and absence (τ_D) of an acceptor, one can calculate the FRET efficiency using:

$$E = 1 - \frac{\tau_{DA}}{\tau_D} \quad (2.19)$$

During FRET, the donor molecule transfers energy to the acceptor molecule and fluorescence lifetime becomes shorter. The FLIM-FRET method has been used for several investigations inside cells [55, 56]. Additionally, quantitative identification of protein-protein interaction in living cells can be achieved with the FLIM-FRET method [57].

2.3.1 FLIM setup

The Micro-Time 200 time-resolved confocal microscope (PicoQuant GmbH, Berlin, Germany) was used to determine the fluorescence lifetimes of the fluorophores.

The lifetime of A546 on the labelled PP and CaM constructs with and without DY647 fluorophore was measured in solution as free diffusion through focal volume. The instrument is a commercial system based on an Olympus microscope body (IX71S1F-3, Olympus, Hamburg, Germany) equipped with a water immersion objective lens (UPLSAPO 60XW, 60x/1.2 W, Olympus, Hamburg, Germany). Figure 2.6 represents the experimental setup. A small fraction of the laser light (530 nm or 405 nm) produced by a diode laser (PicoQuant, Berlin, Germany) was reflected by the beam splitter to a photodiode (PD) and a CCD camera. The photodiode measured the laser power, and the CCD camera was used to adjust the focus. The remaining laser light is passed on to a dichroic mirror (DS1) and then into an objective lens, which illuminates a small volume of the sample. The emitted fluorescence light from the sample passes through the same dichroic mirror (DS1) into a pinhole (P, diameter = 100 μm), which is used to suppress out-of-focus signal. Finally, the fluorescent light is detected by the Single Photon Avalanche Diode (SPAD, SPCM-AQR-14, PerkinElmer Inc., Waltham, Massachusetts, USA). The same setup was used for FLIM-FRET imaging of the labelled PP and CaM inside the yeast cells. The lifetime of the donor dye with and without the acceptor dye was measured inside the yeast cells. The labelled yeast cells was scanned in a bidirectional fashion with a pixel integration time of 0.6 ms. For different dye pairs inside the yeast cells, the filters and dichroic mirrors were changed accordingly. All measurements were carried out in a dark chamber at room temperature.

2.3.2 Fluorescent Lifetime Determination

The fluorescence lifetime of the donor dye was determined by using time-correlated single photon counting (TCSPC). PP and CaM constructs were labelled with A546 and DY647 dyes and diluted to final concentrations of 5 nM in 50 mM Tris-HCl, 300 mM NaCl, pH 7.4. The detected fluorescence lifetime decay was fitted with the Instrument Response Function (IRF) (red). After deconvolution, the lifetime of A546 is extracted using an exponential fit function (equations 2.20 & 2.21) in the SymPhoTime program (PicoQuant GmbH, Berlin, Germany). The amplitude and lifetime values were extracted from the fitted data decay (Figure 2.7). The fitted curve (black) is overlapping with the decay curve.

The decays were fitted with a double and triple exponential functions. Here, single (equation 2.20) and multi (equation 2.21) exponential function are shown.

$$I(t) = I(0)e^{\frac{-t}{\tau}} \quad (2.20)$$

$$I(t) = I(0) \sum_i \alpha_i e^{\frac{-t}{\tau_i}} \quad (2.21)$$

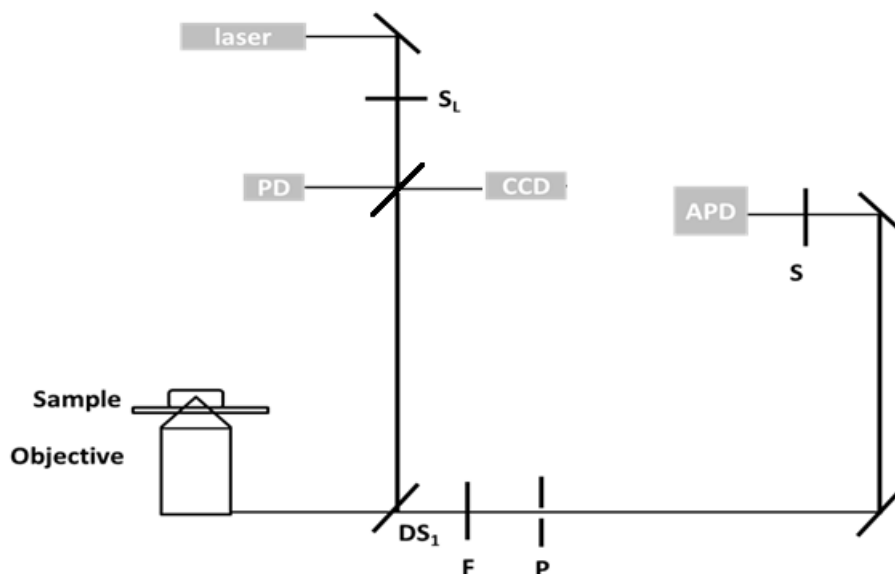


Figure 2.6: Schematic representation of the excitation and detection paths. It includes the dichroic mirror DS1, filter F (HQ580/70 or LP450 for the donor and HQ690/70 M for the acceptor channels, both Chroma, AHF), pinhole P, shutter S, the Single Photon Avalanche Diode SPAD, the electronic shutter SL, the photodiode PD and the CCD camera.

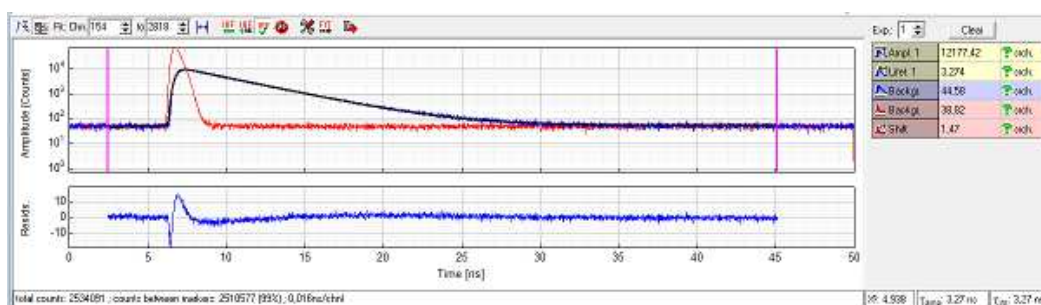


Figure 2.7: The fluorescence lifetime decay fitting process. The lifetime decay is the blue line in the upper panel, which is fitted with a mono-exponential fit function ($\tau = 3.27$ ns: black line). The red line represents the instrument response function (IRF).

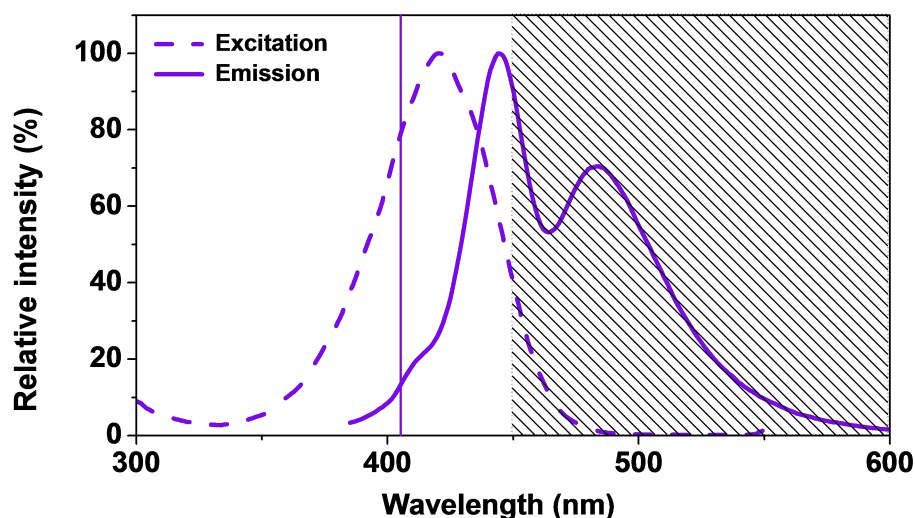


Figure 2.8: Absorbance and emission spectra of the SNAP-Cell 430 dye. The vertical line and shadow show the 405 nm laser excitation and the filter range used for the experiment, respectively, in respect to the excitation (dashed line) and the emission (solid line) spectra of the dye.

where τ and α_i are the lifetime and fractions, respectively. $I(t)$ shows fluorescence intensity.

2.3.3 FLIM-FRET Measurements

FLIM-FRET measurements were performed using the time-resolved fluorescence confocal microscope MicroTime 200 (PicoQuant GmbH, Berlin, Germany). The FLIM-FRET method was utilized for yeast cells transformed with the PP and CaM constructs with different FRET pairs. Live yeast cells transformed with the S-CaM-C construct were labelled with CLIP-CellTM 430 (Figure 2.8) and SNAP-Cell[®] TMR-Star dyes as a donor and an acceptor, respectively and were loaded in a cell chamber for lifetime imaging. The donor dye in yeast cells was excited by a 405 nm single-mode pulsed laser. The excitation laser was filtered out using a long pass filter with a 450 nm cutoff. Fluorescence emission from the donor was collected in the presence and absence of the acceptor in different samples to determine the mean lifetime.

For FLIM-FRET measurements on the PP construct, the snap- and clip-tags was labelled with A546 and DY647 fluorophores, respectively (the same fluo-

rophores as used for *in vitro* labelling). After labelling, the yeast cells were fixed and loaded in the cell chamber for imaging. In the microscope setup for the measuring on the PP construct, the LDH-P-FA-530 diode laser (530 nm laser), the HQ590/70 filter and the excitation dichroic mirror zt470-532-640rdc were used.

2.4 Fluorescence Anisotropy

2.4.1 Time-Resolved Anisotropy

A liquid sample of fluorophore can be excited by a pulsed and polarized excitation; and the fluorescent emission of the fluorophore can be changed by changing the excitation polarization. The variables in this experiment are the intrinsic properties of the fluorophore and its environment. These factors bring about a change in the lifetime and variable rotational diffusion of the fluorophore. For instance, when the fluorophore binds to another substance, the rotational diffusion decreases and anisotropy value increases.

The angle of linear polarization of light with respect to the absorption transition vector of the fluorophore decides whether a fluorophore excites or doesn't. An excited fluorophore aligns to the plane of linearly polarized light. The excitation energy of this fluorophore is released through a linearly polarized fluorescence emission or one of the other processes. The fluorescence emission is not instantaneous following excitation. A fluorophore which rotationally diffuses within the time of excitation and emission would emit an unpolarized light. The ratio of polarized to unpolarized light reveals characteristics of the fluorophore like size and polarizability and that of its environment.

In figure 2.9, the vertically polarized light excites the fluorophore and the fluorescence emission is split by a polarization filter into vertically polarized light (I_{VV}) and Horizontally polarized light (I_{VH}) and its fluorescence decays were analyzed independently. The anisotropy (r) was determined from these decays as a function of time [3].

To the resulting anisotropy decay data, we fitted polarized VV and VH decays by

$$VV(t) = F_0[2r_0 \exp[\frac{-t}{\tau_F \tau_r}] + \exp(\frac{-t}{\tau_F})] \quad (2.22)$$

$$VH(t) = F_0[-r_0 \exp[\frac{-t}{\tau_F \tau_r}] + \exp(\frac{-t}{\tau_F})] \quad (2.23)$$

$$r = \frac{VV(t) - (G \times VH(t))}{VV(t) + (2 \times G \times VH(t))}, \quad (2.24)$$

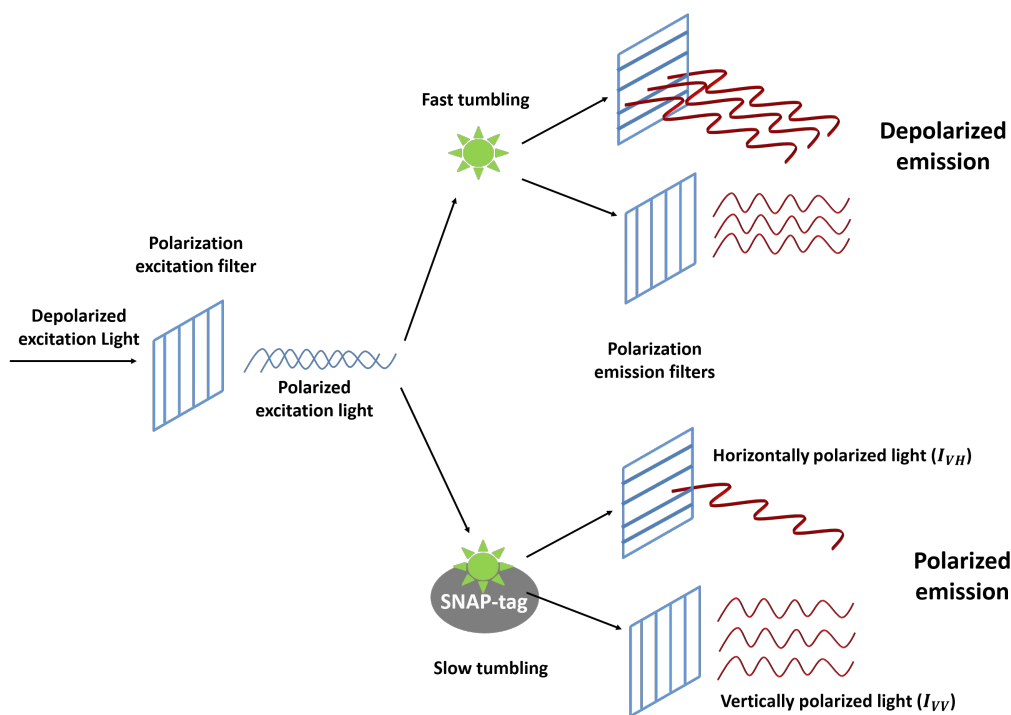


Figure 2.9: Fluorescence polarization diagram. Due to the fast tumbling of fluorophore (in green color), the emission light is not polarized, while the slow tumbling of attached fluorophore on the SNAP-tag shows polarized emission. Image adopted from www.hi-techsci.com/techniques/anisotropy/.

where $VV(t)$ and $VH(t)$ are the observed fluorescence intensities of vertical and horizontal polarization components, respectively, which obey double exponential kinetics. G is the instrument dependent ratio towards vertically and horizontally polarized light. F_0 is a measured initial intensity, r_0 is the initial anisotropy; and τ_F and τ_r are the fluorescence decay and rotational relaxation times, respectively. τ_r and r_0 can be recovered by fitting of each polarization decay.

2.4.2 Anisotropy Measurements

Anisotropy decay data were recorded using the PicoQuant MicroTime 200 confocal microscope described above (PicoQuant GmbH, Berlin, Germany). The SNAP-Surface 546 dye and the SNAP-tag labelled with SNAP-Surface 546 dye were measured at concentration of ≈ 100 pM in PBS buffer (pH 7.2). The fluorophores were excited by vertically polarized pulsed diode laser (530 nm, LDH-P-FA-530, PicoQuant). Fluorescence emission signal was filtered by a band pass filter (HQ590/70)

and an emission dichroic (620DXXR). Micro Photon Devices (MPDs) were used to collect the emission light.

The emission light was split by a polarization beam splitter into vertical I_{VV} and horizontal I_{VH} components and their fluorescence decays were analyzed as vertical and horizontal decays independently. The anisotropy (r) was determined from these decays as a function of time [3]. The VV and VH decays from A546 fluorophore and bound A546 to the SNAP-tag were fitted with a double exponential fit function convolved with an appropriate IRF using 2.22 and 2.23 equations. τ_F was the lifetime of A546 in solution, applied as a fixed value (equal to 3.9 ns) during fitting.

Chapter 3

Materials and Methods

3.1 Polyproline constructs

Polyproline (PP) of varying lengths were used as linkers between a SNAP-tag (S) and a CLIP-tag (C) (Figure 3.1). In the following sections, the preparation of PP constructs are described.

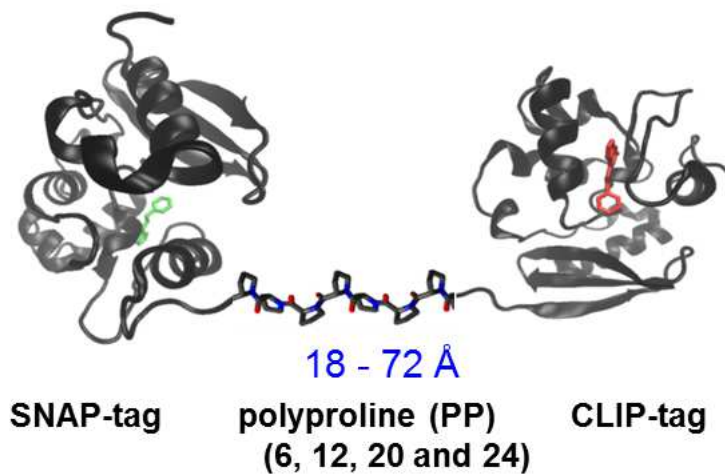


Figure 3.1: Cartoon representation of the SNAP-PP-CLIP construct (SNAP-tag PDB code: 3KZY).

S-PP-C plasmids were prepared by substituting the PP linker (6, 12, 20, and 24 residue PP) for the Nbp2 gene (744 bp) in pET51b-S-Nbp2-C (Nbp2 vector). The Nbp2 vectors were double digested using BamHI and XhoI (Promega, Mannheim, Germany) by incubating for 1 h at 37 °C. The digested vectors were loaded onto a

1.5% agarose gel. After running the gel, two separate bands were observed. One of them corresponded to the Nbp2 gene (744 bp), while the other corresponded to the linearised vector without the Nbp2 gene. The linearised vector band was cut and extracted from the agarose gel with a Gel Extraction Kit (Promega, Mannheim, Germany) (Figure 3.2). Complementary DNA single strands coding for four different lengths of PP (6, 12, 20 and 24-residue) (Biomers, Ulm, Germany) were ordered and annealed in annealing buffer (10 mM Tris-HCl, 50 mM NaCl, 1 mM EDTA, pH 7.5) by incubating at 95 °C for 3 min and cooled to room temperature over 1 h. The sequences of the PP oligonucleotides are listed in Table A.2. The linearised vector and the PP oligonucleotides were ligated using the Quick Ligation™ Kit (New England Biolabs, Frankfurt am Main, Germany) for 30 min at room temperature. Chemically competent *Escherichia coli* (*E. coli*) XL1-Blue cells were transformed with the ligated plasmids and screened by plating on agar plates (75 mg/ml Ampicillin (Amp)) and incubated overnight at 37 °C. Plasmids from single colonies were cultured in 5 ml of 2YT-medium containing 75 mg/ml Amp and purified using PureYield™ Plasmid Miniprep System (Promega, Mannheim, Germany) for further screening procedures.

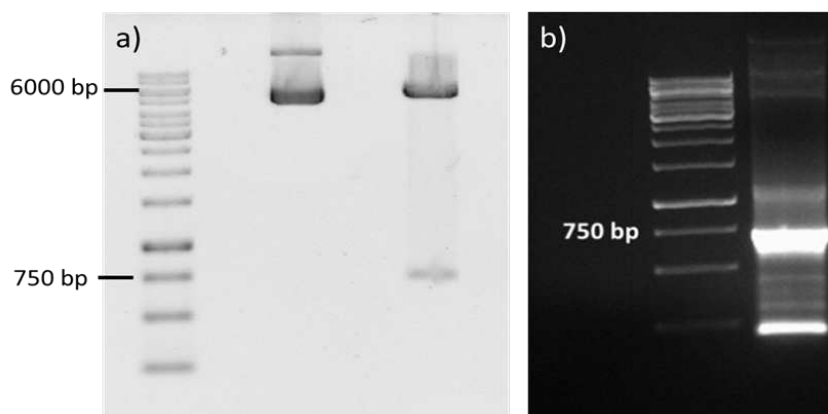


Figure 3.2: linearisation of the Nbp2 vector and amplified SNAP-6PP-CLIP gene. a) linearisation of the Nbp2 vector. In the electrophoresis gel, the lanes from left to right: Marker (GeneRuler 1kb DNA, Fermentas), non-cleaved vector, and cleaved vector. b) Electrophoresis gel of a PCR screen for the 6-residue PP construct (primers: T7-981079 and PP-CLIP-tag, Table A.2).

PP linker insertions were screened by PCR and restriction enzyme digestion. For PCR screening, a forward and a reverse primer (T7-981079 and PP-CLIP-tag, Table A.2) were used to amplify the SNAP-tag to the end of the 6PP linker inside the selected vector (Figure 3.3). The presence of an amplified fragment of the vector confirmed the insertion of the PP gene between the snap- and clip-

tags. In addition to PCR screening, selected constructs were analysed by double restriction enzyme digestions using XbaI and XhoI to check for the presence of DNA fragments at the expected sizes (Figure 3.3). Finally, screened vectors were sequenced by GATC BIOTECH (Köln, Germany). The same preparation process was performed for the 12-, 20- and 24-residue PP constructs.

To express the PP constructs in yeast cells, we subcloned them into the pRS313-MET3 yeast expression vector. The pRS313-MET3 vector was linearised using the NotI/ApaI sites, and the amplified PP constructs were ligated as described above. All primers were purchased from Integrated DNA Technologies (IDT, Leuven, Belgium). For validation, we repeated the screening procedures described in the previous section (PCR and restriction digest screening).

3.1.1 Preparation of the S-PP-C Plasmid for Expression in Yeast cells

A yeast expression vector was prepared by subcloning the S-PP-C gene from the pET51b-S-PP-C vector into the pRS313-MET3 vector between ApaI and NotI sites according to the protocol described in the previous section (Figure 3.4). The target gene was amplified from the pET51b-S-PP-C vector using two primers (NotI-pRS313 F and ApaI-pRS313 R) listed in Table A.2.

3.2 15 Amino Acid Construct and 15 Amino Acid (15 aa) Peptide

The 15 aa construct (SNAP-15 aa-CLIP) was a gift from our project collaborator, Prof. N. Johnsson (Institut für Molekulare Genetik und Zellbiologie, Universität Ulm, Germany). The 15 aa peptide was commercially synthesized and labelled with Alexa Fluor 546 (A546) and Alexa Fluor 647 (A647) on both ends by the Peps4LS GmbH Company in Heidelberg, Germany (Figure 3.5).

3.3 CaM Construct

3.3.1 Preparation of the S-CaM-C Plasmid for Bacterial Expression

The SNAP-CaM-CLIP (S-CaM-C) containing vector (pET-51b-S-CaM-C) was prepared by substituting the CaM gene (447 bp) for the Nbp2 (744 bp) gene in the Nbp2 vector. Procedures described in section 3.2.2 were followed with the exception that the inserted CaM gene was PCR amplified from the Yellow Cameleon 3.6 vector (AAV-6PSEW-YC3.6) using two primers (XhoI-CaM R and BamHI-CaM

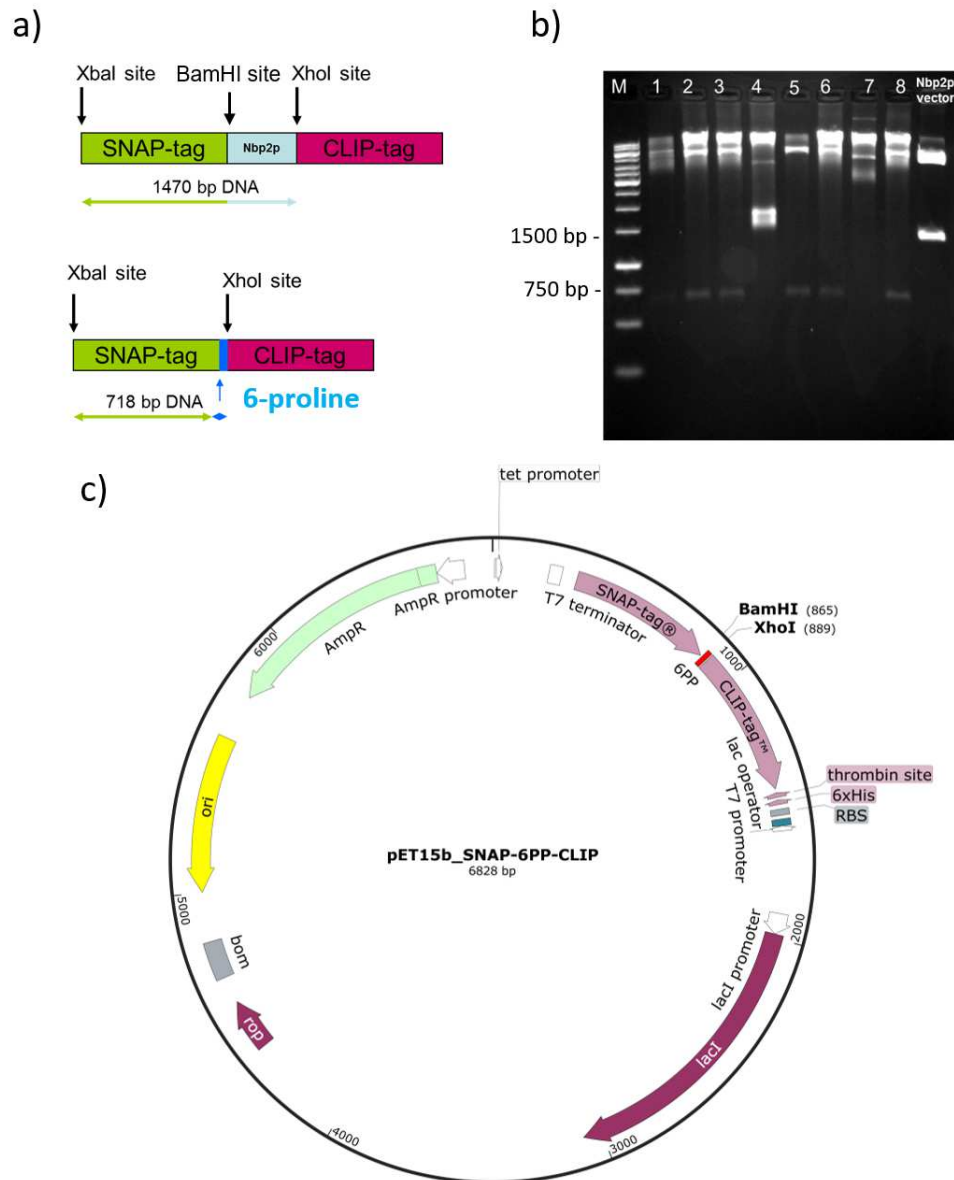


Figure 3.3: Restriction enzyme screening of the 6PP construct. a) Schematic design of restriction enzyme screening. XbaI and XhoI restriction enzymes were used to digest both constructs shown. The size of the cut-out gene is longer for the Nbp2 construct than for the 6-residue PP. b) Eight purified plasmids were digested by restriction enzymes and ran in 1.5% agarose gel. First lane: 1kb ladder, lanes 1-8: purified plasmids from different colonies, last lane: negative control (Nbp2 construct). Samples in lanes 2, 3, 5, 6, 8 show the presence of an expected ≈ 750 bp band. The lowest band in the negative control lane (Nbp2 vector) is at ≈ 1500 bp. c) The vector map of pET51b-SNAP-6PP-CLIP.

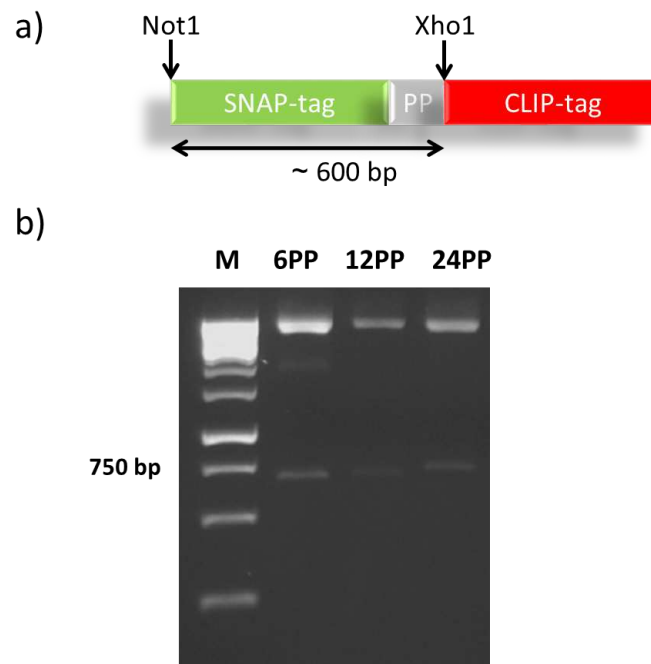


Figure 3.4: Restriction enzyme screening for the S-PP-C gene in the pRS313-MET3 vector. a) Schematic of the restriction sites of the S-PP-C gene in the pRS313-MET3 vector. b) Gel electrophoresis of double-digested plasmids (S-6PP-C, S-12PP-C, S-24PP-C) in 1.5% agarose gel. The second band from the top is at ≈ 600 bp, which is the expected size for the digested construct (lanes 2-4).

F, Table A.2). Schematic representations of these proteins and the final vector map are depicted in Figure 3.6.

3.3.2 Preparation of the S-CaM-C Plasmid for Yeast Cell Expression

The yeast expression vector containing the S-CaM-C gene (pRS313-MET3-S-CaM-C) was prepared by subcloning the S-CaM-C gene from the pET51b-S-CaM-C vector into the pRS313-MET3 vector between *Apa*I and *Not*I restriction sites following the protocol described in the previous section (Figure 3.7). The target gene was amplified from the pET51b-S-CaM-C vector using two primers (*Not*I-pRS313 F and *Apa*I-pRS313 R, sequences given in Table A.2).

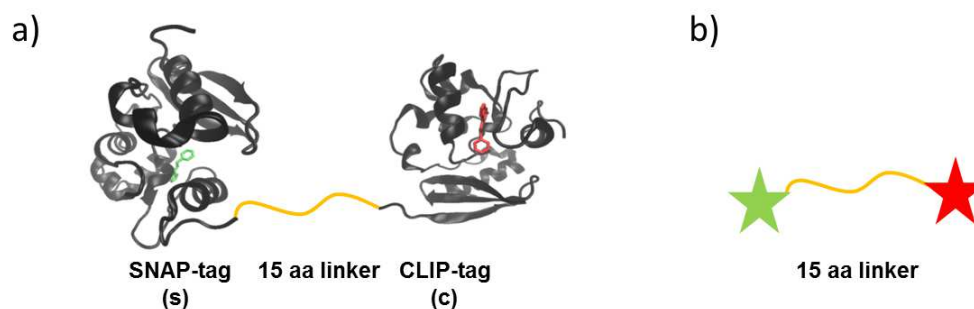


Figure 3.5: Cartoon representations of the 15 aa construct and the 15 aa peptide. a) SNAP-15 aa-CLIP (S-15 aa-C, sequence GRLEVLFQGPKAFLE) construct. b) 15 aa peptide (sequence: GRLEVLFQGPRAFLC). The green and red stars present A546 and A647 fluorescent dyes, respectively. (SNAP-tag PDB code: 3KZY)

3.4 Nbp2 Constructs

The Nbp2 constructs (S-Nbp2-P and S-Nbp2-SH3-C) and peptide constructs (S-Bck1, S-Pbs2, S-Cla4 and S-Ste20) in bacterial vector pET-51b were gifts from our project collaborator, Prof. N. Johnsson. Figure 3.8 depicts schematic representations of the proteins used in the Nbp2 study described in Chapter 4.1. The Nbp2 protein and the Nbp2-SH3 domain are fused between the SNAP-tag (N-terminus) and the CLIP-tag (C-terminus). The peptides also each has a SNAP-tag (N-terminus), but they are not labeled with a fluorophore during our measurements. All constructs have a hexa-histidine-tag on the C-termini.

3.5 Expression and Purification of Recombinant Proteins

All constructs including S-Nbp2-C, S-Nbp2-SH3-C, S-PP-C, S-15aa-C and S-CaM-C in the bacterial expression vector were transformed and expressed in chemically competent *E. coli* cells (BL21-DE3). 100 ml of an overnight culture was added as a starter to 5 L of Lysogeny Broth (LB) medium and grown to an Optical Density (OD) at 600 nm (OD600) of 0.6-0.8 at 37 °C at 220 rpm. The cell culture was induced by adding Isopropyl- β -D-thio-galactoside (IPTG) to the final concentration of 1 mM and grown overnight at 18 °C at 160 rpm. The cells were harvested by centrifugation at 5,000 g for 20 min (SIGMA 4-16K, 13350 rotor, Newtown, UK) at 4 °C. The cell pellet was re-suspended in 15 ml of the lysis buffer and incubated for 30 min on ice. The re-suspended solution was sonicated (5% pulsation and 85% amplitude; Bandelin Sonoplus, Berlin, Germany) for a total of 16 min with

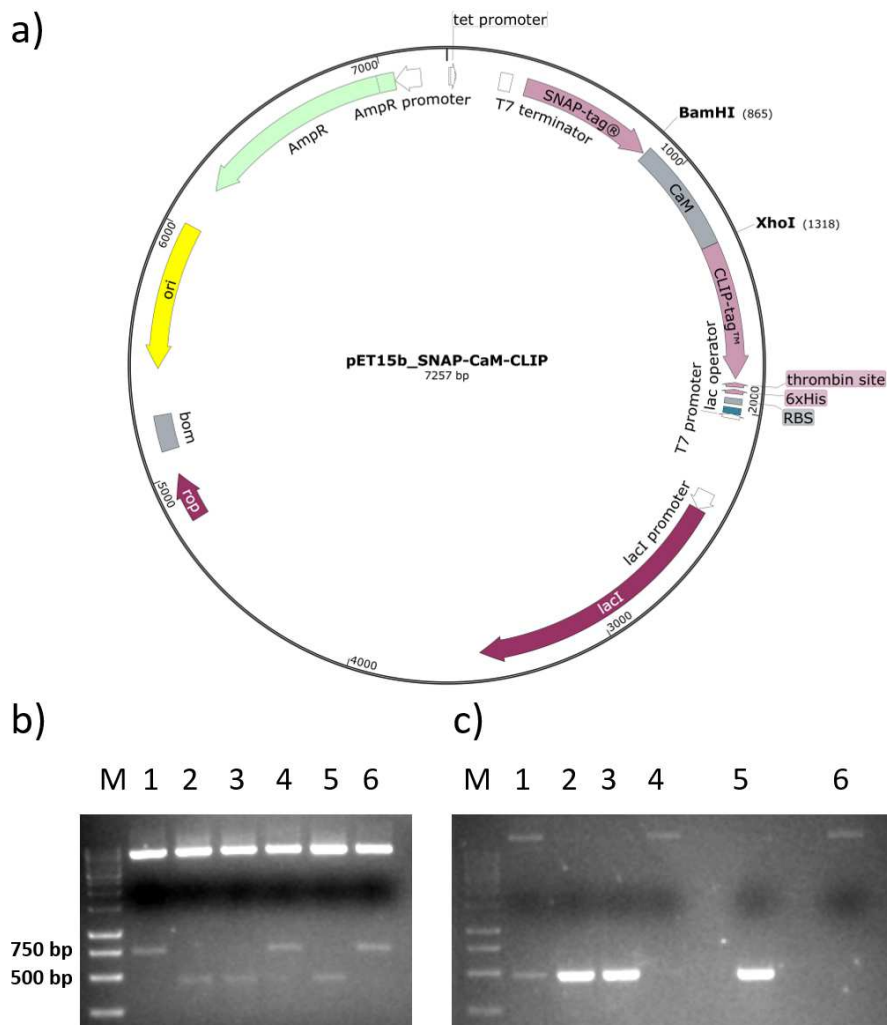


Figure 3.6: S-CaM-C expression vector preparation. a) The vector map of the SNAP-CaM-CLIP construct. b) An example of a restriction enzyme screening for six colonies ran in a 1.5% agarose gel. S-CaM-C constructs were doubly digested with the BamHI and XhoI enzymes. Samples in lanes 2, 3 and 5 showed the band near 500 bp marker, which is expected size for CaM. c) The gel result for PCR screening for the same six plasmids used for the double digest screening. Samples in lanes 2, 3 and 5 presented a clear positive band for CaM. Colony 1 also showed a very faint band at about 500 bp. M: Marker (GeneRuler 1 kb DNA Ladder, Fermentas).

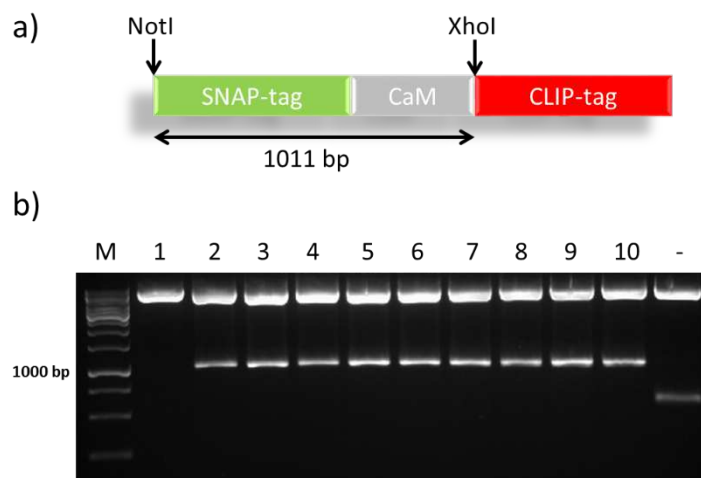


Figure 3.7: S-CaM-C yeast cell expression vector preparation. a) Schematic of the restriction sites of the S-CaM-C gene in the pRS313-MET3 vector. b) Restriction enzyme screening for the S-CaM-C gene in the pRS313-MET3 vector. Doubly digested plasmids (lanes 1-10) ran in 1.5% agarose gel. The second band from the top shows the expected size (≈ 1000 bp) of the digested construct (lanes 2-10). The last lane marked by "-" corresponds to the pRS313-6PP construct, which was ran as a negative control.

a 5 min break every 2 min. The lysate was centrifuged at 20,000 g for 20 min at 4 °C. Next, the supernatant of the centrifuged lysate was loaded to the His-tag column (6 ml Profinity IMAC resin, Bio-Rad, Munich, Germany) attached to a Fast Protein Liquid Chromatography (ÄKTAexplorer 10, GE Healthcare, Munich, Germany) system. Prior to loading, the column was washed with 5 column volumes of the washing buffer with a flow rate of 2 ml/min. The protein was eluted by running a linear gradient (0-100%) with the elution buffer over 30 min with a flow rate of 2 ml/min. The imidazole from eluted protein aliquots was removed by exchanging the buffer with Phosphate-Buffered Saline (PBS) using Vivaspin 20 centrifugal concentrator. The purities of all protein aliquots were checked using 4-20% polyacrylamide SDS Polyacrylamide Gel Electrophoresis (SDS-PAGE) gels and the concentrations of protein stock solutions were quantified by absorbance spectroscopy. Finally, glycerol was added to the protein solutions to a final concentration of 25%. The solutions were flash frozen with liquid nitrogen and stored at -80 °C. The protocol of all prepaid buffers are listed in Table A.1.

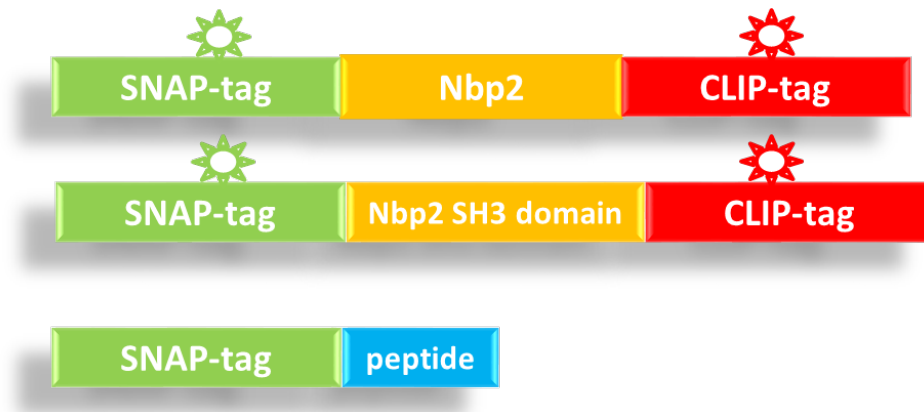


Figure 3.8: Schematic representations of full-length Nbp2, the Nbp2-SH3 domain and peptides. The SH3 domain and full-length Nbp2 protein include snap- and clip-tags labeled by fluorophores (green: donor dye and red: acceptor dye).

3.5.1 Bacterial Cell Transformation

Transformation of all plasmids into chemically competent bacterial cells was completed according to the following procedure. First, an aliquot of the competent cells was thawed on ice. 100 ng of the plasmid was added to 500 μl competent cells and kept on ice for 30 min. After the incubation, the mixture was heat shocked by incubating in a 42 $^{\circ}\text{C}$ water bath for 45 s and immediately transferred back into ice for 5 min. Then, 700 μl of pre-warmed LB medium was added to the competent cell solution, and cells were cultured at 37 $^{\circ}\text{C}$ at 220 rpm for 1 h. Finally, between 50-200 μl of cell suspension was plated on a LB agar plate with an appropriate antibiotic and incubated at 37 $^{\circ}\text{C}$ overnight.

3.5.2 Yeast Cell Transformation

Yeast cells from frozen stock were inoculated in 5 ml of YPD medium and grown at 30 $^{\circ}\text{C}$ at 200 rpm overnight. The overnight culture was added to 50 ml YPD medium (OD600 = 0.3-0.4) and grown to a density OD600 of 0.6-0.8 at 30 $^{\circ}\text{C}$ at 160 rpm. The culture was centrifuged for 5 min at 1,000 g, and the supernatant was discarded. The remaining pellet was re-suspended in 25 ml sterile H_2O and centrifuged at 15,700 g for 15 s. The supernatant was removed and the cell pellet was re-suspended to a final volume of 500 μl with 100 mM LiAc/1x TE buffer. Cells were aliquotted (100 μl each) and incubated on ice for 2 h. Extra aliquots were stored at -80 $^{\circ}\text{C}$ without adding glycerol and were used within the next 2

weeks for additional transformations [58].

An aliquot of the cell suspension was centrifuged for 1 min at 1,000 g, and the supernatant was discarded. The transformation mixture, consisting of 240 μl PEG3000 (50% (w/v)), 36 μl 10x 1 M LiAc and 15 μl stock solution of heated salmon sperm DNA, was prepared and vigorously mixed. 45 μl of the plasmid (total $\approx 4.5 \mu\text{g}$) was added to the mixture, which was re-suspended with the cell pellet for 15 s. The cell mixture was incubated for 30 min at 30 °C in a Thermomixer at 1,400 rpm. The cell suspension was heat shocked at 42 °C in the water bath for 20 min and was then placed on ice for 1 min. Following this, the supernatant was removed by centrifuging for 15 s at 15,700 g. The cell pellet was re-suspended in 100 μl H₂O and plated on 1.5% agarose without histidine (Synthetic Defined (SD)-His medium for the selection). After 2 days of incubation at 30 °C, isolated colonies became visible and used for further experiments.

3.6 Yeast Cell Labelling

3.6.1 Fixed Cell Labelling

To label snap- and clip-tags inside yeast cells, cultured yeast cells were re-suspended in 100 μl Lyticase digestion solution at 30 °C for 30 min. After incubation, cells were washed by adding 900 μl PBS buffer and centrifuged for 5 min at 4 °C at 1,306 g. This step was repeated twice, and cell pellets were suspended in a ratio of 1:20 (v/v) in PBS buffer. Then, 10 μl of re-suspended cells were spotted on polylysine coated slides (prepared according to the manufacturer's instruction, Sigma Aldrich, Munich, Germany) and left for 20 min. The cells were washed twice with PBS buffer (20 °C) and fixed in MeOH for 5 min at -20 °C, followed by acetone for 20 min at -20 °C. The fixed cells were dried overnight at room temperature. The next day, cells were washed twice with PBS (4 °C) and then incubated for 15 min in PBS buffer with 0.1% (w/v) Triton X-100. The block solution (2% BSA (w/v), 0.1% Tween 20 (w/v) in PBS) was added to the cells and incubated for 1 h at room temperature to avoid non-specific binding. Next, the block solution was removed and the cells were incubated with permeable SNAP and CLIP dyes diluted in the block solution for 1 h at room temperature. The cells were then washed 3 times for 5 min each time in PBS buffer containing 0.1% Triton X-100 (w/v) at room temperature. Finally, the cells were washed again with PBS (4 °C) for 15 min and stored with PBS at 4 °C before imaging [25, 59].

3.6.2 Live Cell Labelling

Yeast cells stably transformed with the pRS313-MET3-S-CaM-C construct were grown in 5 ml of SD-medium, devoid of histidine and methionine, at 30°C overnight. The overnight culture was centrifuged for 5 min at 1,500 g to remove the medium. The cell pellet was re-suspended in 50 ml of freshly warmed histidine-lacking SD-medium with 70 μ M methionine and grown to an OD600 of 0.8. After this, the cells were collected by centrifuging for 5 min at 1,500 g, and the cell pellet was incubated with SNAP-Cell 430 and CLIP-Cell™ TMR-Star dye solutions (5 μ M of each dye in 100 μ l of warmed histidine-lacking SD-medium) for 30 min at 30 °C. Cells were subsequently centrifuged and the supernatant was removed. The cell pellet was re-suspended in fresh SD medium and was kept at 30 °C for another 30 min to further remove free dye. Labelled cells were diluted and sealed between a microscope slide (25 mm x 75 mm) and a coverslip (24 mm x 32 mm, #1.0) using Wirozil duplicating silicone (BEGO, USA). The prepared cell chamber was imaged under the microscope from the coverslip side.

3.7 Labelling Proteins *in vitro*

All purified constructs including PP, CaM, 15 aa, Nbp2-SH3 and full length Nbp2 were labelled with both SNAP-Surface® Alexa Fluor®546 (A546) and CLIP-Surface™ 647 (DY647) dyes (NEW ENGLAND BioLabs, Frankfurt am Main, Germany) in a 1:2 ratio (protein:dye, 2.5 μ M:5 μ M in 500 μ l of buffer) in PBS buffer, pH 7.4, with 1 mM Dithiothreitol (DTT) by incubating at room temperature for 1.5 h. The dyes covalently bind to the reactive cysteines of the snap- and clip-tags. Following the incubation step, labelled proteins were separated from free dyes using a NAP5 column (GE Healthcare, Munich, Germany) and concentrated by Vivaspin® Centrifugal Concentrators (Invitrogen, Darmstadt, Germany) or by a Bio-Spin 6 column (Bio-Rad, Munich, Germany) according to Ref. [12] but omitting the concentrating step.

After labelling, the absorbance of the protein solution was recorded to determine the concentration and the labelling efficiency with a commercial spectrometer (Cary 100 Scan, Varian/Agilent Technology, Santa Clara, USA or NanoDrop 2000c, Thermo Scientific, Wilmington, USA). The theoretical extinction coefficient at 280 nm based on the protein sequence (PortParam tool, <http://web.expasy.org/-protparam/>) and the specific extinction coefficient of the dyes were used to calculate the protein concentration and labelling efficiency of dyes on protein (Table A.3 & Table A.5).

3.8 Ensemble Fluorescence Measurements

We measured the ensemble FRET signal (fluorescence emission of the acceptor achieved upon donor excitation) of all labelled constructs on a Fluorolog-3 spectrofluorometer (Horiba Jobin Yvon Inc., Edison, NY) prior to smFRET measurements. Fluorescence spectroscopy was used to examine the binding affinities of CaM and the Nbp2-SH3 domain constructs with their ligands. The labelled CaM construct was incubated with different concentrations of Ca²⁺ or M13 peptide, and fluorescence spectra were measured for each Ca²⁺ or peptide concentration. A546 and DY647 were used as donor and acceptor, respectively. The excitation wavelength of 532 nm was used to excite the A546 dye, and fluorescence spectra were detected from 545 to 750 nm with a slit width of 5 nm. Each set of fluorescence spectra was normalized to the peak intensity of the donor at 571 nm.

3.8.1 Single-Molecule Detection with Confocal Microscopy

Single-molecule FRET (smFRET) measurements of labelled snap- and clip-tags constructs (15 aa, PP and CaM) were carried out on a custom-build confocal microscope based on a Zeiss Axiovert 135 TV (Figure 3.9). The donor and acceptor dyes were excited by a 532 nm diode-pumped solid state laser (Excelsior 532-100-SLMCDRH, Spectra Physics, Santa Clara, CA) at a power of 43 kW cm⁻² and the 640 nm line at 110 kW cm⁻² of another solid-state laser (DL 638-100, CrystaLaser, Reno, NV), respectively, in Alternating-Laser Excitation [52] (ALEX) mode. The excitation was switched between the two lasers by an acousto-optical tunable filter (AOTF, AOTFnC-400.650-TN, AA Opto-eletronic, Orsay, France) at a frequency of 10 kHz with a duty cycle of 70% for the donor excitation and 30% for the acceptor excitation. Data collected within the first 5 μ s after each excitation switching were discarded to avoid temporal crosstalk between laser excitations.

The laser beams were transmitted into the AOTF and the microscope body. The sample stage was equipped with a piezo drive (Model: P-731.20, Physik Instrumente GmbH & Co. KG, Karlsruhe, Germany) to move the slide in the lateral plane. The fluorescence emission from the sample was collected by the objective (C-Apochromat 63x/1.2 W, Zeiss). Thereafter, it was passed through the Acousto-Optical Beam Splitter (AOBS) and then through lens L1 ($f_1 = 125$ mm) to refocus the fluorescence emission at the confocal pinhole, P. The pinhole was used to filter out the light from non-focal planes. The lens L2 ($f_2 = 200$ mm) projected the emission light on two detectors. The fluorescence emission from the donor and the acceptor were separated by a dichroic mirror (HQ640DCXR, AHF, Tuebingen, Germany) between lens L2 and the detectors. Appropriate bandpass fluorescence filters (550 – 610 nm for the donor and 650 – 750 nm for the acceptor channel) were also used to reduce the spectral crosstalk (Figure 3.10). Filtered

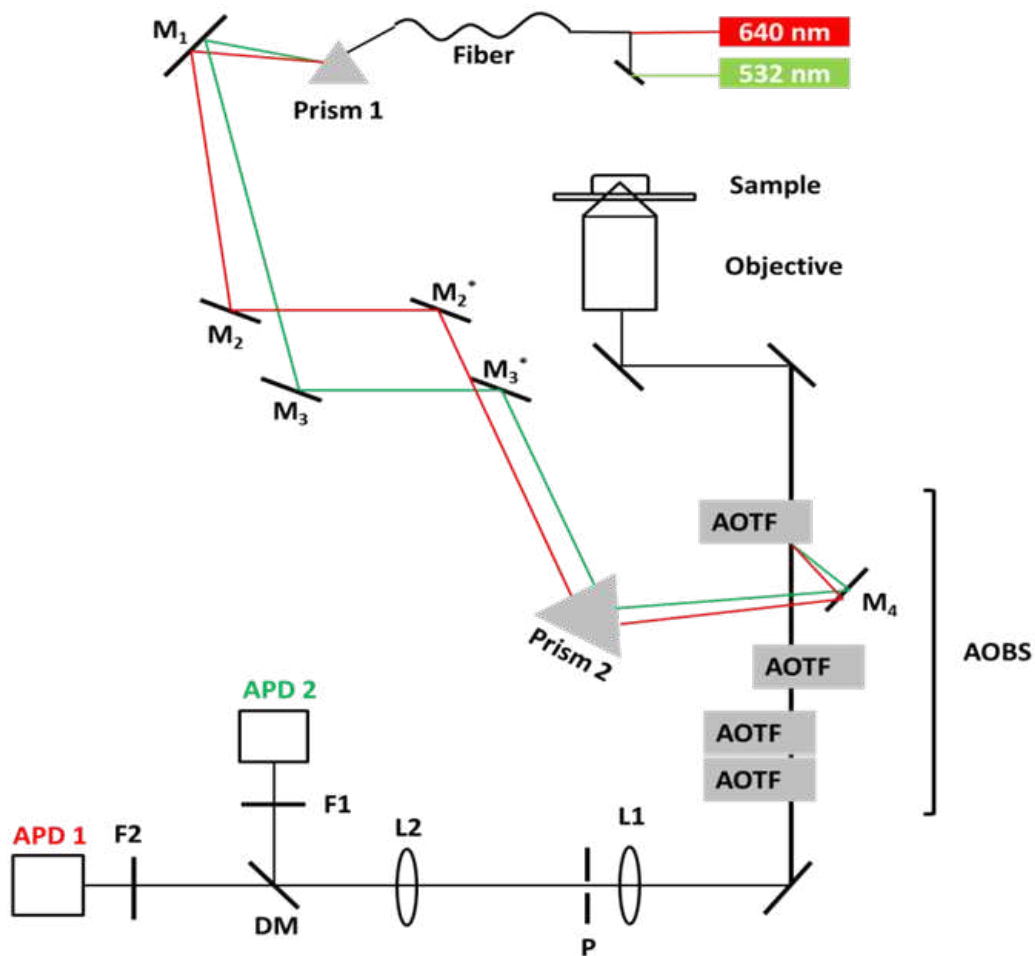


Figure 3.9: Construction of the confocal microscope. Two lasers are coupled to a fiber leading to the excitation beam path of the microscope. Through a prism, the excitation beams are spectrally separated and distributed to the mirror M_1 in two different beam paths. In each of these beam paths, there are two sets of mirrors (M_{2-3} and M_{2-3}^*), which allows the adjustment of two beams for a maximum overlap of excitation volumes. With prism 2, the beams are recombined and reflected into an AOTF via mirror M_4 and into the objective lens. The collected fluorescence light is separated from the excitation light by the AOBS, passed through the pinhole P, separated by a dichroic mirror (DM), filtered by bandpass filters F1, F2 and finally detected by APDs. L: Lens, M: Mirror, F: Filter [60].

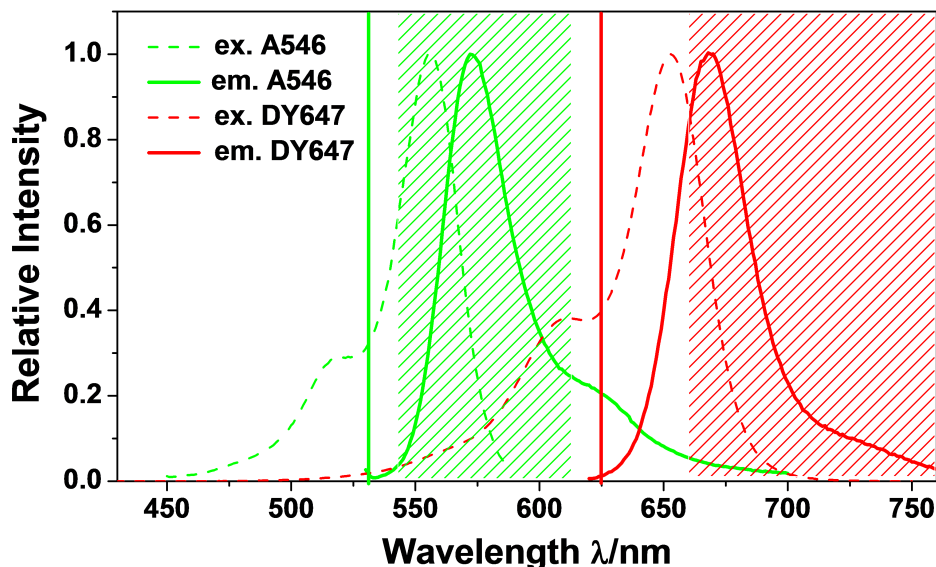


Figure 3.10: Excitation and emission spectra for the A546-DY647 dye pair is presented by dashed and solid lines, respectively. The Tetramethylrhodamine (TMR) dye has excitation and emission spectra that are similar to those of the A546 dye. The green and red hatched areas represent the filter set used in the smFRET experiment setup. The excitation wavelengths are shown as green and red vertical lines at 532 nm (donor) and 635 nm (acceptor).

photons were detected by two avalanche photo diodes (APDs) (SPCM-CD 3017, PerkinElmer, Boston, MA) and counted with a data acquisition card (NI PCI-6229, National Instruments, Munich, Germany). The detector alignments were done using reference solutions (donor channel: 50 nM Rhodamine 6G; acceptor channel: 50 nM Alexa Fluor 647).

The PP, the CaM, the 15 aa constructs and the 15 aa peptide were dissolved in 50 mM Tris-HCl, 300 mM NaCl buffer at pH 7.4, 2 mM ascorbic acid (Sigma Aldrich, St. Lois, MO, USA), and 2 mM methyl viologen (Sigma Aldrich, St. Lois, MO, USA) were used as a reducing and oxidizing system (ROXS) for triplet states depletion from the sample solution to retain the brightness of the fluorescent dyes. 0.001% of Tween 20 as a non-ionic surfactant was used to avoid non-specific adsorption of proteins on the glass surface.

A glass coverslip (24 x 32 mm, Menzel, Braunschweig, Germany) was flamed and sealed by a piece of Parafilm with a cut-out hole (Sigma Aldrich, roll size 4 in. x 125 ft, St. Lois, MO, USA) (Figure 3.11). The hole was washed three times with pure water and once with buffer solution. Then, 50 μ l of the prepared

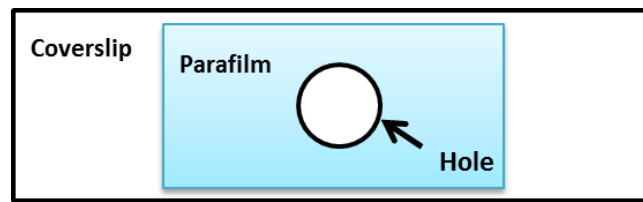


Figure 3.11: Schematic of the sample holder.

protein solution was loaded into the hole. The coverslip with the sample solution was placed over the objective lens inside a chamber, which was filled with nitrogen gas to reduce the amount of dissolved oxygen in the sample buffer. The sample was kept for 5 min in the closed chamber to reduce the oxygen concentration prior to the measurement [54].

Chapter 4

Results and Discussion

4.1 Protein Peptide Interaction Study

The relationship between the conformations of the protein and its function is of a great interest in understanding a wide array of biological processes, such as signal transduction, viral entry, molecular trafficking and vesicular transport [61]. There are a number of physical techniques that can investigate the conformational changes of proteins, such as nuclear magnetic resonance, electron paramagnetic resonance, FRET and tryptophan fluorescence [62, 63, 64]. However, the conformation of a protein is sensitive to its local environment and could be different *in vitro* or inside the cell. Most of these techniques can be performed *in vitro*, hence the real cellular information is lost. Furthermore it is interesting to know that the local environment for a protein varies depending on the subcellular localization, and the conformational state could drastically change upon receiving these stimuli. A technique which measures PPI must take this into account.

FRET method and genetically encoded sensors are implemented to observe real-time protein conformation changes. This class of biosensor undergoes a large conformational change upon binding an appropriate ligand and subsequently modulates the fluorescence signal. The FRET approach has been conventionally used to study the local concentration of the ‘ligand’ that binds the target protein, rather than the ‘conformation’ of the protein itself. While genetically fused fluorescent proteins are widely popular, improvements are desired on their photostability and emission wavelengths to reduce the overlap with the autofluorescent background from the host cell.

Our overall goal is to develop the next generation of sensors that would utilize more stable fluorescent probes and are capable of studying the conformational state of proteins inside the cell. As a first step, *in vitro* bulk FRET measurements of the conformational changes of the yeast protein Nbp2-SH3 and full length Nbp2 genet-

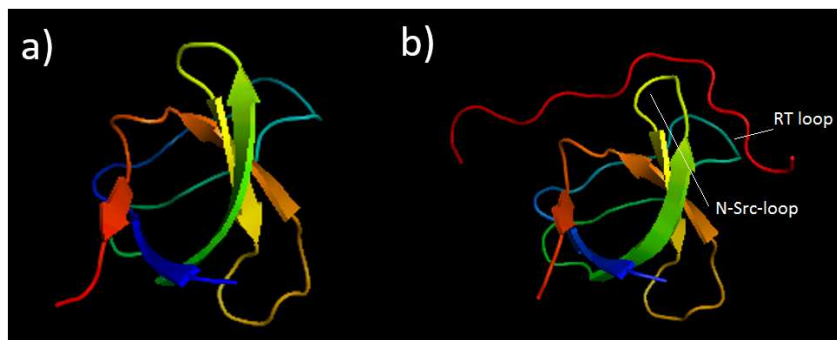


Figure 4.1: Structure of Nbp2-SH3 domain and Nbp2-SH3-Ste20 complex. (a) The Nbp2-SH3 domain crystal structure (rainbow, PDB code 1YN8). (b) The Nbp2-SH3 domain (rainbow) in complex with the Ste20 peptide (red, PDB code 2LCS).

ically fused to the SNAP-tag and CLIP-tag (S-Nbp2-SH3-C and S-Nbp2-C) has been performed. The interaction of four different peptides (Pbs2p, Bck1p, Ste20p and Cla4p) with S-Nbp2-SH3-C and S-Nbp2-C protein constructs was investigated based on the conformational change of Nbp2-SH3 or Nbp2 proteins. The feasibility and limitations of the use of these tags to investigate these conformational states are critically evaluated through these experiments.

4.1.1 Bulk FRET Measurements to Study Nbp2-SH3 Domain-Peptide Interactions

The interactions of dual-labeled Nbp2-SH3 with different peptides (Pbs2p, Bck1p, Ste20p and Cla4p) were studied using the FRET assay. The binding of a peptide to the Nbp2-SH3 domain is assumed to induce major conformational changes in RT loop and N-Src-loop in the peptide binding region (Figure 4.1). The structure of Nbp2-SH3 domain in complex with Ste20 peptide displays a similar folds with typical SH3 domain (PDB code 1YN8) except at the peptide binding region [65].

To study the peptide dependent conformational change of Nbp2-SH3 domain (S-Nbp2-SH3-C), we recorded the fluorescence emission spectra as a function of peptide (Pbs2-S and Ste20-S) concentrations (Pbs2: Figure 4.2a; Ste20: Figure 4.3a). Upon addition of either Pbs2-SNAP or Ste20-SNAP, we observed a decrease in the FRET efficiency (i.e., decrease of acceptor emission and the anticorrelated increase of the donor fluorescence emission). We assumed that the interacting peptide changed the conformation of S-Nbp2-SH3-C domain in a way that the distance between the donor and the acceptor dyes increased. The snap- and clip-

tags on the Nbp2-SH3 domain and SNAP-tag on the Ste20 peptide may affect the affinity between SH3 domain and peptide, unlike the known conformational change in Nbp2-SH3 domain in complex with Ste20 peptide [29]. The conformation of Nbp2-SH3 domain may also be affected by snap- and clip-tags. An increase in the distance between two dyes (by conformational change) decreases the FRET. Surprisingly, no change in the fluorescence signal was observed upon addition of Cla4 or Bck1.

To quantify the effective binding affinity, K_d , of the peptide to induce a conformational change on Nbp2-SH3, we plotted the mean acceptor fluorescence signals from the normalized spectra as a function of peptide concentrations (Figure 4.2c and Figure 4.3c). The binding affinities given by Hill function fitting were 122 ± 35 nM (n: 2.3 ± 0.50) and 37 ± 5 nM (n: 1.3 ± 0.01), for Pbs2 and Ste20, respectively. The concentration of Nbp2-SH3 was 5 nM. The Hill coefficients higher than 1 describe positive cooperative binding.

Similar measurements were previously done by Davidson and colleagues [29] using tryptophan fluorescence to detect the binding affinity between a Nbp2-SH3 domain (residues 110-172) and the same set of peptides. Their proteins did not contain any SNAP-tag nor CLIP-tag. Table 4.1 shows the comparison of the binding affinities of Davidson's results, $K_d - D$, and our binding affinities, K_d . While Ste20 showed higher affinity as compared to Pbs2 in both measurements, Davidson's results show about one order of magnitude higher values. We expected lower affinity between the Nbp2-SH3 domain and peptides in comparison to Davidson's results due to snap- and clip-tags in the protein and peptide structure. There are several possible reasons for these differences. The most obvious reason may be a change of the protein activity introduced by large terminal tags. In the current construct, the core SH3 domain (13 kD) and all peptides were tagged to relatively large (20 kD each) tags. Another possible cause for the difference, particularly for Cla4 and Bck1, where we do not observe any change of the FRET efficiencies, is that the binding of these peptides does not induce any conformational change of the SH3 domain or not enough to see a change. The tryptophan fluorescence assay detects the binding by the change of native tryptophan's local environment, while, our assay detects the change in the distance between two fluorophores as a result of the conformational change. The fact that our current construct lacks other peripheral domains, may play a role in the conformational change and could also contribute to this discrepancy. We tested the binding of the peptides to Nbp2-SH3 using the tryptophan fluorescence assay, but were unable to observe a significant difference in the signal so as to measure the binding. This could most likely be caused by the SNAP-tag and CLIP-tag themselves containing four tryptophans and hence reducing the signal to noise ratio.

To rule out the effect due to the absence of peripheral domains, we prepared

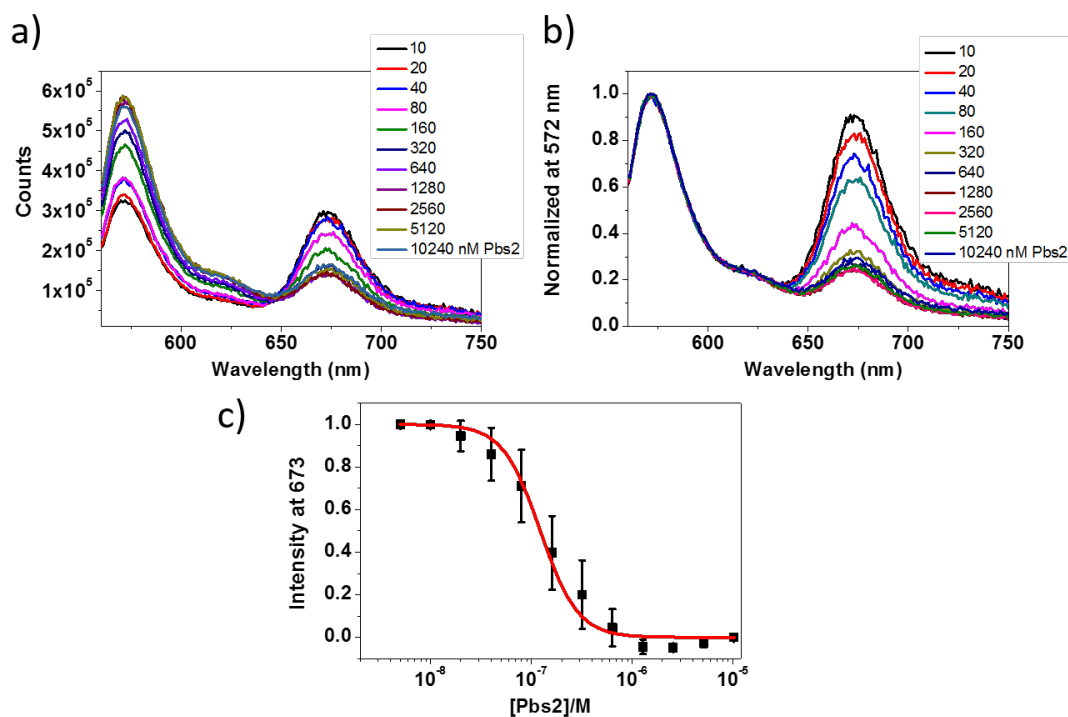


Figure 4.2: Bulk fluorescence measurements of Nbp2-SH3 with Pbs2 peptide. a) Raw fluorescence spectra of labeled Nbp2-SH3 (5 nM) with Pbs2 at different concentrations (0 to 10.24 μM). b) Raw fluorescence spectra was normalized at 572 nm to show trend in different concentration (FRET). c) Data represent the average of acceptor fluorescence signals from the normalized spectra at 673 nm plotted as a function of the peptide concentration. The error bars denote standard deviation of these sets.

Table 4.1: Comparison of Nbp2-SH3 binding affinities

Peptides	Current Results (K_d) (μM)	Tryptophan Fluorescence Results (K_d -D) (μM) [61]
Ste20	0.037 ± 0.005	0.20 ± 0.01
Pbs2	0.12 ± 0.04	3 ± 0.30
Cla4	Not detected	0.65 ± 0.09
Bck1	Not detected	0.81 ± 0.15

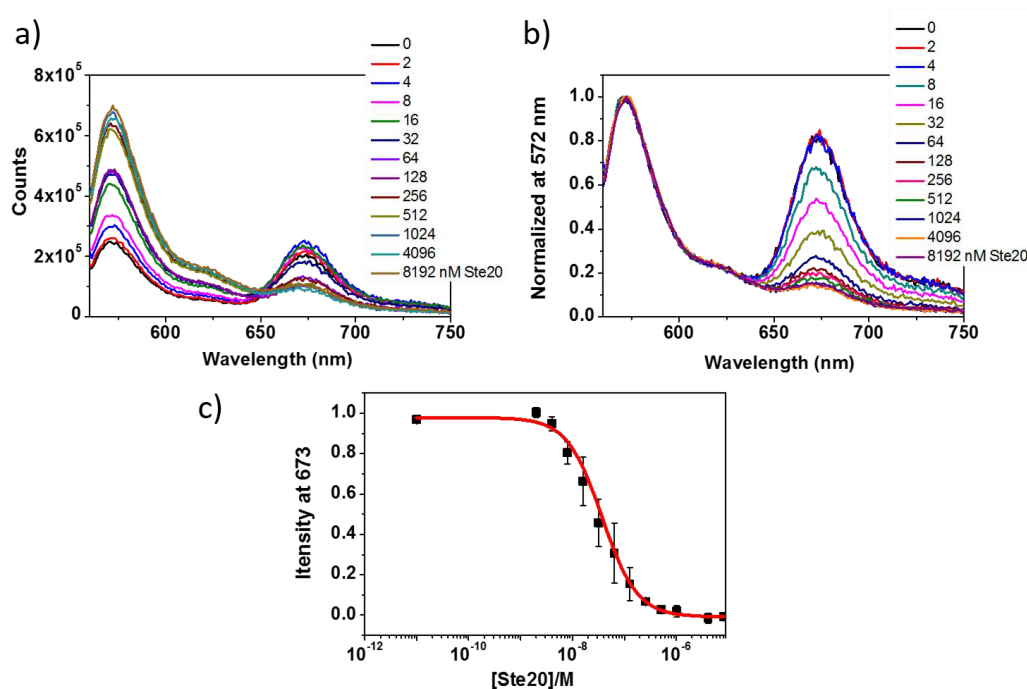


Figure 4.3: Bulk fluorescence measurements of Nbp2-SH3 with Ste20 peptide. a) Raw fluorescence spectra of labeled Nbp2-SH3 (5 nM) with Ste20 at different concentrations (0 to 8.192 μM). b) Raw fluorescence spectra was normalized at 572 nm to show trend in different concentration (FRET) c) Data represent the average of acceptor fluorescence signals from the normalized data points of two sets of independent experiments at 673 nm plotted as a function of the peptide concentration. The error bars indicate standard deviation of these sets.

a full length Nbp2 with snap- and clip-tags and orthogonally labeled the protein with the same donor and acceptor dye pair. We titrated all four peptides and measured the FRET efficiencies as done previously. With the full length Nbp2, the initial acceptor fluorescence was lower than that of Nbp2-SH3 under the same condition. No change in the FRET efficiency was observed upon addition of the peptides in any of the tested concentrations. Figure 4.4 shows the emission spectra upon adding the Ste20 peptide to the full length Nbp2. The mean acceptor intensities show no significant change over the entire peptide concentration range (Figure 4.4b). The re-introduction of the peripheral domains gives SH3 domain more space; however, this most likely moved the snap- and clip-tags outside of the FRET sensitive distance range.

To investigate, whether the SNAP-tag on peptides (Figure 4.2 & Figure 4.3)

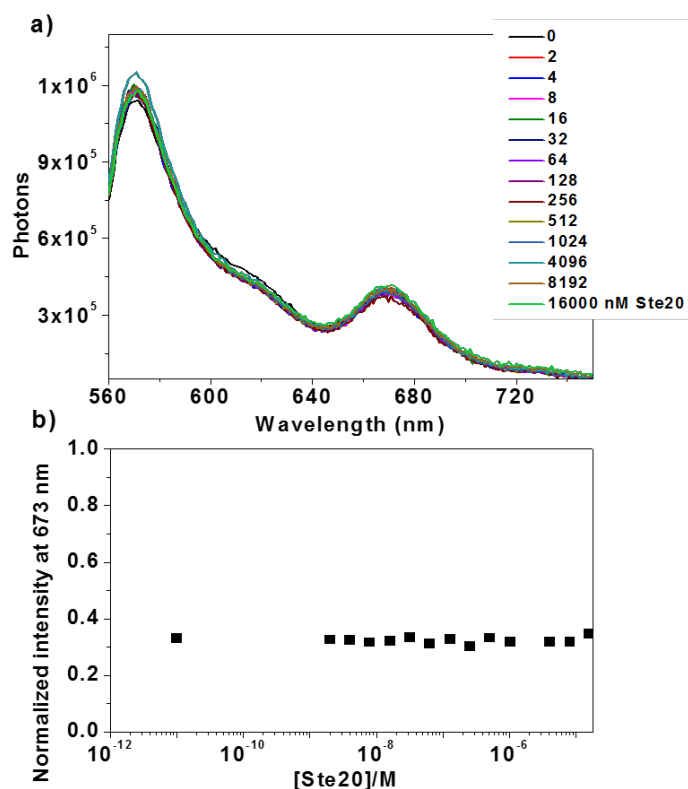


Figure 4.4: Bulk fluorescence measurements of full length Nbp2 with Ste20 peptide. a) Fluorescence spectra of labeled Nbp2 full length (5 nM) with Ste20 at different concentrations (0 to 16 μM). The concentration of peptides in each measurement was calculated based on known stock concentration from company. b) Normalized data points of acceptor intensity at 673 nm in different concentration of Ste20 peptide plotted as an affinity plot.

affects the interaction between Nbp2-SH3 domain with peptides, we applied Ste20 and Pbs2 synthesized peptides (Centic Biotec, Heidelberg, Germany) without a SNAP-tag to interact with SH3 domain. The SH3 domain was titrated with different concentrations of synthesized Ste20 and Pbs2 peptides to probe changes in FRET upon binding (Figure 4.5).

The protein interaction between SH3 domain and peptides was tracked for one hour (incubation time). Every two minutes, the fluorescence intensity was measured at the maximum fluorescence intensity of the acceptor dye, 673 nm (Figure 4.6). The results show no FRET change during this period (1 h). We conclude that the FRET change is quite small after protein-peptide interaction, which may not be measure using bulk FRET measurement. The peptide-SNAP-

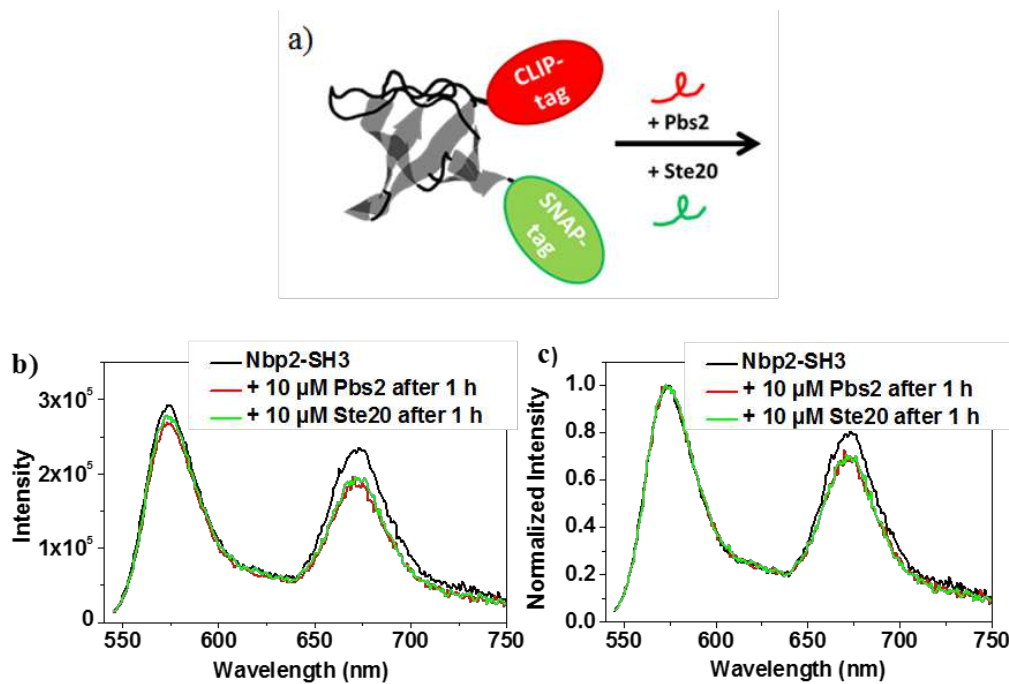


Figure 4.5: Study of the interaction between Nbp2-SH3 domain and peptides without SNAP-tags. a) Schematic design of doubly labeled Nbp2-SH3 domain, which interacts with Pbs2 and Ste20 peptides without SNAP-tag. b) Fluorescence spectra of the Nbp2-SH3 domain before incubating with peptide and after 1 h incubation. c) The fluorescence spectra were normalized at the maximum donor emission and the change at acceptor emission spectra considered.

tag fusion may show false positive results due to snap- and clip-tags on the protein and peptide.

As the conformational changes on Nbp2-SH3 domain are known after binding of Ste20 peptide [65], our results do not show any agreement with known results. More control experiments using different Nbp2-SH3 constructs are necessary to refine the assay. Building on the current results between Nbp2-SH3 and Ste20 and Pbs2, the terminal ends of the Nbp2-SH3 domain could be orthogonally labeled with small organic dyes by various conjugation strategies that are available [66]. While this is not ultimately helpful for *in vivo* applications, it will be helpful to assess the issue of change in protein activity.

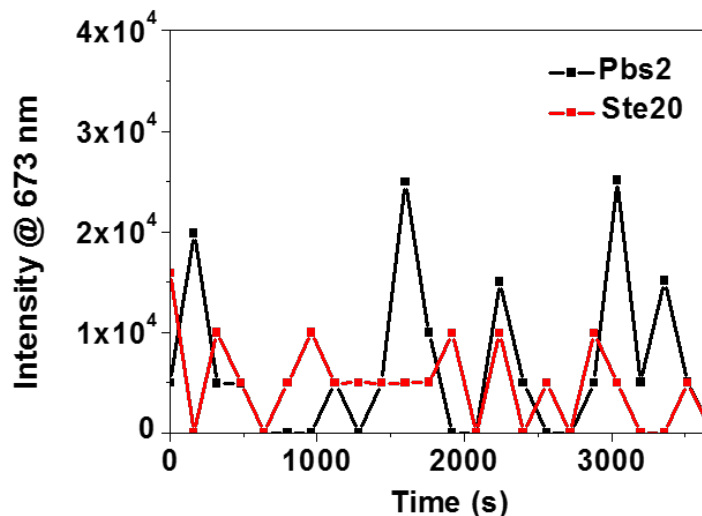


Figure 4.6: Tracking of the fluorescence intensity at 673 nm every two minutes during one hour. No significant change in intensity was detected for both peptides.

4.2 Single-Molecule FRET Studies

4.2.1 Single-Molecule FRET Study of the 15-aa Construct

To quantify the effect of the tag size, we compared smFRET distributions from the directly labeled 15-aa peptide and 15-aa construct (S-15aa-C). The 15-aa construct was labelled on snap- and clip-tags with the donor and the acceptor dyes (S-15-aa-C; donor: A546; acceptor: Dy647), and the degree of labelling was determined from the absorbance measurements (Figure A.5). The exact labelling ratio was impossible to calculate due to the protein impurity in purified 15-aa construct. However, the fluorescence spectrum of the labelled 15-aa construct shows clear peaks from the donor and the FRET emission upon donor excitation, thus confirming the dual labelling of the construct with both the donor and the acceptor dyes.

The smFRET measurements of directly labelled 15-aa peptide and two S-15aa-C constructs each showed pronounced single high E_{FRET} peak with differences in the peak positions and widths (Figure 4.7). No additional FRET subpopulation was observed, indicating that there is no transient interaction between the two tags. As expected, the added distance from the self-labelling tags shifted the E_{FRET} peak to a lower value (A546-15-aa-A647: $E_{FRET} = 0.81 \pm 0.01$; S-15-aa-C: $E_{FRET} = 0.73 \pm 0.01$) but, surprisingly, only by a small amount.

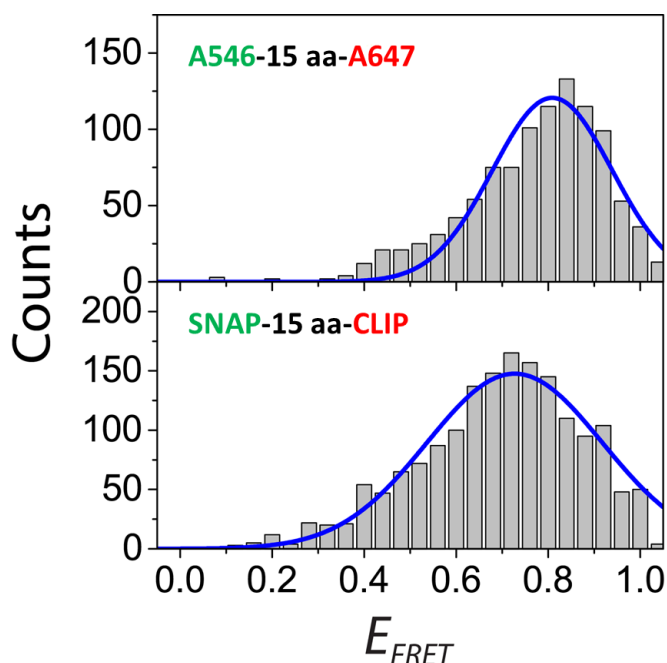


Figure 4.7: Representative smFRET histograms of the directly labelled random 15 amino acids peptide (A546-15aa-A647) and the random 15 amino acids peptide labelled by SNAP-/CLIP-tag (S-15aa-C) both show a single high FRET peak. The S-15aa-C shows a slightly lower FRET peak ($\langle E_{FRET} \rangle = 0.73 \pm 0.01$) in comparison to that of A546-15aa-A647 ($\langle E_{FRET} \rangle = 0.81 \pm 0.01$) due to the additional distance from the self-labelling tags. Blue line presents Gaussian fit.

To further compare 15-aa constructs, we calculated the average distance between two dyes using the $\langle E_{FRET} \rangle$ equation (A546/A647: $R_0 = 69 \text{ \AA}$; A546/DY647: $R_0 = 67 \text{ \AA}$). We computed the distances to be $\approx 5.7 \text{ nm}$ for S-15aa-C and $\approx 5.4 \text{ nm}$ for the 15aa peptide. This is an unexpectedly small change. The average end-to-end distance (d) of 15aa peptide calculated using the Gaussian chain model is $\approx 3.1 \text{ nm}$, ($d = b \times l^{0.5}$), where b (0.8 nm) is an effective bond length and l is the number of residues. If we include the length of dye linkers, there is an agreement between measured and estimated average distance. On the other hand, the distances between the reactive thiol group (on C145) and the N- and C-terminus from the crystal structure of the SNAP-tag (PDB ID: 3KZY) are 2.5 nm and 1.7 nm, respectively. Therefore, the average distance between two dyes may increase about 4 nm and also about 2 nm more due to the length of dye linkers. The observed change in distance of $\approx 0.3 \text{ nm}$ indicates that the snap- and clip-tags is, on average, inclined toward each other. Part of this work has been

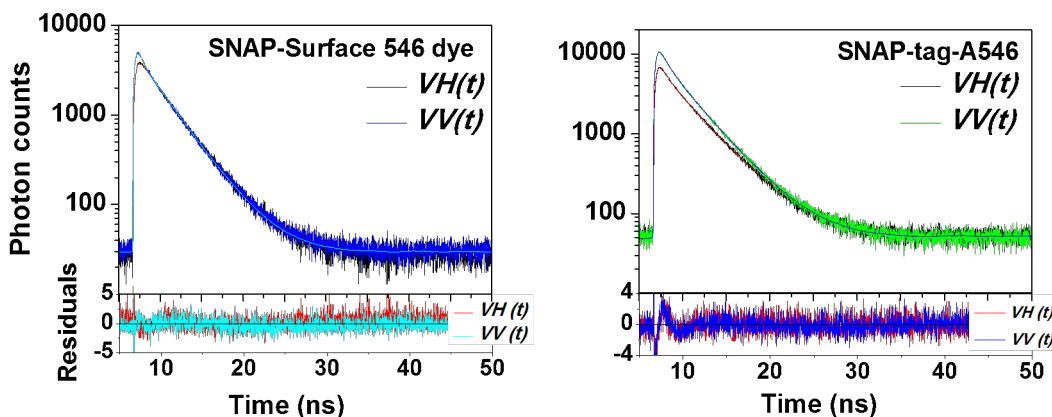


Figure 4.8: $VV(t)$ and $VH(t)$ polarized decays of free SNAP-Surface Alexa Fluor 546 and Alexa Fluor 546 conjugated to the SNAP-tag. The horizontal (VH) and vertical (VV) anisotropy decays were fitted using Exponential fit function; and the lifetimes and the rotational correlation time of dyes were extracted from fit result (Table A.32). The residuals of fitted decays display sufficient fitting of decays. A clear difference between vertical and horizontal anisotropy decays was observed for the bound dye on the SNAP-tag.

published in Ref. [67].

The greater width of the S-15 aa-C distribution compared to the 15aa construct (0.38 ± 0.02 and 0.26 ± 0.01 , respectively, mean $\pm \sigma$) can be mostly explained by the large tags, tumbling of fluorophores around their attachment site and much larger volume of the sample resulting in a wider $\langle E_{FRET} \rangle$ distribution value. In addition, existence of tryptophan and tyrosine amino acids around the attachment site of the dye may quench the fluorophore. These photophysical effects may result in the broadening of $\langle E_{FRET} \rangle$ distributions in smFRET measurements [67].

4.2.2 Rotational Freedom

Results of single-molecule FRET of the S-15aa-C construct indicates that the peptide is not in the extended conformation. Since the SNAP-, CLIP-tag and the corresponding dyes are rotationally free, understanding the origin of peak broadening becomes extremely complex. The evaluation of rotational freedom of the dye attached to the SNAP-tag protein plays an important role in FRET histogram broadening. The rotational freedom of the free dye (SNAP Surface-Alexa Fluor 546) and the dye bound on the SNAP-tag was probed by fluorescence anisotropy measurements (Figure 4.8).

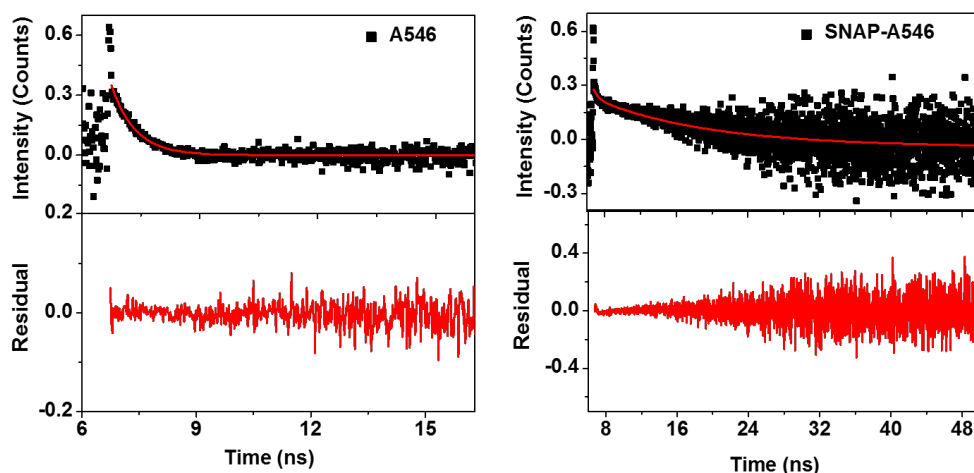


Figure 4.9: Anisotropy decays curve calculated in OriginPro from $VV(t)$ and $VH(t)$ for A546 and labelled SNAP-tag with A546 fluorophore, assuming $G = 1$. The anisotropy decays were fitted with exponential decay (Red line). Lower panel shows the residuals from the exponential fit.

Based on the equation 2.24, the anisotropy decays for A546 and SNAP-A546 were calculated. The anisotropy decay measurements were fitted by single and double exponential fit functions for the free and bound dyes, respectively (Figure 4.9). The rotational correlation time extracted from these fits displayed a slow rotation of bound dye on the SNAP-tag. The rotational correlation times of the dye labelled on the SNAP-tag is more than 27 times slower (13 ± 1 ns) than that of the freely diffusing dye (0.6 ± 0.02 ns). The significantly longer correlation time for the SNAP-tag conjugated dye shows that the dye is interacting with surrounding amino acids near the catalytic site of the tag. The rotation time of the bound dye is comparable to that of a 20 kDa protein [3].

4.2.3 Distance Characterisation

To investigate the distance sensitivity of the snap- and clip-tagged FRET system, we introduced PP spacers of lengths varying from 1.8 nm to 7.2 nm between the tags (Figure 4.10). Here, we present *in vitro* FRET measurement results from the PP constructs and discuss the distance and conformation sensitivity.

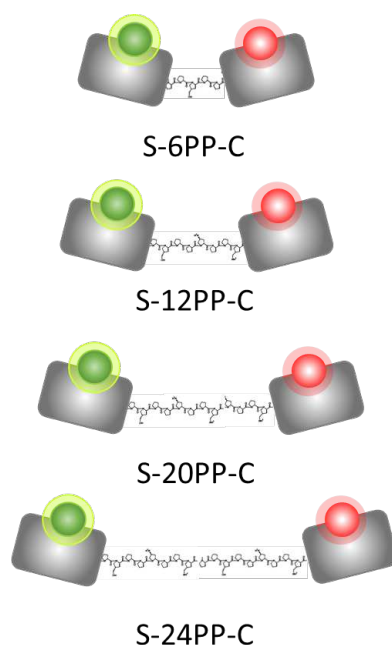


Figure 4.10: Cartoon of S-xPP-C construct designs ($x = 6, 12, 20,$ and 24)

4.2.4 Average FRET value Measurements

SNAP-tag/CLIP-tag constructs with polyproline linkers (S-xPP-C, $x = 6, 12, 20$ and 24 prolines) were dual labelled and absorbance measurements were done to verify the labelling and to quantify the labelling efficiencies (Figure 4.11). The absorbance at maxima at 280 nm , 555 nm and 655 nm correspond to the aromatic amino acids in the protein, A546 or TMR-Star and DY647 dyes, respectively. A546 and TMR-Star dyes have the same maximum absorbance at 555 nm . The typical labelling efficiencies of the donor and the acceptor were obtained between 43% and 74% (see Table A.5 for more details).

In the next step, the fluorescence spectra of doubly labelled PP constructs were measured to verify the existence of the FRET signal in the PP constructs. An additional 6PP construct was labelled with only the donor dye, A546, to verify that the emission of the acceptor (FRET signal) originates from donor excitation in presence of acceptor. All constructs were excited at 540 nm (donor excitation) and the emission was collected between 545 and 750 nm . We detected FRET signals ($650\text{-}720\text{ nm}$) upon donor excitation for double-labelled constructs, but not for the 6PP donor-only labelled construct (Figure 4.12).

Although this verifies the presence of FRET in these constructs, different FRET values can result from different degrees of labelling for each PP construct (6PP,

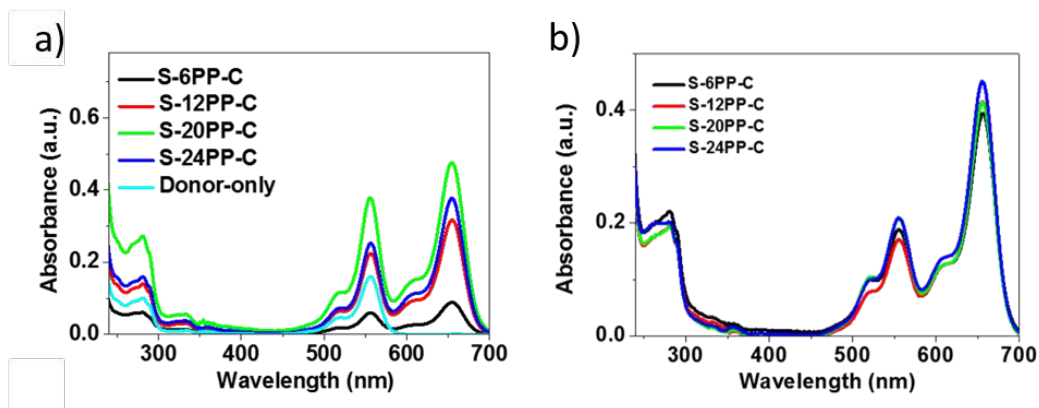


Figure 4.11: Absorbance spectra of labelled PP constructs. S-xPP-C constructs ($x = 6, 12, 20$ or 24 residues of Pro) were labelled with the A546-DY647 (set A) (a) and TMR-Star-DY647 (set B) (b) dye pairs. Absorbance maxima for the protein, the donor dye and the acceptor dye were observed at 280 nm, 555 nm and 655 nm, respectively. The donor only sample (6PP construct labelled only with the A546 dye) has absorbance maxima at 280 nm and 555 nm.

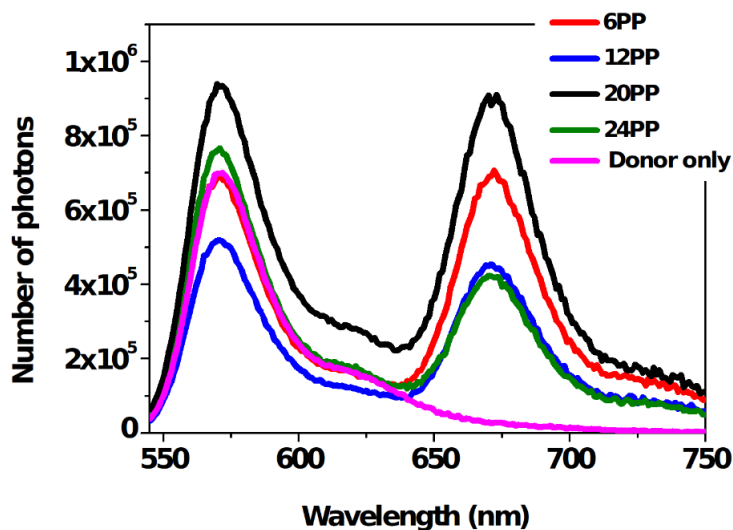


Figure 4.12: Fluorescence spectra of PP constructs. The PP constructs were labelled on the snap- and clip-tags with A546 and DY647, respectively. The 6PP construct was also labelled only on the SNAP-tag as donor only sample.

12PP, 20PP, and 24PP). Therefore, we cannot definitively conclude that the increase in FRET arises from decreased PP length. Here, we utilized a series of SNAP-(x)PP-CLIP constructs (x: 6-24 polyproline residues) and bulk FRET measurements to interrogate FRET efficiency between snap- and clip-tags separated by polyproline linkers of different lengths. The data from bulk FRET measurement cannot completely describe the molecular behaviour due to the averaging of all FRET efficiencies in the measurement, but by examining the acceptor peak, the relative amount of folding in the system can be inferred. Therefore, the values of the acceptor peaks of the different lengths of the same construct can be qualitatively compared to each other. In this measurement, the ratio of acceptor to donor fluorescence decreases with increasing length of the PP linker between snap- and clip-tags. This bulk FRET experiment does not disagree with earlier smFRET measurements and suggests the existence of linker-length dependent FRET.

While bulk FRET measurements allow us to discern general relationships between donor and acceptor distance, the fluorescence values measured are ensemble-averaged and do not contain clear information about rapid fluctuations and species subpopulations. At the individual molecule scale, each construct can be investigated using smFRET method to collect information about subpopulations and conformational fluctuations of each single molecule.

4.2.5 Single-Molecule FRET Study of Polyproline

Single-molecule FRET measurements of the SNAP-PP-CLIP constructs were made to obtain unbiased FRET efficiency distributions. Two sets of PP constructs were prepared by using either A546 (set A) or TMR (set B) as the donor to test the dye effect. The smFRET results in FRET efficiency histograms from these PP constructs are shown in Figure 4.13. The PP smFRET results from the labelled construct with set A shows two broad subpopulations in each distribution (Figure 4.13 a). The lower FRET subpopulation progressively decreases towards lower FRET efficiencies as the PP length between the two tags increases. On the contrary, the higher FRET subpopulations did not show a significant change in the peak position, except that the peak width increases as the PP length increases. The *cis-trans* isomerization of the polyproline oligomers has been widely discussed and analysed using different methods [42, 68, 69]. Therefore, we initially attributed the two main FRET subpopulations to two different conformational states (Figure 4.14).

An extra FRET subpopulation in set A was recorded, which may be attributed to the photophysical effects of A546 dye. The Trp amino acids in the SNAP-tag may quenched the A546 dye and affected FRET histogram. Haenni et al. [70] combined FRET and photo-induced electron transfer (PET) to obtain accurate distance information and the kinetics of intramolecular contact formation. They

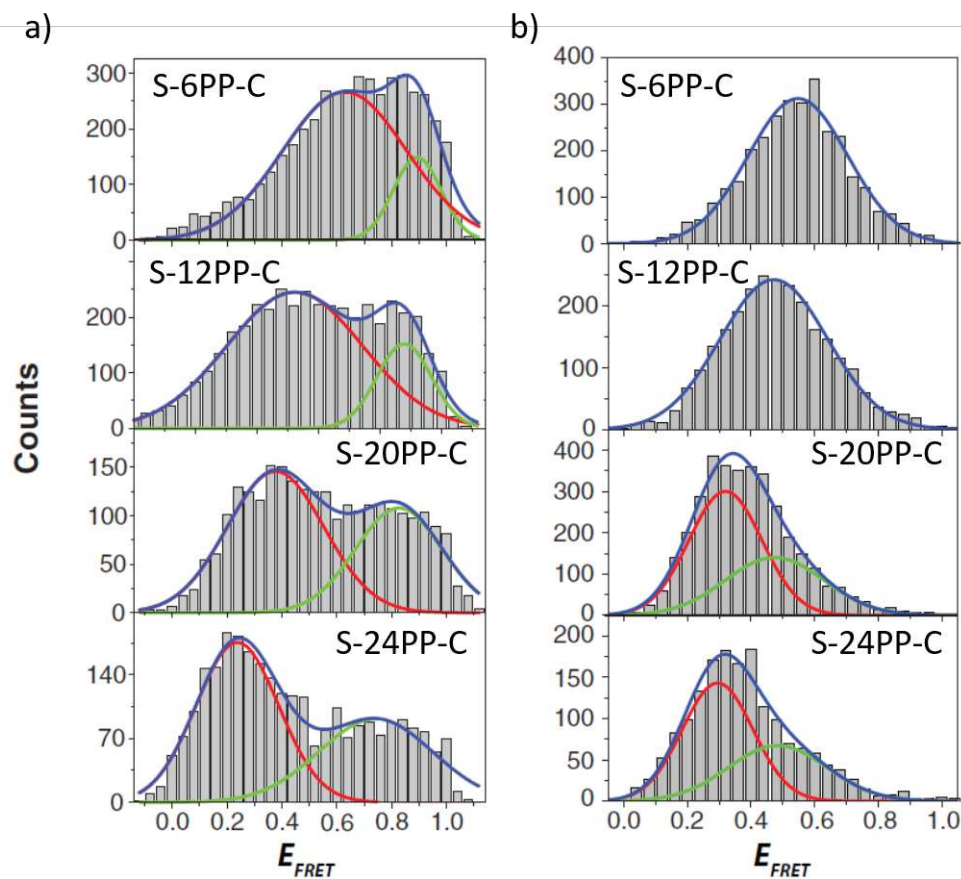


Figure 4.13: smFRET histogram of PP constructs for different lengths of PP constructs. a) PP constructs were labelled with set A. Two separate subpopulations are observable (red and green lines indicate each fitted subpopulation). b) PP constructs labelled with set B, which shows one FRET peak. FRET subpopulations were fitted by Gaussian fit function (equation 2.14) for each construct. Blue line presents the overall fit.

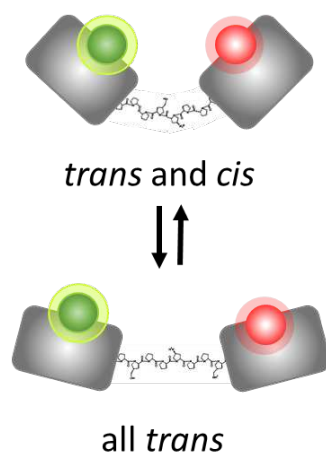


Figure 4.14: *cis-trans* isomerization of polyproline oligomers. The proline residues can be observed in *cis* or *trans* conformation. Most residues are in *trans* conformation, but few of them are in *cis* conformation. The average end-to-end distance may change based on the combinations of conformation of each proline residue.

labeled 20 polyproline peptide with Alexa 488 and Alexa 594 dyes and used different Trp amino acid positions at the end of the peptide. The sequence of peptide was GP20CGS(W3)GS(W5)GS(W7)GS(W9), which WX indicate the position of Trp amino acid. The distance between the fluorophores and the Trp amino acid was varied to investigate the effect of PET quenching on the FRET efficiency histogram. One of the PET quenching effects is the change of quantum yield of the donor dye. The presence of Trp slightly increased the uncorrected transfer efficiencies, because the quantum yield of the donor dye changed. In addition, the dynamic quenching effect of Trp on the donor dye was more pronounced than the acceptor dye. In contrast, static donor quenching did not change the FRET efficiency but it affected the average molecular brightness of the entire FRET system. As a summary, PET quenching systematically affected on uncorrected (or apparent) transfer efficiencies [70]. Due to observed mirror change of FRET efficiency, we may not only attributed the high FRET population to the quenching.

Various smFRET studies of polyproline linkers show one [71, 72, 73] or two [42] FRET populations, with the two FRET populations are due to *cis-trans* isomerization. Therefore, we first considered that the smFRET result of the labelled PP construct with set A was the correct result. However, the result could be due to a systematically high FRET peak, as evidenced by the unchanged FRET position of that FRET population while increasing the distance between the donor and acceptor dyes. Therefore, we repeated all smFRET measurements by exchanging

TMR for the donor dye, on the assumption that the TMR dye may be less affected by photophysical effects than the A546 dye.

The smFRET results of PP constructs labelled with set B has shown more promising results, because we recognized that no high FRET subpopulation such as those of set A and single FRET. Set A and single FRET populations show a progressive decreases towards lower FRET efficiencies as the PP length between the two tags increases. As shown in figure 4.13, S-20PP-C and S-24PP-C constructs fit to two subpopulations, which may be due to the bending of PP linkers or possibly due to presence of *cis* and *trans* configurations.

The $\langle E_{FRET} \rangle$ values for directly labelled 20PP [74] and construct has an qualitative agreement, which the $\langle E_{FRET} \rangle$ values are $\langle E_{FRET} \rangle \approx 0.37$ and $\langle E_{FRET} \rangle \approx 0.57$ for the directly labelled 20PP (black triangles in Figure 4.15) and $\langle E_{FRET} \rangle \approx 0.32$ and $\langle E_{FRET} \rangle \approx 0.45$ for S-20PP-C (black squares in Figure 4.15). As we mentioned in the previous section, the lower $\langle E_{FRET} \rangle$ values for both subpopulations are due to the increased distance between two dyes related to the size of tags. In addition, the FRET histograms of the S-20PP-C construct show broader distribution than the directly labelled 20PP. Therefore, this result shows that the two labelling methods was not significantly affected the conformational state of the peptide especially by the presence of the tags. Part of this work was published in [67].

To determine if snap- and clip-tags can be used as a labelling system for smFRET measurements application (providing quantitative distance information in single-molecule fluorescence experiments), we measured the FRET efficiency for donor and acceptor dyes on tags. Our experimentally observed single population FRET histogram for each construct strongly indicates the possibility of FRET in this length regions using snap- and clip-tags. In addition, lower FRET efficiency for 20PP construct compare to the directly labelled 20PP [74] (Figure 4.15) confirms the applicability of this tag system even with an extra distance between the end of the linker and the dye attachment site on each tag for smFRET measurements. However, it would be difficult to measure linkers smaller than 6 residues due to the challenge of separating the low FRET population from donor-only population, even using ALEX method. In conclusion, the distance sensitivity of snap- and clip-tags system was resolved by smFRET measurements even on the order of four proline amino acids (≈ 1.2 nm) [73].

We used polyproline linkers as a spectroscopic reference to test the applicability of the chemical tag system in single-molecule applications. For relatively large tags, this labelling method did not complicate single-molecule experiments. In addition, our results confirm that additional complication arises from photophysical effects from tags are negligible. The dye pair is a very important issue, which can affect smFRET results, and different dye pairs must be tested at the single-molecule

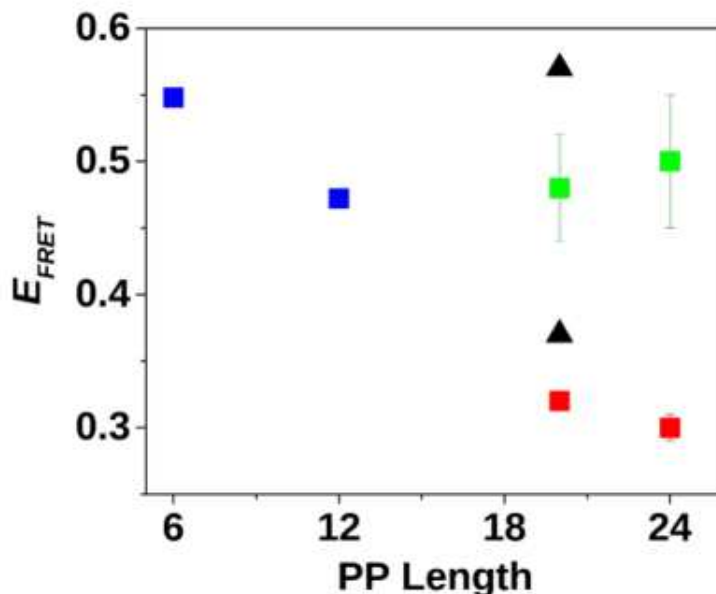


Figure 4.15: $\langle E_{FRET} \rangle$ (black squares) and corresponding errors of the Gaussian fit from smFRET histograms (Figure 4.13) for the S-xPP-C constructs. The $\langle E_{FRET} \rangle$ values were compared with values from directly labelled 20-PP sample [74] (black triangles).

level to calibrate the system before the real smFRET measurement. Bulk FRET measurement is not a sufficient method to clarify the effect of tag protein on the dye due to averaging of all subpopulations.

4.3 Conformation Characterization by the Single-Molecule-FRET Method

CaM is an ideal system for our study, because its large conformational change can easily be induced by the addition of Ca^{2+} and by adding certain peptides. While CaM is a well-studied multi-domain protein, its folding dynamics is complex, and it remains a subject of protein folding studies. The Ca^{2+} -free Apo protein is highly flexible and in unfolded state, but upon Ca^{2+} binding, the conformation of CaM changes to more stable and rigid Holo state. This conformation conversion may be happened for each globular domain independently. More studies have been conducted on the CaM protein to better understand its conformational states upon binding to Ca^{2+} or other proteins using various biophysical techniques, such

as smFRET, single-molecule fluorescence lifetime spectroscopy and single-molecule force microscopy by optical tweezers [51, 75, 76]. Stigler and Rief [77] have studied the folding behavior of CaM at 10 mM concentrations of calcium by the optical tweezer method. The complete kinetic and energetic behavior of the N- and C-terminal domains was modeled. They were able to determine the kinetic folding pathway in detail [77]. Park and his colleagues [78] investigated CaM fluctuation changes upon binding of ions and peptides. They incorporated the two different unnatural amino acids into specific positions of CaM [78]. The smFRET method was used to study the conformational change of the globular domains caused by Ca^{2+} , Ethylene Glycol Tetraacetic Acid (EGTA) and the M13 peptide.

In this section, the SNAP-CaM-CLIP probe was utilized to test the applicability of chemical tag system to study the conformational change of the protein. *In vitro* FRET results of S-CaM-C under various conditions is presented, and its applicability for FRET measurements is discussed.

4.3.1 Affinity Binding Study of Ca^{2+} Ions to the CaM Construct

To check the functionality of the labelled S-CaM-C construct, we performed bulk FRET measurements to probe Ca^{2+} dependent conformational changes. The labelling efficiency of the CaM construct (labelled with TMR and DY647) was characterized from absorbance measurements as done for other constructs (Figure A.3).

In bulk FRET measurements, we detected the conformational change of CaM protein in response to EGTA and Ca^{2+} (Figure 4.16). In the presence of 8.3 mM Ca^{2+} , the emission at 671 nm markedly increased, indicating that the Holo or folded state of CaM proteins were formed. Upon addition of 1 mM EGTA, the emission decreased, which may be related to the residual Ca^{2+} in the buffer or bound on the protein during purification (CaM proteins were in an Apo, unfolded, state).

To determine the apparent Ca^{2+} affinity, the fluorescence intensity of double-labelled CaM was measured and the fluorescence spectra at different Ca^{2+} concentrations were recorded for each calcium concentration. The raw spectra were normalized to a maximum fluorescence point of the donor emission (576 nm) to yield intensities at the acceptor peak (671 nm) as the relative change of emission at 671 nm. All background-corrected spectra were plotted as a function of Ca^{2+} concentration. The data were fitted using the Hill equation (solid line in Figure 4.16), $I_{671} = (I_{start} + (I_{end} - I_{start})) \left(\frac{[\text{Ca}^{2+}]^n}{K_d^n + [\text{Ca}^{2+}]^n} \right)$, where I_{671} is the emission intensity at 671 nm after normalization at 576 nm, representing the relative population of folded CaM, I_{start} and I_{end} are the emission intensities at the start and end of the titration. n denotes the Hill coefficient, $[\text{Ca}^{2+}]$ is the Ca^{2+} ion concentration, and K_d is the equilibrium dissociation coefficient.

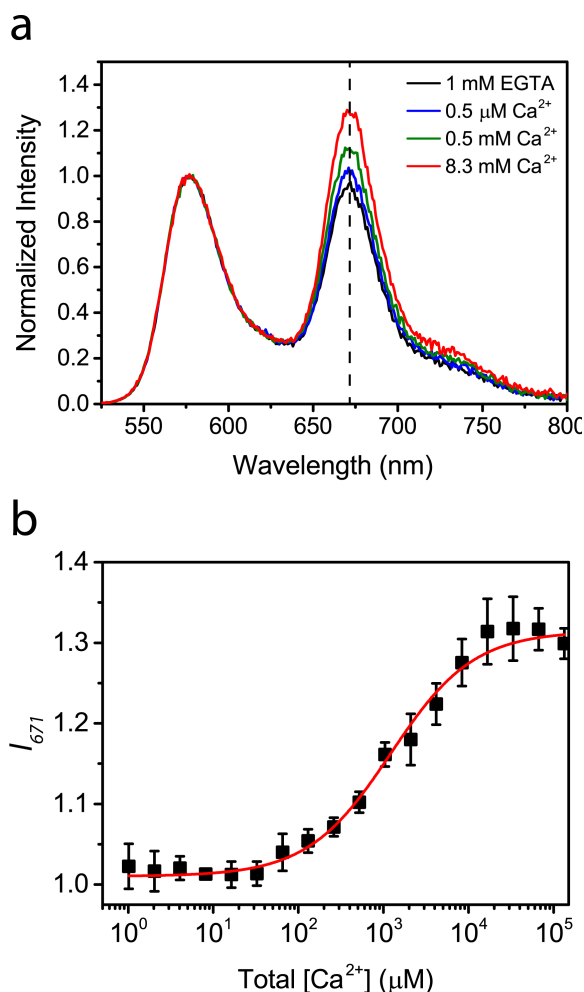


Figure 4.16: Bulk fluorescence measurements of CaM construct. a) 5 nM doubly labelled CaM construct (BG-TMR/BC-DY647) was supplemented with 1 mM EGTA (black), 0.5 μM (blue), 0.5 mM (green), and 8.3 mM (red) of Ca^{2+} in Tris buffer (25 mM Tris-HCl, 100 mM KCl, pH 7.5). To observe the relative change of the emission at 671 nm, spectra were normalized at 576 nm. b) The emission points at 671 nm were plotted as a function of total Ca^{2+} ion concentration to calculate the affinity binding curve. The curve was fitted by Hill fit function in OriginPro software. Three sets of measurements were taken and the mean value and standard deviation were calculated from those three set of data.

The fitted binding affinity of the CaM protein fused with snap- and clip-tags to Ca^{2+} was lower than that of the reported CaM protein without tags [79]. The binding affinity between the CaM protein and Ca^{2+} was determined as two K_d values of 2 and 13 μM for C- and N-terminal domains, respectively [79], while only one dissociation constant in the millimolar range was found (k_d : 1.2 ± 0.1 mM, n : 0.89 ± 0.08), which could be related to interference of the snap- and clip-tags with Ca^{2+} affinity.

Generally, the folding of the S-CaM-C construct can be confirmed by our bulk FRET measurement but we are unable to resolve the binding affinity for individual EF hand motif or even for each globular domain. In addition, there is no significant interference effect was found from tags on CaM function except of slightly lower affinity of CaM to the Ca^{2+} . This lower affinity may be due to steric hindrance of two large tags or other experimental issues such as buffer composition, labelling position, organic dye and tryptophan fluorescence, or NMR and fluorescence.

4.3.2 Single-Molecule FRET investigation of the CaM Construct

To resolve conformations of the CaM protein in detail, a smFRET experiment was attempted since this information cannot be obtained using ensemble FRET measurements (section 4.3.1). The absorbance and fluorescence spectra of the double-labelled CaM construct were measured and to validate FRET effects before the smFRET experiment was performed on the CaM construct.

The CaM construct was labelled with TMR-Star-DY647 dye pair and the smFRET data of the fluorescently labelled CaM were obtained. FRET values for each labelled molecule were calculated and plotted as a FRET efficiency histogram. smFRET data were obtained for various conditions such as 10 mM EGTA, 1 mM Ca^{2+} concentrations and 10 μM M13 in the presence of 1 mM Ca^{2+} (Figure 4.17). After adding 10 mM EGTA, one narrow FRET peak was detected with $\langle E_{FRET} \rangle = 0.40 \pm 0.01$. EGTA, an ion chelating agent, has a very high affinity for calcium ions, leading to Ca^{2+} ion depletion from the surrounding buffer. EGTA changed the width and the FRET efficiency position to a lower FRET efficiency, which indicates that the CaM protein is in a highly dynamic and flexible Apo conformation. In presence of 1 mM Ca^{2+} concentrations, two broad FRET populations were observed, one of which was fixed at $\langle E_{FRET} \rangle = 0.40$ as an Apo conformation and a second at $\langle E_{FRET} \rangle = 0.65 \pm 0.02$ with fractional populations of 57% and 43%, respectively. Then, an overall weighted average $\langle E_{FRET} \rangle = 0.51 \pm 0.05$ was computed from those data, which shows that CaM is more prevalently in a compact and folded conformation. Moreover, the FRET efficiency underwent a small shift to a higher overall average $\langle E_{FRET} \rangle$ of 0.58 ± 0.06 and an increase in the high E_{FRET} subpopulation fraction ($\langle E_{FRET} \rangle = 0.65 \pm 0.02$) to 72% after the addition of M13 peptide and 1 mM Ca^{2+} . These findings are consistent with CaM

conformation stabilization in the folded state upon binding of M13 peptide in the presence of Ca^{2+} .

The CaM construct was also labelled with a A546-DY647 dye pair. Similar to the smFRET results with PP constructs, a high FRET population for 1 mM Ca^{2+} and 10 μM M13 in the presence of 1 mM Ca^{2+} conditions were observed (Figure A.13, Figure A.14). Therefore, these high FRET populations were undue to conformational changes, because these FRET peaks were removed by changing the donor dye from A546 to TMR-Star. As a result, the TMR-Star dye showed no photophysical properties changes compare to the A546 dye by tryptophan amino acids in the SNAP-tag.

All conditions were repeated three times to check the reproducibility of measurements in different buffers.

It is encouraging to compare our smFRET result with the study by Park and his colleague [78] who measured conformational changes of directly labelled CaM by smFRET (Figure 4.18). The CaM protein directly and site-specifically labelled with a Cy3/Cy5 dye pair at positions 34 and 113 by using unnatural amino acids [78]. In Figure 4.18, the results from directly labelled CaM and CaM construct agree that upon addition of M13/ Ca^{2+} , the $\langle E_{FRET} \rangle$ increased. Kim *et al.* [78] did not observe a significant difference for directly labelled CaM in E_{FRET} with or without Ca^{2+} , but the width of FRET populations changed from $\sigma_{EGTA} = 0.12$ to $\sigma_{\text{Ca}^{2+}} = 0.20$. This change of width indicates that the attachment sites of the dye pair were not chosen in a way to resolve other conformational states. Also, our results for CaM construct are supported by an optical tweezer measurement, which shows that even in presence of M13/ Ca^{2+} both unfolded and folded states are obvious. Therefore, our result shows that using a tag-based system adds a necessary distance between attachment site of dyes and protein to uncover other conformational states. This shows that attachment sites are important for smFRET measurements. Part of this work has been published in Ref. [67]

Our smFRET experiments based on tag-labelled CaM indicate the Holo to Apo transition of CaM protein upon addition of Ca^{2+} and M13 peptide. The importance of selected dye pair for labelling of tags was also critical like as PP constructs to get the accurate smFRET result. The broad FRET histograms also indicates conformational fluctuation upon addition of Ca^{2+} in addition of photophysical effects and the motional freedom of the attached dye on the tag. However, using snap- and clip-tags system in smFRET measurements indicates the calcium-dependent folding of CaM protein in a physiologically relevant regime in single-molecule level. In addition, previously reported intermediate state between Holo and Apo conformation [80] was not observed via our measurements. So far, it may be difficult due to the limitation on the large tags and widening of FRET histograms, which hide other subpopulations.

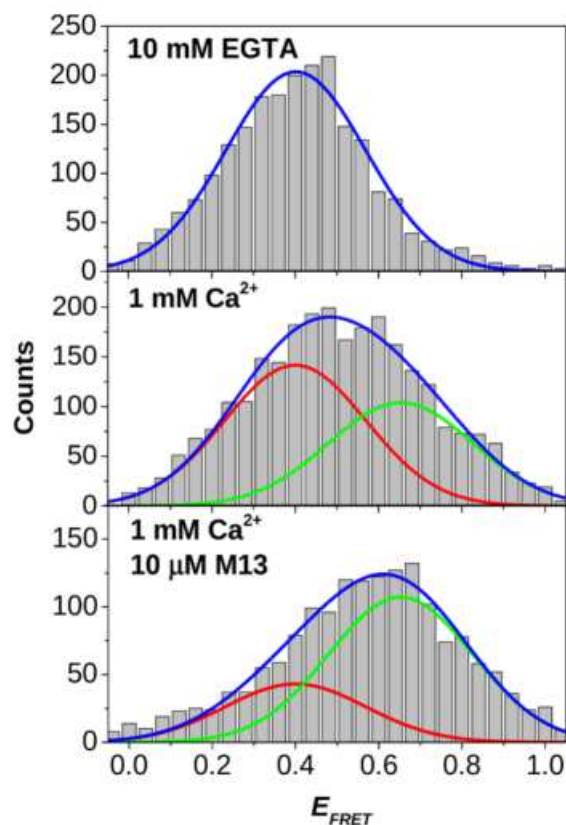


Figure 4.17: smFRET measurements of the CaM construct in 25 mM Tris, 100 mM KCl, pH 7.5. All measurements were performed on PEG surfaces. TMR-Star-DY647 dye pair was used for labelling of CaM construct. Three different conditions (10 mM EGTA, 1 mM Ca²⁺ and 10 μM M13 with 1 mM Ca²⁺) were performed. FRET histograms were fitted by Gaussian functions (equation 2.14). Two main FRET peaks (low and high FRET efficiencies as green and red lines, respectively) were obtained. The blue line shows the overall fit of all subpopulations.

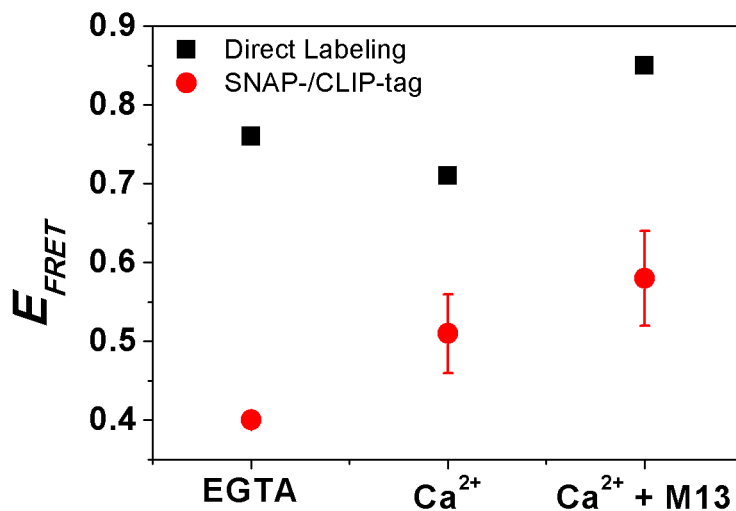


Figure 4.18: Comparison of smFRET results obtained with the CaM construct (labelled with TMR-Star-DY647 dye pair) and directly labelled CaM protein by Kim *et al.* [78]. E_{FRET} peak positions and widths from a Gaussian fit function (equation 2.14) of CaM construct and from published smFRET result from the directly labelled CaM protein are shown here. Both samples were measured at the same buffer conditions.

4.4 Fluorescence Lifetime and FLIM-FRET Imaging Studies

Fluorescence lifetime method is another technique to quantify FRET by measuring of the lifetime of the donor dye, which decrease in presence of the acceptor dye. The lifetime of the donor dye also measures in living cells, which decrease by the nearby acceptor dye. To measure the lifetime of each construct including PP construct and CaM constructs *in vitro* or *in vivo*, diluted sample about 100 pM concentration or transformed and labelled yeast cells was loaded in their sample chambers and the lifetime of the donor dye in the presence and the absence of the acceptor dye were measured. The lifetime decay of the donor dye for each construct was collected and convoluted with IRF decay to fit the decay using single and double exponential fit functions. The lifetime of the only-donor sample was first determined to fix it in the next decay fitting analysis from a donor dye in the presence of the acceptor dye. Therefore, the second lifetime was extracted after fixing of lifetime from the donor-only lifetime, which is the shorter lifetime for the donor dye due to the energy transfer to the nearby acceptor. So, by known

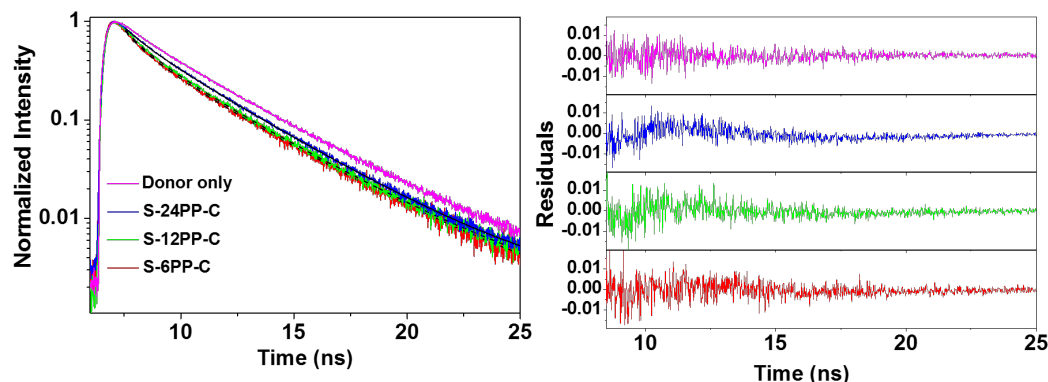


Figure 4.19: Fluorescence lifetime decays of the PP constructs. a) Lifetime decays of donor only labelled 6PP and doubly labelled 6PP, 12PP and 24PP constructs are shown here, with shorter lifetimes being due to shorter PP linkers. b) The three lifetime decays were fitted by exponential fit functions and all related residuals are shown here. The donor dye (A546) was excited using a 532 nm pulsed laser and the lifetime of the donor dye was measured in the absence (donor only) and the presence of the acceptor dye (DY647).

two lifetimes, the FRET can be calculated using Equation 2.19.

4.4.1 Fluorescence Lifetime Study of PP Constructs *in vitro*

To investigate whether the different length of PP linker between snap- and clip-tags can be resolved using the fluorescence lifetime method, we measured the lifetimes of the labelled PP constructs *in vitro*.

The microtime data contains lifetime information (e.g. in an ensemble measurement), which the lifetime data can be extracted independent to the sample concentration. In the smFRET method, the concentration of sample and labelling efficiencies of the donor and the acceptor dyes was more critical than in fluorescence lifetime measurement. Here, we measured the lifetime of the donor dye in presence of the acceptor dye in different PP constructs. 6PP construct were labelled only with the donor dye without the acceptor dye. The lifetime decay from 6PP construct were fitted with a double exponential function. We observed two lifetimes as 3.8 ns and 1.85 ns (Figure 4.19 & Table 4.2). The A546 dye has only one lifetime as 4.1 ns, but the bound A546 on SNAP-tag shows two lifetimes. If we fit the decay lifetime with single exponential function, we could not get a proper fit. The first lifetimes from donor-only labelled 6PP construct were kept unfixed during fitting, and the second lifetime was characterized as shortened-donor lifetime

Table 4.2: Extracted lifetimes from fitting the lifetime decays of the PP constructs and calculated FRET efficiencies for the second lifetime based on equation 2.19. All lifetime decays were deconvoluted from IRF.

	τ_1 (ns) (A%)	τ_2 (ns) (A%)	E_{FRET}
S-6PP-C	3.3 (53 ± 4)	1.3 (14 ± 2)	0.66 ± 0.01
S-12PP-C	3.8 (50 ± 8)	1.4 (16 ± 1)	0.63 ± 0.01
S-24PP-C	3.8 (40 ± 9)	1.7 (23 ± 9)	0.55 ± 0.02
Donor-only	3.8 ± 0.01 (53 ± 4)	1.85 (32 ± 2)	

via nearby the acceptor dye. Therefore, the $\langle E_{FRET} \rangle$ was calculated from the second lifetime. Calculated FRET efficiencies from the lifetimes displayed decreasing FRET efficiency by increasing the length of the PP linkers between tags.

4.4.2 FLIM-FRET Imaging of PP Constructs Inside Fixed Yeast Cells

We investigated the PP constructs (6PP, 12PP and 24PP) inside yeast cells by the FLIM-FRET method. The yeast cells were transformed with 6PP, 12PP and 24PP constructs, and the snap- and clip-tags labelled with A546 and A647. An additional 6PP construct was labelled only with A546 (SNAP-tag) as the donor-only control sample. Then, the yeast cells were loaded into the sample chamber and observed by confocal microscopy to measure the lifetime of the donor dyes in the absence and presence of the acceptor. The labelled PP constructs were localized in the cytoplasm. In the lifetime measurement, both the intensity and lifetime images were recorded (Figure 4.20). The SymPhoTime program (PicoQuant, Berlin, Germany) were used to analysis of recorded intensity and lifetime images. To determine the average lifetime, the lifetime decay of a selected area of interest (Figure 4.20 a) was fitted with a double exponential function for doubly labelled PP constructs (similar to *in vitro* fitting of the lifetime decays), and then the fitted lifetimes were fixed to create the lifetime-based weighting of confocal image for each cell (n= 7-10 cells). From all images, the average-weighted lifetime was extracted for each PP construct. The average-weighted lifetime decreased from 3.6 ± 0.6 as a donor-only lifetime to 2.9 ± 0.5 ns in the 6PP doubly labelled yeast cells (Figure 4.20 b). The reduction of the mean lifetime is due to the shortening of the

Table 4.3: Average lifetimes of PP constructs in yeast cells.

	Average lifetime (ns)
6PP	2.9 ± 0.5
12PP	3.1 ± 0.5
24PP	3.3 ± 0.4
Donor	3.6 ± 0.6

PP linker length between the snap- and clip-tags. The frequency (counts) from the average-weighted lifetime data points were normalized and the lifetime histograms (Figure 4.20 b) were fitted by a Gaussian fit function; the peak positions are listed in Table 4.3. The errors are the width of the Gaussian fit function. As shown in Table 4.3, different lengths of PP linkers cannot be distinguished using average lifetimes in yeast cells. As a result, lifetime measurements were not as sensitive as smFRET experiment. *In vivo* measurement showed a decrease in the average lifetime as the lengths of the PP linkers were shortened, but the distance sensitivity was incomparable with the smFRET study. However, the *in vitro* fluorescence lifetime experiment confirmed the smFRET results.

4.4.3 Fluorescence Lifetime Study of CaM Construct *in vitro*

To examine the agreement between the smFRET and the fluorescence lifetime results and finally to show the application of our snap- and clip-tags system inside the yeast cell, we tested our construct using FLIM method. The lifetime of the doubly labelled CaM construct was measured in 25 mM Tris-HCl, 100 mM KCl, pH 7.5 (Figure 4.21). The donor-only and doubly labelled CaM constructs were measured to compare the lifetime of donor dye in the absence and presence of the acceptor dye. The doubly labelled CaM construct were influenced by 1 mM Ca^{2+} and 10 μM M13 peptide in the presence of 1 mM Ca^{2+} . First, the lifetime decay of the donor-only labelled CaM construct was fitted by a double exponential fit function (lifetimes were 3.5 ± 0.005 ns and 1.3 ± 0.006 ns) and donor-only lifetimes were used to extract the lifetime of the donor in the presence of the acceptor. The lifetime of doubly labelled construct were fitted by double exponential fit function by fixing of the first lifetime. Three sets of measurements were taken for the doubly labelled CaM construct. All extracted lifetimes are listed in Table 4.4.

In the presence of 1 mM Ca^{2+} or 10 μM M13 peptide/1 mM Ca^{2+} , the lifetimes of donor dye on CaM construct are shorter than the donor-only lifetime. The errors are standard deviations of mean value from three sets of measurements.

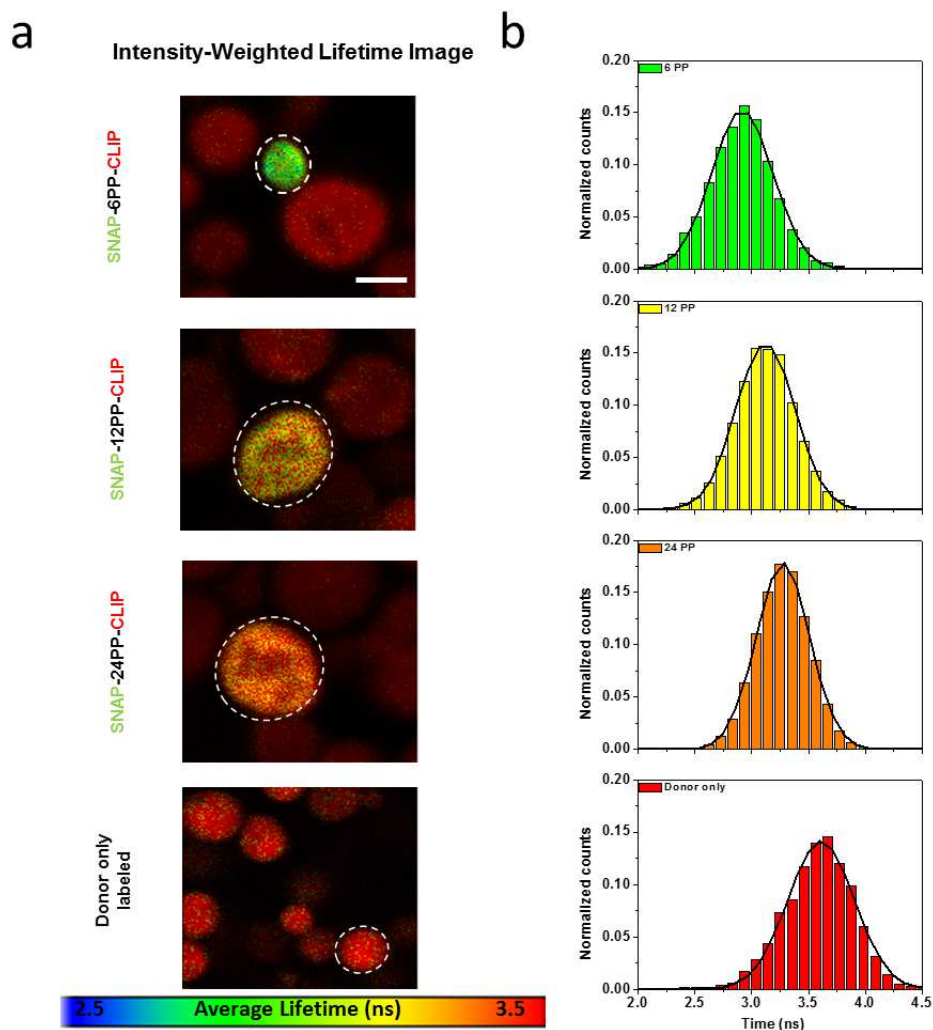


Figure 4.20: FLIM-FRET analysis of PP constructs in yeast cells. a) Representative FLIM-FRET images. The donor lifetimes of expressed and labelled PP constructs were measured in the absence and presence of the acceptor. The lifetimes of the donor dye (A546) in selected areas (indicated by broken circles) were analyzed to calculate FRET efficiencies in order to compare them with smFRET data. snap- and clip-tags were labelled with A546 and DY647, respectively. Scale bar, $3 \mu\text{m}$. b) The selected areas ($n = 7-10$ cells) in intensity-weighted lifetime images were plotted based on the lifetime in each pixel and the plot was normalized for the frequency (Normalized counts). Then, the data were fitted with one Gaussian (black line) to obtain the maximum value of the average lifetime.

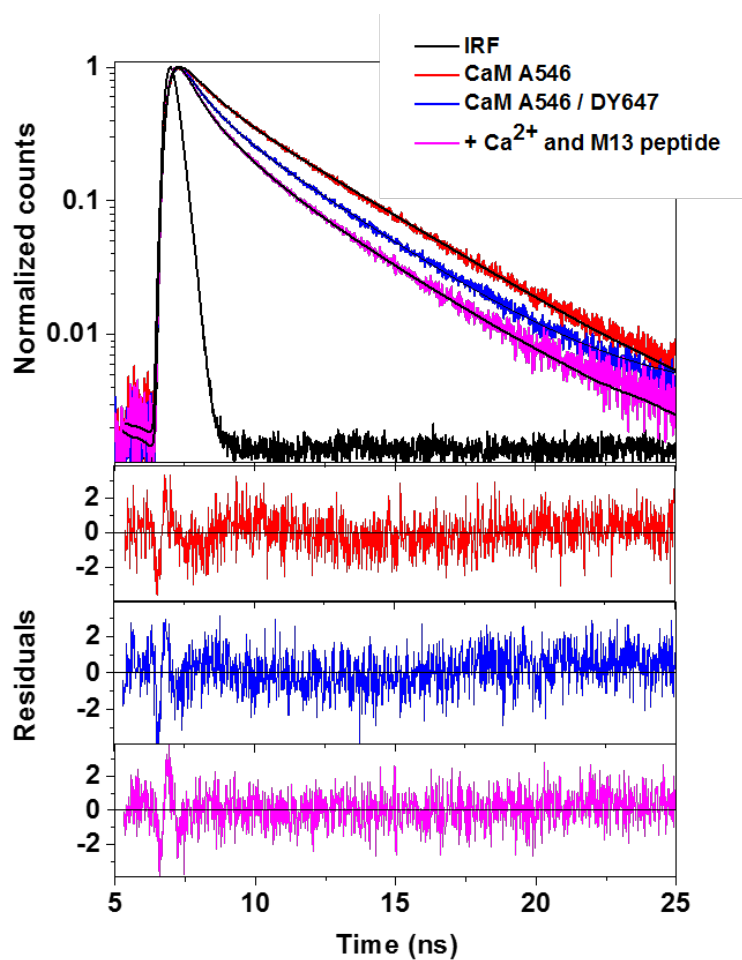


Figure 4.21: Fluorescence lifetime measurements of the CaM construct. Lifetime of the donor dye was measured in the absence and presence of the acceptor in the addition of Ca^{2+} and M13. 1 mM Ca^{2+} and 10 μM M13 was induced shorter lifetimes than induced CaM by only 1 mM Ca^{2+} . The residuals of the fitted lifetime decays by exponential fit functions are shown in the three last panels.

Table 4.4: Calculated lifetimes and FRET efficiencies from fitted lifetime decays for different conditions.

S-Cam-C	$\tau_1(ns)$ (A%)	$\tau_2(ns)$ (A%)	E_{FRET}
Donor-only	3.5 ± 0.005 (55 \pm 4)	1.3 ± 0.006 (44 \pm 5)	
+ 1 mM Ca^{2+}	3.5 (37 \pm 1)	1.1 ± 0.002 (63 \pm 4)	0.68 ± 0.01
+ 1 mM Ca^{2+} +10 μM M13	3.5 (16 \pm 3)	1 ± 0.002 (84 \pm 2)	0.71 ± 0.006

4.4.4 FLIM-FRET Imaging of CaM Constructs In Living Yeast Cells

To illustrate how the conformational change of proteins can be investigated *in vivo*, the CaM constructs expressed in yeast cells were analyzed by FLIM-FRET method. The different localizations and conformations of CaM protein in yeast cells provided us with the opportunity to investigate the application of SNAP-CLIP system in living cells. The expressed CaM construct in yeast cells were transformed and fluorescently labelled with CLIP-CellTM 430 and SNAP-Cell[®] TMR-Star dyes. The yeast cells were labelled and measured as donor-only and doubly labelled samples. After removing of extra free dyes in the cell solution, the labelled yeast cells were placed in the sample chamber to be measured on the Microtime 200 microscope. Depending on the stage of budding, the CaM constructs were localized in various cellular compartments such as the bud-neck, the cytoplasm and in the tip. In fluorescence lifetime measurements, both the intensity and lifetime-weighted images were recorded for labelled yeast cells with only CLIP-CellTM 430 or with both donor and acceptor dyes (Figure 4.22). The average lifetime was calculated from donor-only and doubly labelled CaM construct in yeast cells ($n = \approx 12$ cells). The average lifetime was shortened from 5.3 ± 1.1 ns for donor-only labelled yeast cells to 3 ± 0.5 ns in the tip growth region. The average lifetimes are shown in Figure 4.22 b in the range of 1 to 10 ns for all lifetime images.

CaM protein localized at the region of cell growth in *Saccharomyces cerevisiae*, which has an interdependent distribution with actin protein. During yeast cell division, CaM can be found at the tip of budded cells, and before cytokinesis concentrate in the neck region [81]. We found the same localization for our CaM construct, which means the fused tags did not change the distribution positions of CaM protein. Additionally, that lifetime histogram indicates the change of average lifetime between donor-only sample and doubly labelled CaM construct.

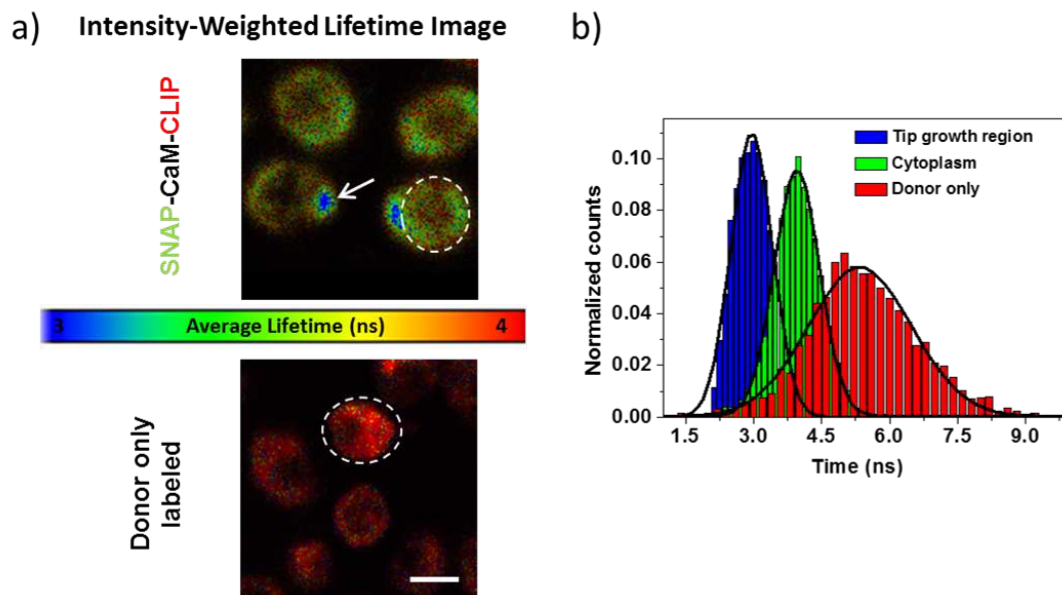


Figure 4.22: FLIM-FRET analysis of CaM constructs in yeast cells. a) Representative FLIM-FRET images. The donor lifetimes of expressed and labelled CaM constructs were measured in the absence and presence of the acceptor. Lifetimes of selected areas (indicated by broken circles) were analyzed to calculate FRET efficiencies to compare them with smFRET data. CLIP- and SNAP-tags were labelled with CLIP-Cell surface 430 and SNAP-Cell TMR, respectively. Scale bar is $3 \mu\text{m}$. b) Normalized intensity-weighted lifetime histograms were plotted for selected areas ($n \approx 12$ cells/data point). Different lifetimes were detected for tip growth and cytoplasm areas due to different local concentrations of calcium. All detected lifetimes from selected areas of all 12 cells was averaged and plotted as a histogram. Then, average lifetime (AV. Lifetime) histograms were fitted by Gaussian fit function (black line) and the maximum value from Gaussian curve was determined as an average value. The error bars indicate the widths of the Gaussian curve (σ).

Table 4.5: Average lifetimes of CaM construct in yeast cells.

	Average lifetime (ns)
Tip growth region	3 ± 0.5
Cytoplasm	4 ± 0.5
Donor only	5.3 ± 1.1

The lifetime of the donor dye was shortened due to the transferring energy to the nearby acceptor dye specially in the tip of budded cells. As a result, we were able to measure the sensitivity of our snap- and clip-tagss labelling system to localize and characterize conformational fluctuation of the CaM protein inside the cell.

However, the distance between snap- and clip-tagss cannot be quantified, because the lifetime decay of each pixel in the image cannot be extracted. Additionally, no single-molecule condition can be found inside the cell, therefore the calculated lifetime would be the average of all existence molecules in the selected region.

In conclusion, we show that the lifetime of the donor dye can be used to probe the conformational changes of CaM protein *in vitro* or *in vivo*. The shortening of the donor lifetime confirms our claim about the sensitivity of tag system to characterize the changing in distance or conformational fluctuation even using the ensemble lifetime method. However, it is difficult to obtain information about specific conformation with heterogeneity in subpopulation, which is known from smFRET measurement.

Summary

Protein interactions with other proteins, ligands, and ions trigger conformational changes that ultimately give rise to protein phenotype and activity. To date, the snap- and clip-tags labeling technique has been applied in the identification of protein co-localization and protein-protein interactions. It was found to be a specific and efficient labeling method *in vitro* and *in vivo*. Additionally, when these tags are used for Förster Resonance Energy Transfer (FRET) experiments, conformational changes within molecular complexes can be experimentally elucidated as well as protein interactions. The snap- and clip-tags labeling technique and bulk FRET methods have been used to study protein-protein interaction, but these have not sufficiently elucidated the formation of subpopulations during interaction yet. Therefore, we decided to combine snap- and clip-tags labeling and single molecule FRET (smFRET) for access to more details about the existence of protein subpopulations, particularly the diversity of individual conformational changes and distances upon binding.

This work introduces the application of the self-labelling SNAP- and CLIP-protein-tags, as tools for orthogonal fluorophore labeling for smFRET measurements. We focused on three model proteins, the Nbp2-SH3 domain, polyproline peptides, and CaM, to demonstrate that nanometer-scale protein conformational changes and various subpopulations of conformations can be observed by our approach. In addition to the *in vitro* smFRET measurements, we also demonstrate that *in vivo* FRET based fluorescence lifetime imaging microscopy (FLIM-FRET) measurements are also feasible with our approach.

The first model system which illustrates peptide-protein interaction analysis using bulk FRET technique was the yeast Nbp2-SH3 domain construct and the interaction of the SH3 domain with Bck1, Cla4, Ste20 and Pbs2 peptides. We observed a FRET change upon binding of the Ste20 and Pbs2 peptides to the SH3 domain, while no FRET change for Bck1 and Cla4 peptides was observed. Our data from these measurements are to some degree in disagreement with known conformational changes of Nbp2-SH3. This disagreement could be caused by the snap- and clip-tags on the protein and peptides. In addition, the minor conformational change of Nbp2-SH3 domain after interaction with peptides seems to be

difficult to measure by bulk FRET method.

Next, a model system of polyproline linkers with varying lengths between the snap- and clip-tags was used to demonstrate distance resolution. We in fact observed an overall increase in the distance measured by FRET as the number of polyproline was increased.

The third model system, the calmodulin (CaM) protein, was used to demonstrate the feasibility of observing externally triggered conformational changes. In this case, conformational changes were induced by adding variable concentrations of calcium ions and/or M13 peptide. Bulk FRET measurements of the CaM construct against various calcium concentrations showed that the snap- and clip-tags reduce binding affinity, but these ensemble measurements do not resolve conformational subpopulations. In contrast, we demonstrated the existence of subpopulations of CaM upon calcium binding by single-molecule FRET method as evidenced by FRET peak broadening. Binding between the CaM construct and the M13 peptide also displayed a higher FRET peak, which indicates the folding of the N- and C-terminals domains around the M13 peptide into a closed conformation.

In this study, we validated and demonstrated the utility of snap- and clip-tags for single-molecule FRET in a systematic fashion. We showed that individual subpopulations can be elucidated at the single-molecule level, which are not resolvable in bulk FRET measurements. This thesis examined and expanded the utility of snap- and clip-tags for measuring inter- and intra-molecular distances, understanding protein folding, and studying protein-interactions with single-molecule FRET.

Zusammenfassung

Interaktionen zwischen Proteinen, Proteinen und Liganden oder Proteinen und Ionen können Konformationsänderungen auslösen, die letztlich für den Phänotyp des Proteins und die Proteinaktivität verantwortlich sind. Zurzeit wird für die Identifikation von Protein Co-Lokalisationen und Protein-Protein Interaktionen anderem die snap- and clip-tags Labeling Technik verwendet. Sie erweist sich als eine spezifische und effiziente Labeling Methode sowohl *in vitro* als auch *in vivo*. Wenn diese Tags in Förster-Resonanz-Energietransfer Messungen (FRET) genutzt werden, lassen sich hiermit sowohl Konformationsänderungen innerhalb molekularer Komplexe als auch Protein-Interaktionen beobachten. Zwar wurden in der Vergangenheit bereits snap- and clip-tags und FRET Methoden in Ensemble Messungen genutzt, um Protein-Interaktionen zu untersuchen, diese konnten aber keine zufriedenstellenden Erkenntnisse über die Formationen von Sub-Populationen während der Interaktion zwischen Proteinen liefern.

In der vorliegenden Arbeit haben wir die snap- and clip-tags Labeling Technik und Einzelmolekül-FRET (smFRET), miteinander kombiniert, um mehr Details über die Existenz von Konformations-Teilpopulationen zu erfahren, insbesondere bezüglich der Diversität individueller Konformationsänderungen und Bindungslängen. Wir stellen die Anwendung von Self-Labeling SNAP- und CLIP-Protein-Tags als eine Methode für orthogonales Fluorophor-Labeling in smFRET Messungen vor. Um zu zeigen, dass sowohl Konformationsänderungen von Proteinen auf der Nanometer-Skala als auch unterschiedliche Teilpopulationen von Proteinkonformationen mit unserem Ansatz beobachtet werden können, haben wir uns auf Proteine mit drei verschiedenen Faltungstypen, die Nbp2-SH3 Domäne, Polyprolin-Peptide und das Protein Calmodulin (CaM), konzentriert. Neben den *in vitro* smFRET Messungen zeigen wir außerdem, dass unser Ansatz auch in FRET-basierten Fluoreszenz-Lebensdauer-Mikroskopie (FLIM-FRET) Messungen *in vivo* nutzbar ist.

Das erste Modell-System, das Peptid-Protein-Wechselwirkung unter Verwendung der Bulk-FRET-Technik veranschaulicht, war ein Hefe Nbp2-SH3-Domäne-Konstrukt und die Wechselwirkung der SH3-Domäne mit Bck1, CLA4, Ste20 und PBS2 Peptiden. Wir beobachteten eine FRET Änderung bei der Bindung der Ste20 und PBS2 Peptide an die SH3-Domäne, während kein FRET Änderung für

Bck1 und CLA4 Peptide beobachtet wurde. Unsere Daten aus diesen Messungen sind zu gewissem Grad in Widerspruch mit bekannten Konformationsänderungen der Wechsel der Nbp2-SH3-Domäne. Diese Uneinigkeit könnte durch die SNAP und CLIP-Tags auf dem Protein und den Peptiden verursacht werden. Darüber hinaus scheint die kleine Konformationsänderung der Nbp2-SH3-Domäne nach der Wechselwirkung mit Peptiden mit der Bulk-FRET-Methode schwierig zu messen zu sein.

Ein Modellsystem eines Polyprolin-Linkers mit variabler Länge zwischen SNAP- und CLIP-Tags wurde genutzt, um die Längenauflösung der Methode zu zeigen. Mit steigender Zahl von Prolinen konnte mittels FRET in der Tat ein vergrößerter Gesamtabstand beobachtet werden.

Das dritte Modellsystem, CaM, wurde genutzt, um zu zeigen, dass definierte Konformationsänderungen beobachtet werden können. Diese Konformationsänderungen wurden durch Zugabe verschiedener Konzentrationen von Kalziumionen und/oder M13 Peptiden induziert. Bulk-FRET Messungen des CaM Konstruktes mit unterschiedlichen Kalziumkonzentrationen zeigten, dass SNAP- und CLIP-Tags die Bindungsaffinität verringern. In diesen Ensemble-Messungen konnten jedoch keine Konformations-Teilpopulationen gezeigt werden. Im Gegensatz hierzu ließen sich mittels Einzelmolekül-FRET Teilpopulationen von CaM nach Kalziumbindung durch die Verbreiterung der FRET-Bande nachweisen. Die Bindung zwischen CaM Konstrukt und M13 Peptid zeigte ebenfalls ein höheres FRET-Signal. Dies deutet auf die Faltung der N- und der C-Terminus Domänen um das M13 Peptid in eine geschlossene Konformation hin.

In dieser Arbeit validieren und demonstrieren wir auf systematische Art und Weise die Nützlichkeit von SNAP- und CLIP-Tags für Einzelmolekül-FRET Messungen. Wir zeigen, dass individuelle Teilpopulationen auf Einzelmolekülebene beobachtet werden können, die mittels Bulk-FRET Messungen nicht aufgelöst werden können. Die Arbeit untersucht und erweitert die Anwendbarkeit von SNAP- und CLIP-Tags für Messungen von inter- und intramolekularen Abständen, um Proteinfaltung zu verstehen und Protein-Interaktionen mit Hilfe von FRET Einzelmolekülmessungen zu untersuchen.

Acronyms

A	Acceptor
AF	Alexa Fluor
ALEX	Alternating-Laser Excitation
Amp	Ampicillin
BC	Benzyl Cytosine
BG	Benzyl Guanine
CaM	Calmodulin
CLIP	CLIP-tag
D	Donor
DTT	Dithiothreitol
DY	Dyomics
<i>E. coli</i>	<i>Escherichia coli</i>
EGTA	Ethylene Glycol Tetraacetic Acid
FLIM	Fluorescence-Lifetime Imaging Microscopy
FRET	Förster Resonance Energy Transfer
GFP	Green Fluorescent Protein
hAGT	O6-alkylguanine-DNA-alkyltransferase
IPTG	Isopropyl β -D-1-thiogalactopyranoside
IRF	Instrument Response Function
LB	Lysogeny Broth
OD	Optical Density
PBS	Phosphate-Buffered Saline
PCR	Polymerase Chain Reaction
PP	Polyproline
PPI	Protein-Protein Interaction
SD	Synthetic Defined
SDS-PAGE	SDS Polyacrylamide Gel Electrophoresis
smFRET	Single-Molecule Förster Resonance Energy Transfer
SNAP	SNAP-tag
TCSPC	Time-Correlated Single Photon Counting

Bibliography

- [1] Keskin, O., Gursoy, A., Ma, B. & Nussinov, R. Principles of protein-protein interactions: what are the preferred ways for proteins to interact? *Chem. Rev.* 108, 1225-1244 (2008).
- [2] Lodish, H., Berk, A., Zipursky, S. L., Matsudaira, P., Baltimore, D., and Darnell, J. *Molecular Cell Biology*, W. H. Freeman & Company, New York, 5th edn (2004).
- [3] Lakowicz, J. R. *Principles of Fluorescence Spectroscopy*, 3rd ed.; Springer: New York, (2008).
- [4] Tirat, A., Freuler, F., Stettler, T., Mayr, L. M. & Leder, L. Evaluation of two novel tag-based labelling technologies for site-specific modification of proteins. *Int. J. Biol. Macromol.* 39, 66-76 (2006).
- [5] Gautier, A., Juillerat, A., Heinis, Ch., Corrêa, I. R., Kindermann, M., Beau-fils, F., Johnsson, K. An engineered protein tag for multiprotein labeling in living cells. *Chem. Biol.* 15, 128-136 (2008).
- [6] Jones, S. A., Shim, S.-H., He, J. & Zhuang, X. Fast, three-dimensional super-resolution imaging of live cells. *Nat. Methods* 8, 499-508 (2011).
- [7] Los, G. & Encell, L. HaloTag: a novel protein labeling technology for cell imaging and protein analysis. *ACS Chem. Biol.* 3, 373-382 (2008).
- [8] Watanabe, S., Mizukami, S., Hori, Y. & Kikuchi, K. Multicolor protein labeling in living cells using mutant β -lactamase-tag technology. *Bioconjug. Chem.* 21, 2320-6 (2010).
- [9] Gallagher, S. S., Sable, J. E., Sheetz, M. P. & Cornish, V. W. An *in vivo* covalent TMP-tag based on proximity-induced reactivity. *ACS Chem. Biol.* 4, 547-56 (2009).

- [10] Sun, X., Zhang, A., Baker, B., Sun, L., Howard, A., Buswell, J., Maurel, D., Masharina, A., Johnsson, K., Noren, C. J., Xu, M., Corrêa, Ivan R. Development of SNAP-tag fluorogenic probes for wash-free fluorescence imaging. *Chembiochem* 12, 2217-2226 (2011).
- [11] Hinner, M. J. & Johnsson, K. How to obtain labeled proteins and what to do with them. *Curr. Opin. Biotechnol.* 21, 766-76 (2010).
- [12] Keppler, A., Gendreizig, S., Gronemeyer, T., Pick, H., Vogel, H., Johnsson, K. A general method for the covalent labeling of fusion proteins with small molecules *in vivo*. *Nat. Biotechnol.* 21, 86-89 (2003).
- [13] Keppler, A., Pick, H., Arrivoli, C., Vogel, H. & Johnsson, K. Labeling of fusion proteins with synthetic fluorophores in live cells. *Proc. Natl. Acad. Sci. U. S. A.* 101, 9955-9959 (2004).
- [14] Angelica, M. D. & Fong, Y. Distance Mapping in Proteins Using Fluorescence Spectroscopy: The Tryptophan-Induced Quenching (TriQ) Method. *Biochemistry*, 16; 49(45): 9722-9731 (2010).
- [15] Gerson, S. L. MGMT: its role in cancer aetiology and cancer therapeutics. *Nat. Rev. Cancer* 4, 296-307 (2004).
- [16] Gemmill, K. B., Diaz, S. A., Blanco-Canosa, J. B., Deschamps, J. R., Pons, T., Liu, H. W., Deniz, A., Melinger, J., Oh, E., Susumu, K., Stewart, M. H., Hastman, D. A., North, S. H., Delehanty, J. B., Dawson, P. E., Medintz, I. L.. Examining the Polyproline Nanoscopic Ruler in the Context of Quantum Dots. *Chem. Mater.* 27, 6222-6237 (2015).
- [17] Correa, I. R., Jr., Baker, B., Zhang, A., Sun, L., Provost, C. R., Lukinavicius, G., Reymond, L., Johnsson, K., Xu, M.-Q. Substrates for Improved Live-Cell Fluorescence Labeling of SNAP-tag. *Curr Pharm Des.* 19(30), 5414-20 (2013).
- [18] Babu, Y. S., Sack, J. S., Greenhough, T. J., Bugg, C. E., Means, A. R., Cook, W. J. Three-dimensional structure of calmodulin. *Nature* 315, 37-40 (1985).
- [19] Park, H. Y., Kim, S. a., Korlach, J., Rhoades, E., Kwok, L. W., Zipfel, W. R., Waxham, M N., Webb, W. W. Pollack, L. Conformational changes of calmodulin upon Ca²⁺ binding studied with a microfluidic mixer. *Proc. Natl. Acad. Sci. U. S. A.* 105, 542-547 (2008).

- [20] Brun, M. A., Tan, K.-T., Nakata, E., Hinner, M. J. & Johnsson, K. Semisynthetic fluorescent sensor proteins based on self-labeling protein tags. *J. Am. Chem. Soc.* 131, 5873-5884 (2009).
- [21] Provost, C. R. & Sun, L. Fluorescent labeling of COS-7 expressing SNAP-tag fusion proteins for live cell imaging. *J. Vis. Exp.* 1-4 (2010).
- [22] Gorur, A., Leung, CM., Jorgens, D., Tauscher, A., Remis, JP., Ball, DA., Chhabra, S., Fok, V., Geller, JT., Singer, M., Hazen, TC., Juba, T., Elias, D., Wall, J., Biggin, M., Downing, KH., Auer, M. Subcellular Localization of Proteins in the Anaerobic Sulfate Reducer *Desulfovibrio vulgaris* via SNAP-tag Labeling and Photoconversion. *Microsc. Microanal.* 16, 4-5 (2010).
- [23] Ward, R. J., Padiani, J. D. & Milligan, G. Ligand-induced internalization of the orexin OX(1) and cannabinoid CB(1) receptors assessed via N-terminal SNAP and CLIP-tagging. *Br. J. Pharmacol.* 162, 1439-1452 (2011).
- [24] Cole, N. B. & Donaldson, J. G. Releasable SNAP-tag probes for studying endocytosis and recycling. *ACS Chem. Biol.* 7, 464-469 (2012).
- [25] Stoehr, K. & Siegbert, D. Quenched substrates for live-cell labeling of SNAP-tagged fusion proteins with improved fluorescent background. *Anal. Chem.* 82, 8186-8193 (2010).
- [26] Parsons, S. J. & Parsons, J. T. Src family kinases, key regulators of signal transduction. *Oncogene* 23, 7906-7909 (2004).
- [27] Birge, R. B., Knudsen, B. S., Besser, D. & Hanafusa, H. SH2 and SH3-containing adaptor proteins: redundant or independent mediators of intracellular signal transduction. *Genes Cells* 1, 595-613 (1996).
- [28] Lowenstein, E. J., Daly R. J., Batzer A. G., Li W., Margolis B., Lammers R., Ullrich A., Skolnik E. Y., Bar-Sagi D., Schlessinger J. The SH2 and SH3 domain-containing protein GRB2 links receptor tyrosine kinases to ras signaling. *Cell* 70, 431-442 (1992).
- [29] Gorelik, M., Stanger, K., Davidson, A. R. A Conserved residue in the yeast Bem1p SH3 domain maintains the high level of binding specificity required for function. *J. Biol. Chem.* 286, 19470-19477 (2011).
- [30] Heuer, K., Kofler, M., Langdon, G., Thiemke, K., Freund, C. Structure of a helically extended SH3 domain of the T cell adapter protein ADAP. *Structure* 12, 603-610 (2004).

- [31] Lougheed, J. C., Holton, J. M., Alber, T., Bazan, J. F., Handel, T. M. Structure of melanoma inhibitory activity protein, a member of a recently identified family of secreted proteins. *Proc. Natl. Acad. Sci. U. S. A.* 98, 5515-5520 (2001).
- [32] Larson, S. M. & Davidson, A. R. The identification of conserved interactions within the SH3 domain by alignment of sequences and structures. *Protein Sci.* 9, 2170-2180 (2000).
- [33] Fernandez-Ballester, G., Blanes-Mira, C., Serrano, L. The Tryptophan Switch: Changing Ligand-binding Specificity from Type I to Type II in SH3 Domains. *J. Mol. Biol.* 335, 619-629 (2004).
- [34] Gorelik, M. Investigation of SH3 Domain Specificity through the Study of Cross-reactive Domains from Yeast Proteins Nbp2p and Bem1p, Ph.D. thesis. (2012).
- [35] Tong, A. H. Y., Drees B., Nardelli G., Bader G. D., Brannetti B., Castagnoli L., Evangelista M., Ferracuti S., Nelson B., Paoluzi S., Quondam M., Zucconi A., Hogue C. W., Fields S., Boone C., Cesareni G. A combined experimental and computational strategy to define protein interaction networks for peptide recognition modules. *Science* 295, 321-324 (2002).
- [36] Landgraf, C., Panni S., Montecchi-Palazzi L., Castagnoli L., Schneider-Mergener J., Volkmer-Engert R., Cesareni G. Protein interaction networks by proteome peptide scanning. *PLoS Biol.* 2, 0094-0103 (2004).
- [37] Schimmel, P. & Flory, P. Conformational energy and configurational statistics of poly-L-proline. *Proc. Natl. Acad. Sci. U. S. A.* 58, 52-59 (1967).
- [38] Horng, J. C. & Raines, R. T. Stereoelectronic effects on polyproline conformation. *Protein Sci.* 15, 74-83 (2006).
- [39] Shi, L., Holliday, A. E., Shi, H., Zhu, F., Ewing, M. A., Russell, D. H., Clemmer, D. E. Characterizing intermediates along the transition from polyproline I to polyproline II using ion mobility spectrometry-mass spectrometry. *J. Am. Chem. Soc.* 136, 12702-12711 (2014).
- [40] Naziga, E. B., Schweizer, F. & Wetmore, S. D. Solvent interactions stabilize the polyproline II conformation of glycosylated oligoprolines. *J. Phys. Chem. B* 117, 2671-81 (2013).
- [41] Stryer, L. & Haugland, R. Energy transfer: a spectroscopic ruler. *Proc. Natl. Acad. Sci. U. S. A.* 58, 719-726 (1967).

- [42] Best, R. B., Merchant, K. a., Gopich, I. V., Schuler, B., Bax, A., Eaton, W. a. Effect of flexibility and cis residues in single-molecule FRET studies of polyproline. *Proc. Natl. Acad. Sci. U. S. A.* 104, 18964-18969 (2007).
- [43] Eldik, L. J. Van & Watterson, D. M. *Calmodulin and signal transduction*. Academic Press; New York: 1998. (1998).
- [44] Linse, S., Thulin, E. & Sellers, P. Disulfide bonds in homodimers and heterodimers of ef-hand subdomains of calbindin-d(9k) - stability, calcium-binding, and nmr-studies. *Protein Sci.* 2, 985-1000 (1993).
- [45] Kukic, P., Lundström, P., Camilloni, C., Evenäs, J., Akke, M., Vendruscolo, M. Structural insights into the calcium-mediated allosteric transition in the C-terminal domain of calmodulin from NMR measurements. *Biochemistry*, 55, 19-28 (2016).
- [46] Ababou, A. & Zaleska, M. Electrostatics effects on Ca^{2+} binding and conformational changes in EF-hand domains: Functional implications for EF-hand proteins. *Arch. Biochem. Biophys.* 587, 61-69 (2015).
- [47] Ikura, M., Barbato, G., Klee, C. B. & Bax, A. Solution structure of calmodulin and its complex with a myosin light chain kinase fragment. *Cell Calcium* 13, 391-400 (1992).
- [48] Meador, W. E., Means, A. R. & Quijcho, F. A. Modulation of calmodulin plasticity in molecular recognition on the basis of x-ray structures. *Science* 262, 1718-1721 (1993).
- [49] Förster, T. Zwischenmolekulare Energiewanderung und Fluoreszenz. *Ann. Phys.* 437, 55-75 (1948).
- [50] Regoes, A. & Hehl, A. B. SNAP-tag mediated live cell labeling as an alternative to GFP in anaerobic organisms. *Biotechniques* 39, 809-10, 812 (2005).
- [51] Kapanidis, A. N., Lee, N. K., Laurence, T. a., Doose, S., Margeat, E., Weiss, S. Fluorescence-aided molecule sorting: analysis of structure and interactions by alternating-laser excitation of single molecules. *Proc. Natl. Acad. Sci. U. S. A.* 101, 8936-8941 (2004).
- [52] Lee, N. K., Kapanidis, A. N., Wang, Y., Michalet, X., Mukhopadhyay, J., Ebright, R. H., Weiss, S. Accurate FRET Measurements within Single Diffusing Biomolecules Using Alternating-Laser Excitation. *Biophys. J.* 88, 2939-2953 (2005).

- [53] Deniz, A. A., Dahan, M., Grunwell, J. R., Ha, T., Faulhaber, A. E., Chemla, D. S., Weiss, S., Schultz, P. G. Single-pair fluorescence resonance energy transfer on freely diffusing molecules: observation of Förster distance dependence and subpopulations. *Proc. Natl. Acad. Sci. U. S. A.* 96, 3670-5 (1999).
- [54] Rieger, R. F. Investigation of a Folding Intermediate of RNase H Using Single Molecule FRET Spectroscopy, Ph.D. thesis. (2012).
- [55] Elangovan, M., Day, R. N. Periasamy, A. Nanosecond fluorescence resonance energy transfer-fluorescence lifetime imaging microscopy to localize the protein interactions in a single living cell. *J. Microsc.* 205, 3-14 (2002).
- [56] Roy, R., Hohng, S. Ha, T. A practical guide to single-molecule FRET. *Nat. Methods* 5, 507-516 (2008).
- [57] Llères, D., Swift, S. Lamond, A. I. Detecting protein-protein interactions *in vivo* with FRET using multiphoton fluorescence lifetime imaging microscopy (FLIM). *Curr. Protoc. Cytom.* Chapter 12, Unit12.10 (2007).
- [58] Gietz, R. D. & Schiestl, R. H. high-efficiency yeast transformation using the LiAc/SS carrier DNA/PEG method. *Nat. Protoc.* 2, 38-41 (2007).
- [59] Stagge, F., Mitronova, G. Y., Belov, V. N., Wurm, C. a. & Jakobs, S. Snap-, CLIP- and Halo-Tag Labelling of Budding Yeast Cells. *PLoS One* 8, 1-9 (2013).
- [60] Manz, C. Einzelmolekülfluoreszenzexperimente zur Untersuchung biomolekularer Dynamik mit Detektion in mehreren Farbkanälen. Karlsruhe Institute of Technology, Diploma thesis. (2013).
- [61] Grossman, M., Sela-Passwell, N., Sagi, I. Achieving broad molecular insights into dynamic protein interactions by integrated structural-kinetic approaches. *Curr. Opin. Struct. Biol.* 21, 678-685 (2011).
- [62] Zuiderweg, E. R. P. Mapping Protein-Protein Interactions in Solution by NMR Spectroscopy. *Biochemistry* 41, 1-7 (2002).
- [63] Elbaz, Y., Tayer, N., Steinfels, E. Substrate-induced tryptophan fluorescence changes in EmrE, the smallest ion-coupled multidrug transporter. *Biochemistry* 7369-7377 (2005).
- [64] Zhang, Z. R., Song, B., McCarty, N. A. State-dependent chemical reactivity of an engineered cysteine reveals conformational changes in the outer

- vestibule of the cystic fibrosis transmembrane conductance regulator. *J. Biol. Chem.* 280, 41997 (2005).
- [65] Gorelik M. & Davidson A. R. Distinct peptide binding specificities of Src homology 3 (SH3) protein domains can be determined by modulation of local energetics across the binding interface. *J Biol Chem.* 287(12), 9168-77 (2013).
- [66] Stephanopoulos, N. & Francis, M. B. Choosing an effective protein bioconjugation strategy. *Nat. Chem. Biol.* 7, 876-884 (2011).
- [67] Ishitsuka, Y., Azadfar, N., Kobitski, A. Y., Nienhaus, K., Johnsson, N., Nienhaus, G. U. Evaluation of Genetically Encoded Chemical Tags as Orthogonal Fluorophore Labeling Tools for Single-Molecule FRET Applications. *J. Phys. Chem. B* 119, 6611-9 (2015).
- [68] Doose, S., Neuweiler, H., Barsch, H. & Sauer, M. Probing polyproline structure and dynamics by photoinduced electron transfer provides evidence for deviations from a regular polyproline type II helix. *Proc. Natl. Acad. Sci. U. S. A.* 104, 17400-17405 (2007).
- [69] Moradi, M., Babin, V., Roland, C., Darden, T. A. & Sagui, C. Conformations and free energy landscapes of polyproline peptides. *Proc. Natl. Acad. Sci. U. S. A.* 106, 20746-20751 (2009).
- [70] Haenni, D., Zosel, F., Reymond, L., Nettels, D., and Schuler. B. Intramolecular Distances and Dynamics from the Combined Photon Statistics of Single-Molecule FRET and Photoinduced Electron Transfer. *J. Phys. Chem. B.* 117, 13015-28 (2013).
- [71] Schuler, B., Lipman, E. A., Steinbach, P. J., Kumke, M. & Eaton, W. A. Polyproline and the 'spectroscopic ruler' revisited with single-molecule fluorescence. *Proc. Natl. Acad. Sci. U. S. A.* 102, 2754-2759 (2005).
- [72] Schuler, B., Lipman, E. A. & Eaton, W. A. Probing the free-energy surface for protein folding with single-molecule fluorescence spectroscopy. *Nature* 419, 743-7 (2002).
- [73] Rüttinger, S., Macdonald, R., Krüner, B., Koberling, F., Roos, M., Hildt, E. Accurate single-pair Förster resonant energy transfer through combination of pulsed interleaved excitation, time correlated single-photon counting, and fluorescence correlation spectroscopy. *J. Biomed. Opt.* 11, 024012 (2006).

- [74] Hoefling, M., Lima, N., Haenni, D., Seidel, C. a. M., Schuler, B., Grubmüller, H. Structural heterogeneity and quantitative FRET efficiency distributions of polyprolines through a hybrid atomistic simulation and Monte Carlo approach. *PLoS One* 6, e19791 (2011).
- [75] Eggeling, C., Berger, S., Brand, L., Fries, J. R., Schaffer, J., Volkmer, A., Seidel, C. a. Data registration and selective single-molecule analysis using multi-parameter fluorescence detection. *J. Biotechnol.* 86, 163-180 (2001).
- [76] Zander, C., Sauer, M., Drexhage, K. H., Ko, D. S., Schulz, A., Wolfrum, J., Brand, L., Eggeling, C., Seidel, C. A. M. Detection and characterization of single molecules in aqueous solution. *Appl. Phys. B Laser Opt.* 63, 517-523 (1996).
- [77] Stigler, J. & Rief, M. Calcium-dependent folding of single calmodulin molecules. *Proc. Natl. Acad. Sci. U. S. A.* 109, 17814-17819 (2012).
- [78] Kim, J., Seo, M-H., Lee, S., Cho, K., Yang, A., Woo, K., Kim, H-S., Park, H-S. Simple and efficient strategy for site-specific dual labeling of proteins for single-molecule fluorescence resonance energy transfer analysis. *Anal. Chem.* 85, 1468-1474 (2013).
- [79] Peersen, O. B., Madsen, T. S. & Falke, J. J. Intermolecular tuning of calmodulin by target peptides and proteins: differential effects on Ca^{2+} binding and implications for kinase activation. *Protein Sci.* 6, 794-807 (1997).
- [80] Chen, Y. & Hummer, G. Slow Conformational Dynamics and Unfolding of the Calmodulin C-Terminal Domain Slow Conformational Dynamics and Unfolding of the Calmodulin C-Terminal Domain. *Communication* 2-4 (2007).
- [81] Brockerhoff, S. E. & Davis, T. N. Calmodulin concentrates at regions of cell growth in *Saccharomyces cerevisiae*. *J. Cell Biol.* 118, 619-29 (1992).
- [82] Johnsson, N. & Johnsson, K. A fusion of disciplines: chemical approaches to exploit fusion proteins for functional genomics. *ChemBiochem* 4, 803-10 (2003).
- [83] Pegg, A. E., Boosalis, M., Samson, L., Mosche, R. C., Byers, T. L., Swenn, K., Dolanl, M. E. Mechanism of Inactivation of Human O^6 -Alkylguanine-DNA Alkyltransferase by O^6 -Benzylguanine. *Biochemistry* 1993, 32, 11998-12006 (1993).

- [84] Reinhard, J., Hull, W. E., von der Lieth, C. W., Eichhorn, U., Kliem, H. C., Kaina, B., Wiessler, M. Monosaccharide-linked inhibitors of O(6)-methylguanine-DNA methyltransferase (MGMT): synthesis, molecular modeling, and structure-activity relationships. *J. Med. Chem.* 44, 4050-4061 (2001).
- [85] Gronemeyer, T., Chidley, C., Juillerat, A., Heinis, C. & Johnsson, K. Directed evolution of O6-alkylguanine-DNA alkyltransferase for applications in protein labeling. *Protein Eng. Des. Sel.* 19, 309-316 (2006).
- [86] Daniels, D. S., Mol, C. D., Arvai, A. S., Kanugula, S., Pegg, A. E., Tainer, J. A. Active and alkylated human AGT structures: a novel zinc site, inhibitor and extrahelical base binding. *EMBO J.* 19, 1719-1730 (2000).
- [87] Guengerich, F. P., Fang, Q., Liu, L., Hachey, D. L. & Pegg, A. E. O6-alkylguanine-DNA alkyltransferase: low pKa and high reactivity of cysteine 145. *Biochemistry* 42, 10965-10970 (2003).
- [88] Daniels, D. S., Woo, T. T., Luu, K. X., Noll, D. M., Clarke, N. D., Pegg, A. E., Tainer, J. A. DNA binding and nucleotide flipping by the human DNA repair protein AGT. *Nat. Struct. Mol. Biol.* 11, 714-720 (2004).
- [89] Rasimas, J. J., Pegg, A. E. & Fried, M. G. DNA-binding mechanism of O6-alkylguanine-DNA alkyltransferase. Effects of protein and DNA alkylation on complex stability. *J. Biol. Chem.* 278, 7973-7980 (2003).
- [90] Gronemeyer, T. Degredation studies and directed evolution of the alkylguanine-DNA-alkyltransferase, Ph.D. thesis. (2005).
- [91] Schena, A., Griss, R. & Johnsson, K. Modulating protein activity using tethered ligands with mutually exclusive binding sites. *Nat. Commun.* 6, 7830 (2015).
- [92] Wille, T., Barlag, B., Jakovljevic, V., Hensel, M., Sourjik, V., Gerlach, R. G. A gateway-based system for fast evaluation of protein-protein interactions in bacteria. *PLoS One* 10, 1-18 (2015).
- [93] Crivici, A. & Ikura, M. Molecular and structural basis of target recognition by calmodulin. *Annu. Rev. Biophys. Biomol. Struct.* 24, 85-116 (1995).
- [94] Lukas, T. J., Burgess, W. H., Prendergast, F. G., Lau, W. & Watterson, D. M. Calmodulin binding domains: characterization of a phosphorylation and calmodulin binding site from myosin light chain kinase. *Biochemistry* 25, 1458-1464 (1986).

-
- [95] Payne, M. E., Fong, Y. L., Ono, T., Colbran, R. J., Kemp, B. E., Soderling, T. R., Means, A. R. Calcium / Calmodulin-dependent Protein Kinase II. *J. Biol. Chem.* 263, 7190-7195 (1988).
- [96] Novack, J. P., Charbonneau, H., Bentley, J. K., Walsh, K. A. & Beavo, J. A. Sequence comparison of the 63-, 61-, and 59-kDa calmodulin-dependent cyclic nucleotide phosphodiesterases. *Biochemistry* 30, 7940-7947 (1991).
- [97] Steiner, J. P., Walke, H. T. & Bennett, V. Calcium/calmodulin inhibits direct binding of spectrin to synaptosomal membranes. *J. Biol. Chem.* 264, 2783-2791 (1989).
- [98] Collins, K., Sellers, J. R. & Matsudaira, P. Calmodulin dissociation regulates brush border myosin I (110-kD-calmodulin) mechanochemical activity *in vitro*. *J. Cell Biol.* 110, 1137-1147 (1990).

Appendix

Buffers and Solutions

Table A.1: The protocol of buffers and solutions.

Buffer	Protocol
LB (lysogeny broth) medium	10 g/l tryptone, 5 g/l yeast extract, 10 g/l NaCl
Yeast YPD medium	10 g/l yeast extract, 20 g/l peptone, pH 5.8. The medium was autoclaved for sterilization and 40% (w/v) filtered glucose was added to the medium at ≈ 65 °C after sterilization to obtain 2% (w/v) glucose as final concentration.
Yeast medium (500 ml)	25 ml of 20x SD (Synthetic Defined) -minimal medium: 134 g/l yeast nitrogen base without amino acids (Formedium) 5 ml of 100x amino acid stock solution: 0.6% (w/v) L-isoleucine, 0.2% (w/v) L-arginine, 0.4% (w/v) L-lysine, 0.6% (w/v) L-phenylalanine, 0.1% (w/v) L-threonine, 0.1% (w/v) L-methionine 2.5 ml of 1% (w/v) adenine: 5 g adenine, 5 ml 10 M NaOH in 500 ml H ₂ O 5 ml of 100x L-histidine: 1 g L-histidine added to 500 ml H ₂ O 5 ml of 100x L-leucine: 3 g L-leucine added to 500 ml H ₂ O 5 ml of 100x L-tryptophan: 2 g L-tryptophan added to 500 ml H ₂ O 2.5 ml of 1% (w/v) uracil stock solution (w/v) All solutions were mixed and H ₂ O was filled to 475 ml; the solution was sterilized by autoclaving. After the medium had cooled down to 65 °C, 25 ml of 40% (w/v), filtered glucose was added (2% glucose final).

continued ...

Table A.1 Continued from previous page

Buffer	Protocol
10x TE buffer	0.1 M Tris-Cl, 10 mM Ethylenediaminetetraacetic acid (EDTA), pH 8.0
100 mM LiAc/1xTE	10% (w/v) 1 M LiAc, 10% 10x TE and 80% H ₂ O
lysis buffer	50 mM Sodium Phosphate buffer, 10 mM imidazole, 500 mM NaCl, pH 7.4, 1 mg/ml lysozyme, protease inhibitor cocktail (according to the manufacturer's instruction, Sigma Aldrich, Munich) and 0.5% Triton X-100
Washing buffer	50 mM KH ₂ PO ₄ , 20 mM imidazole, 300 mM NaCl, pH 7.5
Elution buffer	50 mM KH ₂ PO ₄ , 200 mM imidazole, 300 mM NaCl, pH 8.0

List of Primers

Table A.2: List of primers.

Name	bp	Oligo Sequence	T _m	Intended Purpose
6PP F	18	GATCCCGCCGCCACCG CCACCGC		6PP construct in pET51b vector
12PP F	36	GATCCCGCCGCCACCGC CACCGCCGCCACCAC CGCCGC		construct in pET51b vector
20PP F	60	GATCCCGCCTCCGCCACC ACCGCCACCTCCTCCACC GCCTCCTCCTCCGCCGCC GCCACCGCCGC		20PP construct in pET51b vector

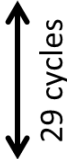
continued ...

Table A.2 Continued from previous page

Name	bp	Oligo Sequence	T _m	Intended Purpose
24PP F	72	GATCCCGCCTCCGCCACC ACCGCCACCTCCTCCACC TCCGCTCCACCGCCTCC TCCTCCGCCGCCGCCACC GCCGC		24PP construct in pET51b vec- tor
T7-981079	18	TAATACGACTCACTATAG	55 °C	screening of PP constructs
PP-CLIP-tag	21	TTGTCCATCTCGAGCGG CGGT	55 °C	PCR screening of PP Con- structs
Not1-pRS313 F	33	GGTGGCGGCCGCATGGA TAAAGACTGCGAAATG	57 °C	PP construct in yeast vector
Apa1-pRS313 R	27	TACCGGGCCCTTATCCAC CCAGACCCG	57 °C	PP construct in yeast vector
CLIP-Cys-C- term F	28	GGCTTGGAAGATCTTG CTAATGAGGCC	60 °C	Cysteine mu- tation on C-terminal CLIP-tag
F24C F	26	AGCACGGCCGAATGCGG GTCGACTAT	60 °C	Cysteine mu- tation on N-terminal CLIP-tag
BamH1-CaM F	36	GGCCGGATCCATGACCA ACTGACAGAAGAGCAGA TT	53 °C	CaM construct in pET51b vector
Xho1-CaM R	36	CATCTCGAGCTTTGCTGT CATCATTTGTACAAACTC	53 °C	CaM construct in pET51b vector

PCR program

Step	Temperature	Duration (minutes)
Initial denaturation	95°C	2
Denaturation	95°C	0.5
Annealing	42-65°C	0.5
Extension	72°C	1 min/kb
Final extension	72°C	5
Soak	4°C	indefinite



29 cycles

Figure A.1: PCR program.

PCR-Master

Necessities	Final volume	Final concentration
5X green GoTaq reaction buffer	10 μ l	1X (1.5 mM MgCl ₂) ²
dNTP Mix, 2mM each	1.25 μ l	0.2 mM each dNTP
Upstream primer	0.16 μ l	1 μ M
Downstream primer	0.16 μ l	1 μ M
GoTaq DNA Polymerase (5u/ μ l)	0.25 μ l	1.25 u
Template DNA	2 μ l	\leq 0.5 μ g/50 μ l
Nuclease-Free water to	36.2 μ l	

Figure A.2: PCR-Master Mix.

SNAP-tag sequence

MDKDCMKR T T L D S P L G K L E L S G C E Q G L H E I I F L G K G
 T S A A D A V E V P A P A A V L G G P E P L M Q A T A W L N A Y F H Q P
 E A I E E F P V P A L H H P V F Q Q E S F T R Q V L W K L L K V V K F G
 E V I S Y S H L A A L A G N P A A T A A V K T A L S G N P V P I L I P C H
 R V V Q G D L D V G G Y E G G L A V K E W L L A H E G H R L G K P G L G

CLIP-tag sequence

MDKDCMKR T T L D S P L G K L E L S G C E Q G L H E I I F L G
K G T S A A D A V E V P A P A A V L G G P E P L I Q A T A W L N A Y
F H Q P E A I E E F P V P A L H H P V F Q Q E S F T R Q V L W K L L K
V V K F G E V I S E S H L A A L V G N P A A T A A V N T A L D G N P V
P I L I P C H R V V Q G D S D V G P Y L G G L A V K E W L L A H E G H
R L G K P G L G G

CaM sequences

M H D Q L T E E Q I A E F K E A F S L F D K D G D G T I T T K E L G T
V M R S L G Q N P T E A E L Q D M I N E V D A D G N G T I Y F P E F L
T M M A R K M K D T D S E E E I R E A F R V F D K D G N G Y I S A A
Q L R H V M T N L G E K L T D E E V D E M I R E A D I D G D G Q V N
Y E E F V Q M M T A K

Cys-CLIP

H H H H H H S S A Met A S T A E C G S T Met D K D C E Met K R T T L D
S P L G K L E L S G C E Q G L H E I I F L G K G T S A A D A V E V P A
P A A V L G G P E P L Met Q A T A W L N A Y F H Q P E A I E E F P V P
A L H H P V F Q Q E S F T R Q V L W K L L K V V K F G E V I S Y S H L
A A L A G N P A A T A A V K T A L S G N P V P I L I P C H R V V Q G D
L D V G G Y E G G L A V K E W L L A H E G H R L G K P G L G R S Stop

CLIP-Cys

H H H H H H S S A Met A S T A E F G S T Met D K D C E Met K R T T L D
S P L G K L E L S G C E Q G L H E I I F L G K G T S A A D A V E V P A
P A A V L G G P E P L Met Q A T A W L N A Y F H Q P E A I E E F P V P
A L H H P V F Q Q E S F T R Q V L W K L L K V V K F G E V I S Y S H L
A A L A G N P A A T A A V K T A L S G N P V P I L I P C H R V V Q G D
L D V G G Y E G G L A V K E W L L A H E G H R L G K P G L G R C Stop

15 amino acid peptide sequence in SNAP- 15 aa-CLIP construct

G R L E V L F Q G P K A F L E

15 amino acid peptide

G R L E V L F Q G P R A F L C

Dye Properties

Table A.3: Spectral characterization of dyes.

Dye	$MW(g/mol)$	$\lambda_{abs}(nm)$	$\lambda_{em}(nm)$	$\epsilon(M^{-1}cm^{-1})$	CF_{280}
SNAP-Surface Alexa Fluor 546		558	574	104000	0.21
CLIP-Surface 647	877	653	672	250000	0.03
Alexa Fluor 647 C2 Maleimide	1300	650	665	250000	0.03
CLIP-Surface 547	851	554	568	150000	0.11
SNAP-Cell TMR-Star	677.1	554	580	91000	
CLIP-Cell 430	473.5	421	484	45000	

Absorbance Spectra and Calculated Labeling Efficiencies of Labeled Constructs

Labeling efficiency can be calculated based on these equations step by step:

$$1. A_{A546,Corr.} = A_{A546} - (A_{DY647} * CF_{571})$$

$$2. \text{Protein Concentration (M)} = \frac{A_{280} - (A_{A546,Corr.} * CF_{280}) - (A_{DY647} * CF_{280})}{\epsilon_{Protein}}$$

$$3. \frac{Dye}{Protein} (\%) = \frac{A_{A546,Corr.}}{\epsilon_{A546} * ProteinConcentration(M)} * 100$$

$$4. \frac{\text{Dye}}{\text{Protein}} (\%) = \frac{A_{\text{DY647}}}{\epsilon_{\text{DY647}} * \text{Protein Concentration (M)}} * 100$$

Table A.4: Correction factors of dyes at 280 and 571 nm.

Dyes	Full Name	CF_{280}	CF_{571}
SS-A546	SNAP-Surface-Alexa Fluor 546	0.12	
CS-DY647	CLIP-Surface-DY 647	0.03	0.1
CS-DY547	CLIP-Surface 547	0.08	

Table A.5: Calculated labeling efficiencies for each constructs. *Due to the protein impurity, the absorbance of the protein at maxima 280 nm is high; therefore, the calculated degree of protein labeling based on this absorbance would be lower than the actual.

		ϵ	Abs. l (nm)	Abs. (A.U.)	Corr.Abs. (A.U.)	Conc. (mM)	dye/protein (%)
S-6PP-C	protein	46325	280	0.06	0.05	1.1	
	SS-A546	112000	555	0.05		0.5	41
	CS-DY647	237000	655	0.09		0.4	34
S-12PP-C	protein	46325	280	0.14	0.11	2.3	
	SS-A546	112000	555	0.19		1.7	74
	CS-DY647	237000	655	0.32		1.3	58
S-20PP-C	protein	46325	280	0.268	0.22	4.6	
	SS-A546	112000	555	0.33		3.0	64
	CS-DY647	237000	655	0.44		1.8	40
S-24PP-C	protein	46325	280	0.16	0.12	2.7	
	SS-A546	112000	555	0.21		1.9	72

continued ...

Table A.5 Continued from previous page

		ϵ	Abs. 1 (nm)	Abs. (A.U.)	Corr.Abs. (A.U.)	Conc. (mM)	dye/protein (%)
	CS-DY647	237000	655	0.38		2	60
S-15 aa-C	protein	40825	280	0.3	0.28	6.93	
	SS-A546	112000	555	0.13		1.1	16
	CS-DY647	237000	655	0.23		1.0	14
S-CaM-C	protein	45295	280	0.35	0.30	6.6	
	SS-A546	112000	555	0.26		2	35
	CS-DY647	237000	655	0.76		3.2	48
15 aa*	protein	250	280			10.00	
	A546	112000	555	0.53		4.8	48
	A647	237000	655	0.84		3.5	35

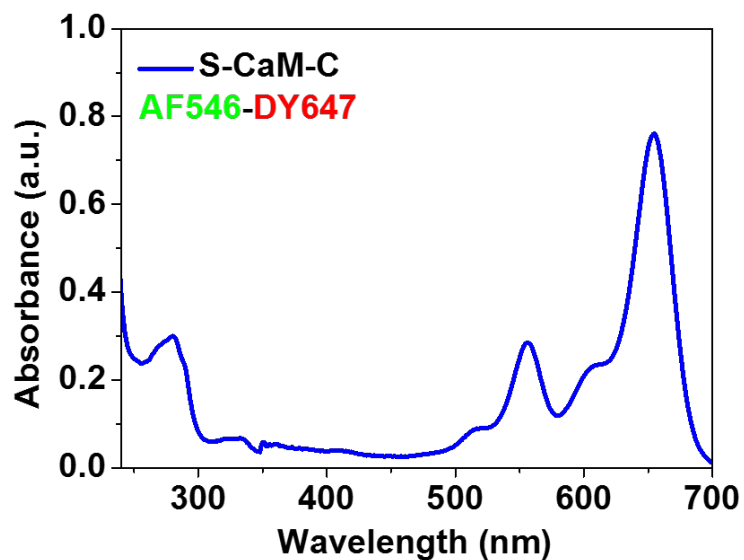


Figure A.3: Absorbance spectrum of labeled CaM construct.

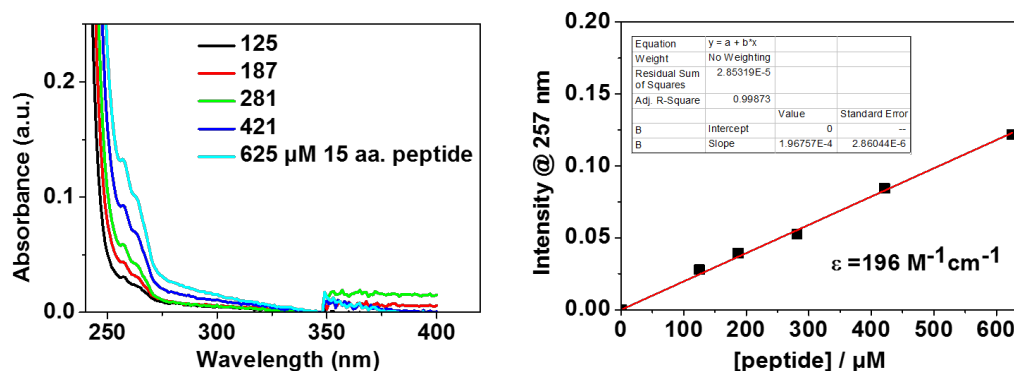


Figure A.4: Extinction coefficient determination of the 15 aa peptide. (Left) Absorbance spectra of the 15 aa peptide at different concentration. (Right) the intensity at 257 nm was plotted against the concentration of peptide. The points were linearly fitted and the extinction coefficient of $196 \text{ M}^{-1}\text{cm}^{-1}$ was extracted from slope.

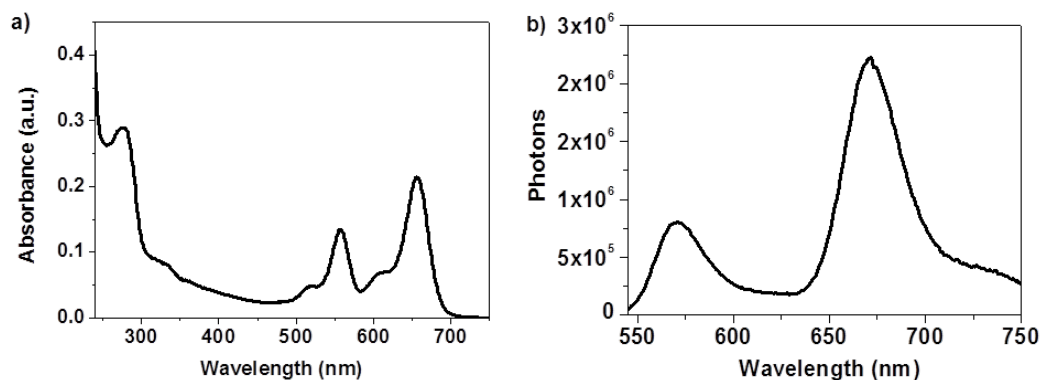


Figure A.5: Absorbance (a) and fluorescence spectra (b) of the labeled 15-aa construct labeled with A546 and DY647. The wavelength range between 630-700 nm shows the acceptor FRET emission upon donor excitation.

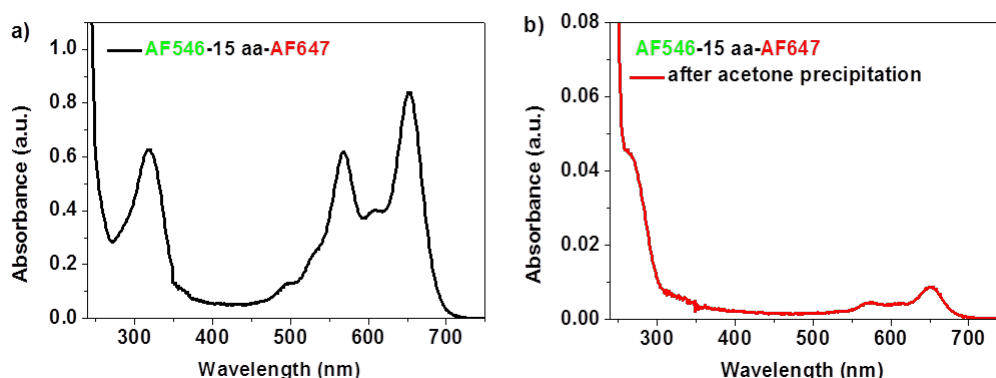


Figure A.6: The synthesized and labeled 15-aa peptide was dissolved first in dimethylformamide (DMF) and then in PBS buffer without further purification. However, an unexpected absorbance peak at 320 nm was observed (a). Therefore, the buffer in the peptide solution was exchanged with fresh PBS buffer using the acetone precipitation technique (b). The impurity may have originated from the contaminated buffer, but more likely from the peptide synthesis procedure. After exchanging the buffer, the absorbance at 320 nm was diminished. Then, the absorbance and fluorescence spectra of the 15-aa linker in fresh PBS buffer were measured in order to determine the labeling efficiency and FRET signal, respectively.

Single-Molecule FRET Histograms

In this section, three individual smFRET histograms and their corresponding fit parameters for PP (6-, 12-, 20-, 24-residues) constructs and CaM construct in different conditions and buffers are shown. All constructs in Figure A.8 to A.18 were labeled with A546-DY647 dyes. The goodness of fit in all FRET histograms (from Figure A.8 to Figure A.18) was indicated by reduced chi-squared value. The χ_{red}^2 in all fitted FRET histograms is ≈ 1 , which shows the goodness of our fit for FRET histograms.

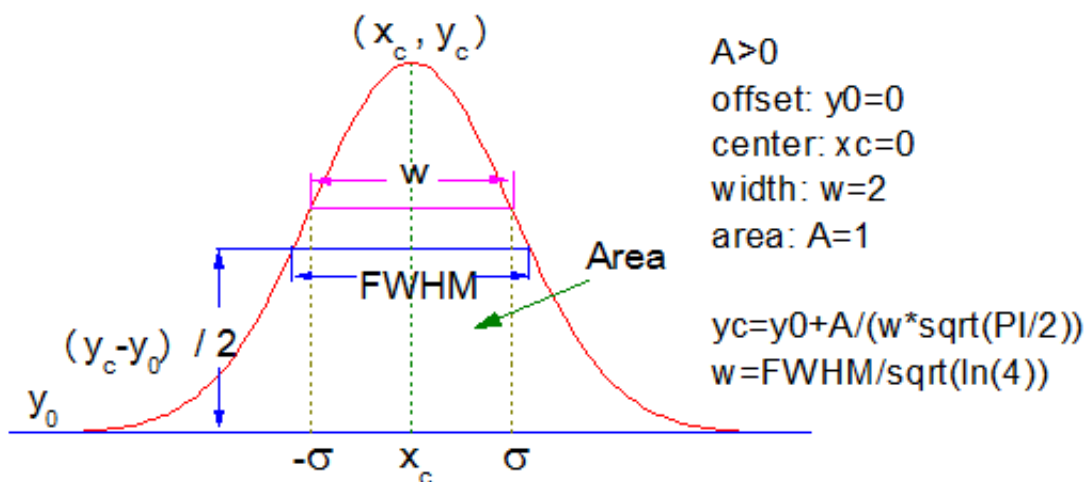


Figure A.7: Gaussian fitting parameter. Gaussian fitting equation is $y = y_0 + \frac{A}{w\sqrt{\pi/2}} e^{-2\frac{(x-x_c)^2}{w^2}}$.

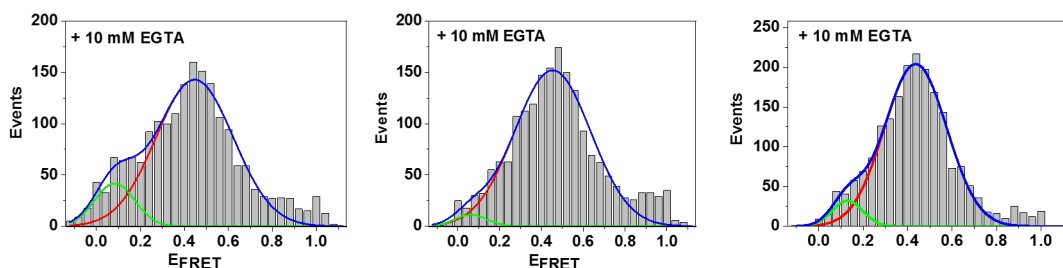


Figure A.8: CaM construct in 25 mM Tris, 300 mM NaCl, pH 7.5 buffer.

Table A.6: Goodness of Fit for Gaussian fitting results of FRET histograms for CaM construct in 25 mM Tris, 300 mM NaCl, pH 7.5 buffer.

Model	Gauss
Equation	$y = y_0 + (A / (w \cdot \sqrt{\pi/2})) \cdot \exp(-2 \cdot ((x - x_c) / w)^2)$
Reduced Chi-Sqr 1	416.18
Adj. R-Square1	0.98
Reduced Chi-Sqr 2	163.17
Adj. R-Square 2	0.98
Reduced Chi-Sqr 3	83.98
Adj. R-Square 3	0.97

Table A.7: Gaussian fitting results of FRET histograms for CaM construct in 25 mM Tris, 300 mM NaCl, pH 7.5 buffer.

	Value	Standard 1	error 1	Standard 2	error 2	Standard 3	error 3
Peak1	y0	0	0	0	0	0	0
Peak1	xc	0.07	0.02	0.12	0.02	0.530	0.006
Peak1	w	0.21	0.04	0.21	0.05	0.26	0.01
Peak1	A	2.75	0.50	1.47	0.35	5.5	0.22
Peak1	sigma	0.10	0.02	0.11	0.02	0.130	0.006
Peak1	FWHM	0.24	0.04	0.25	0.05	0.31105	0.01
Peak1	Height	10.63	1.24	5.54	0.79	16.66	0.48
Peak2	y0	0	0	0	0	0	0
Peak2	xc	0.489	0.006	0.508	0.006	0.18	0.039
Peak2	w	0.34	0.01	0.31	0.01	0.19	0.07
Peak2	A	17203.12	566.781	11072.53	382.55	504.47	201.50
Peak2	sigma	0.169	0.007	0.156	0.006	0.10	0.04
Peak2	FWHM	0.40	0.02	0.37	0.01	0.22	0.09
Peak2	Height	40.56	0.95	28.37	0.61	2.15	0.57

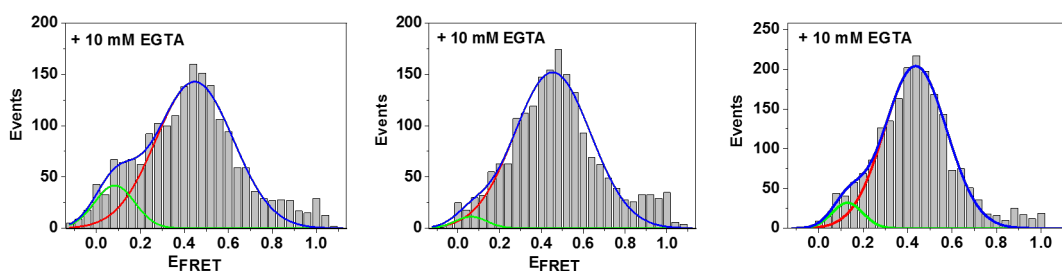


Figure A.9: CaM construct in 25 mM Tris, 300 mM NaCl, pH 7.5 buffer in addition of 10 mM EGTA.

Table A.8: Goodness of Fit for Gaussian fitting results of FRET histograms for CaM construct in 25 mM Tris, 300 mM NaCl, pH 7.5 buffer in addition of 10 mM EGTA.

Model	Gauss
Equation	$y=y_0 + (A/(w*\sqrt{\pi/2}))*\exp(-2*((x-xc)/w)^2)$
Reduced Chi-Sqr 1	31.40
Adj. R-Square1	0.97
Reduced Chi-Sqr 2	55.91
Adj. R-Square 2	0.97
Reduced Chi-Sqr 3	116.57
Adj. R-Square 3	0.99

Table A.9: Gaussian fitting results of FRET histograms for CaM construct in 25 mM Tris, 300 mM NaCl, pH 7.5 buffer in addition of 10 mM EGTA.

	Value	Standard 1	error 1	Standard 2	error 2	Standard 3	error 3
Peak1	y0	0	0	0	0	0	0
Peak1	xc	0	0	0	0	0.517	0.005
Peak1	w	0.29	0.01	0.26	0.02	0.27	0.01
Peak1	A	32	1	46	3	96	3.51
Peak1	sigma	0.145	0.006	0.132	0.008	0.134	0.005
Peak1	FWHM	0	0	0	0	0.31	0.01
Peak1	Height	88.40	2.78	137.99	4.04	286.81	5.59
Peak2	y0	0	0	0	0	0	0
Peak2	xc	0	0	0	0	0.19	0.05
Peak2	w	0.15	0.11	0.24	0.14	0.20	0.08
Peak2	A	1	1	4	3	7	3.31
Peak2	sigma	0.08	0.05	0.12	0.07	0.10	0.04
Peak2	FWHM	0.18	0.13	0.29	0.17	0.24	0.09
Peak2	Height	6.74	3.73	14.51	4.47	28.21	7.12

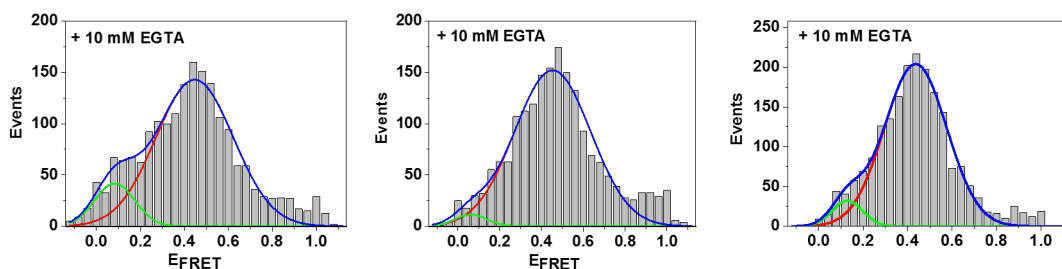


Figure A.10: CaM construct in 25 mM Tris, 300 mM NaCl, pH 7.5 buffer in addition of 1 mM calcium.

Table A.10: Goodness of Fit for Gaussian fitting results of FRET histograms for CaM construct in 25 mM Tris, 300 mM NaCl, pH 7.5 buffer in addition of 1 mM calcium.

Model	Gauss
Equation	$y=y_0 + (A/(w*\sqrt{\text{PI}/2}))*\exp(-2*((x-xc)/w)^2)$
Reduced Chi-Sqr 1	61.91
Adj. R-Square1	0.97
Reduced Chi-Sqr 2	36.55
Adj. R-Square 2	0.95
Reduced Chi-Sqr 3	69.78
Adj. R-Square 3	0.98

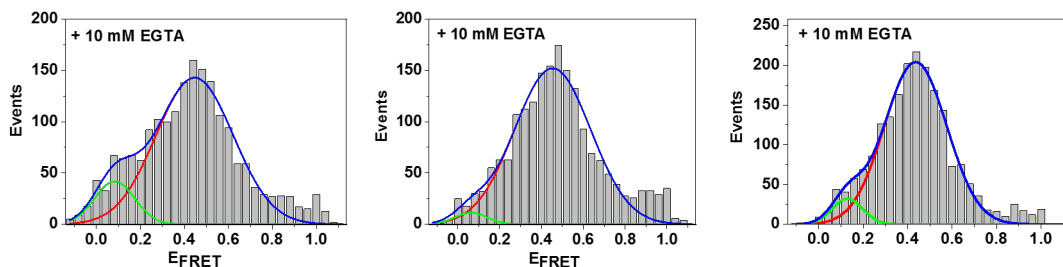
Table A.11: Gaussian fitting results of FRET histograms for CaM construct in 25 mM Tris, 300 mM NaCl, pH 7.5 buffer in addition of 1 mM calcium.

	Value	Standard 1	error 1	Standard 2	error 2	Standard 3	error 3
Peak1	y0	0	0	0	0	-1.13	5.28
Peak1	xc	0.472	0.008	0.530	0.009	0.575	0.007
Peak1	w	0.45	0.02	0.44	0.02	0.42	0.02
Peak1	A	74.61	2.69	43.61	1.86	85.83	5.72
Peak1	sigma	0.23	0.01	0.22	0.01	0.21	0.01
Peak1	FWHM	0.53	0.02	0.51	0.03	0.49	0.02
Peak1	Height	131.73	3.32	79.74	2.57	164.87	5.64
Peak2	y0	0	0	0	0	-1.13	5.28
Peak2	xc	0.95	0.02	0.09	0.02	0.12	0.02
Peak2	w	0.08	0.05	0.15	0.04	0.19	0.03

continued ...

Table A.11 Continued from previous page

	Value	Standard 1	error 1	Standard 2	error 2	Standard 3	error 3
Peak2	A	1.41	0.87	4.26	1.22	10.90	2.27
Peak2	sigma	0.04	0.02	0.08	0.02	0.10	0.02
Peak2	FWHM	0.09	0.06	0.18	0.04	0.23	38
Peak2	Height	14.45	7.55	22.39	4.50	45.41	5.86
Peak3	y0	0	0	0	0		
Peak3	xc	0.064	0.008	0.96	0.02		
Peak3	w	0.13	0.02	0.05	0.03		
Peak3	A	9.78	1.67	0.89	0.53		
Peak3	sigma	0.065	0.009	0.03	0.01		

Figure A.11: CaM construct in 25 mM Tris, 300 mM NaCl, pH 7.5 buffer in addition of 1 mM calcium and 10 μ M M13 peptide.Table A.12: Goodness of Fit for Gaussian fitting results of FRET histograms for CaM construct in 25 mM Tris, 300 mM NaCl, pH 7.5 buffer in addition of 1 mM calcium and 10 μ M M13 peptide.

Model	Gauss
Equation	$y=y_0 + (A/(w*\sqrt{\text{PI}/2})) * \exp(-2*((x-xc)/w)^2)$
Reduced Chi-Sqr 1	115.74
Adj. R-Square1	0.91
Reduced Chi-Sqr 2	68.65
Adj. R-Square 2	0.92
Reduced Chi-Sqr 3	229.55
Adj. R-Square 3	0.90

Table A.13: Gaussian fitting results of FRET histograms for CaM construct in 25 mM Tris, 300 mM NaCl, pH 7.5 buffer in addition of 1 mM calcium and 10 μ M M13 peptide.

	Value	Standard 1	error 1	Standard 2	error 2	Standard 3	error 3
Peak1	y0	0	0	0	0	-2.88	9.18
Peak1	xc	0.13	0.06	0.06	0.01	0.931	0.009
Peak1	w	0.23	0.09	0.1	0	0.15	0.03
Peak1	A	4.14	0	4.14	0	21.25	8.94
Peak1	sigma	0.12	0.05	0.05	0	0.08	0.02
Peak1	FWHM	0.28	0.11	0.12	0	0.18	0.04
Peak1	Height	14.08	5.60	33.03	0	112.73	26.71
Peak2	y0	0	0	0	0	-2.88	9.18
Peak2	xc	0.93	7	0.918	0.005	0.12	0
Peak2	w	0.14	0.02	0.14	0.02	0.19	0
Peak2	A	16.083	5.007	15.39	2.90	7.03	2.91
Peak2	sigma	0.07	0.01	0.070	0.009	0.0 95	0
Peak2	FWHM	0.16	0.03	0.17	0.02	0.22	0
Peak2	Height	92.96	16.08	87.29	9.17	29.53	12.22
Peak3	y0	0	0	0	0	-2.88	9.18
Peak3	xc	0.67	0.05	0.60	0.03	0.67	0.05
Peak3	w	0.41	0.07	0.49	0.05	0.43	0.09
Peak3	A	33.45	6.52	37.28	4.07	55.77	15.65
Peak3	sigma	0.20	0.04	0.24	0.03	0.21	0.04
Peak3	FWHM	0.48	0.09	0.57	0.06	0.51	0.11
Peak3	Height	65.44	5.05	61.08	3.23	103.34	11.84

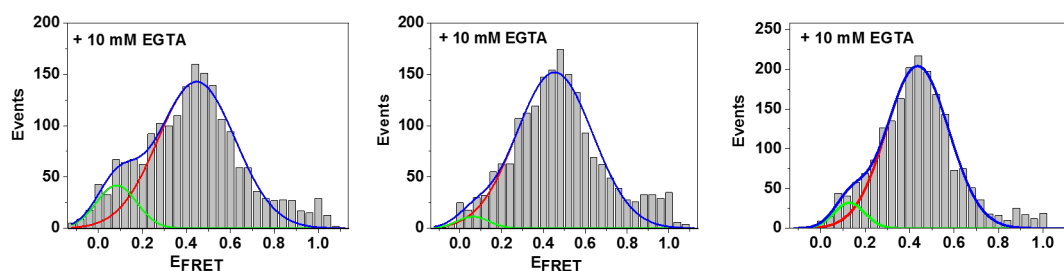


Figure A.12: CaM construct in 25 mM Tris, 100 mM KCl, pH 7.5 buffer in addition of 10 mM EGTA.

Table A.14: Goodness of Fit for Gaussian fitting results of FRET histograms for CaM construct in 25 mM Tris, 100 mM KCl, pH 7.5 buffer in addition of 10 mM EGTA.

Model	Gauss
Equation	$y=y_0 + (A/(w*\sqrt{\pi/2}))*\exp(-2*((x-xc)/w)^2)$
Reduced Chi-Sqr 1	157.11
Adj.R-Square1	0.93
Reduced Chi-Sqr 2	209.42
Adj.R-Square 2	0.92
Reduced Chi-Sqr 3	206.19
Adj.R-Square 3	0.96

Table A.15: Gaussian fitting results of FRET histograms for CaM construct in 25 mM Tris, 100 mM KCl, pH 7.5 buffer in addition of 10 mM EGTA.

	Value	Standard 1	error 1	Standard 2	error 2	Standard 3	error 3
Peak1	y0	0	0	0	0	0	0
Peak1	xc	0.45	0.01	0.45	0.01	0.436	0.008
Peak1	w	0.35	0.03	0.36	0.02	0.28	0.02
Peak1	A	62.89	4.23	69.42	3.84	71.68	3.66
Peak1	sigma	0.18	0.01	0.18	0.01	0.140	0.009
Peak1	FWHM	0.41	0.03	0.43	0.03	0.33	0.02
Peak1	Height	142.66	5.71	151.89	6.50	203.83	7.34
Peak2	y0	0	0	0	0	0	0
Peak2	xc	0.08	0.03	0.06	0.09	0.13	0.03
Peak2	w	0.18	0.05	0.15	0.18	0.14	0.06
Peak2	A	9.55	3.66	2.18	2.91	5.589	3.004
Peak2	sigma	0.09	0.03	0.08	0.09	0.07	0.03
Peak2	FWHM	0.21	0.06	0.18	0.02	0.16	0.07
Peak2	Height	41.79	9.80	11.36	10.56	32.09	11.34

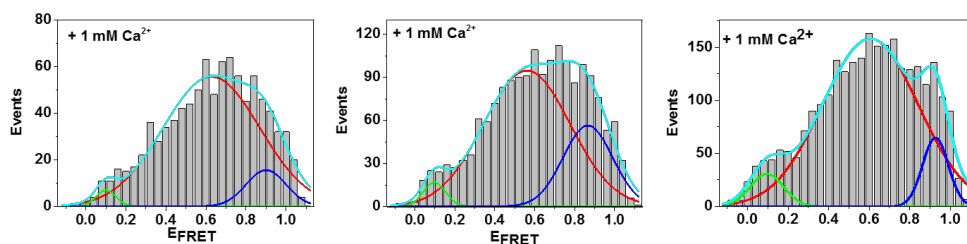


Figure A.13: CaM construct in 25 mM Tris, 100 mM KCl, pH 7.5 buffer in addition of 1 mM calcium.

Table A.16: Goodness of Fit for Gaussian fitting results of FRET histograms for CaM construct in 25 mM Tris, 100 mM KCl, pH 7.5 buffer in addition of 1 mM calcium.

Model	Gauss
Equation	$y=y_0 + (A/(w*\sqrt{PI/2})) * \exp(-2*((x-xc)/w)^2)$
Reduced Chi-Sqr 1	29.09
Adj.R-Square1	0.93
Reduced Chi-Sqr 2	55.64
Adj.R-Square 2	0.96
Reduced Chi-Sqr 3	128.25
Adj.R-Square 3	0.96

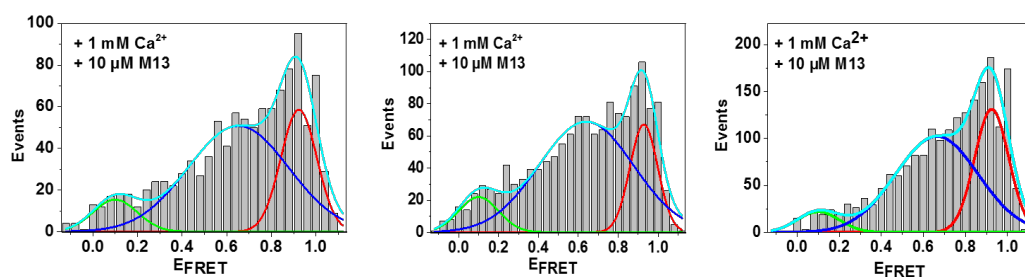
Table A.17: Gaussian fitting results of FRET histograms for CaM construct in 25 mM Tris, 100 mM KCl, pH 7.5 buffer in addition of 1 mM calcium.

	Value	Standard 1	error 1	Standard 2	error 2	Standard 3	error 3
Peak1	y0	0	0	0	0	0	0
Peak1	xc	0.63	0.02	0.56	0.08	0.61	0.01
Peak1	w	0.48	0.04	0.43	0.11	0.47	0.04
Peak1	A	33.68	2.74	51.48	18.24	93.88	6.50
Peak1	sigma	0.24	0.02	0.22	0.06	0.24	0.02
Peak1	FWHM	0.57	0.04	0.51	0.01	0.56	0.04
Peak1	Height	55.62	2.21	94.64	10.33	158.19	4.74
Peak2	y0	0	0	0	0	0	0
Peak2	xc	0.1	0	0.10	0.02	0.10	0.03
Peak2	w	0.1	0	0.11	0.06	0.17	0.05
Peak2	A	0.87	0.51	2.34	1.65	6.35	2.43

continued ...

Table A.17 Continued from previous page

	Value	Standard 1	error 1	Standard 2	error 2	Standard 3	error 3
Peak2	sigma	0.05	0	0.06	0.03	0.08	0.03
Peak2	FWHM	0.12	0	0.13	0.07	0.19	0.06
Peak2	Height	6.91	4.06	16.66	7.24	30.60	8.13
Peak3	y0	0	0	0	0	0	0
Peak3	xc	0.9	0	0.87	0.03	0.93	0.01
Peak3	w	0.2	0	0.25	0.07	0.13	0.03
Peak3	A	3.90	1.86	17.54	16.59	10.27	3.76
Peak3	sigma	0.1	0	0.12	0.04	0.06	0.02
Peak3	FWHM	0.24	0	0.29	0.08	0.15	0.04
Peak3	Height	15.57	7.40	56.33	38.22	64.78	13.06

Figure A.14: CaM construct in 25 mM Tris, 100 mM KCl, pH 7.5 buffer in addition of 1 mM calcium and 10 μ M M13 peptide.Table A.18: Goodness of Fit for Gaussian fitting results of FRET histograms for CaM construct in 25 mM Tris, 100 mM KCl, pH 7.5 buffer in addition of 1 mM calcium and 10 μ M M13 peptide.

Model	Gauss
Equation	$y=y_0 + (A/(w*\sqrt{PI/2}))*\exp(-2*((x-xc)/w)^2)$
Reduced Chi-Sqr 1	72.75
Adj.R-Square1	0.88
Reduced Chi-Sqr 2	75.67
Adj.R-Square 2	0.91
Reduced Chi-Sqr 3	401.47
Adj.R-Square 3	0.88

Table A.19: Gaussian fitting results of FRET histograms for CaM construct in 25 mM Tris, 100 mM KCl, pH 7.5 buffer in addition of 1 mM calcium and 10 μ M M13 peptide.

	Value	Standard 1	error 1	Standard 2	error 2	Standard 3	error 3
Peak1	y0	0	0	0	0	0	0
Peak1	Xc	0.92	0.01	0.93	0.008	0.92	0.01
Peak1	W	0.16	0.04	0.14	0.03	0.16	0.04
Peak1	A	11.86	5.71	11.72	3.68	26.62	13.60
Peak1	sigma	0.08	0.02	0.07	0.01	0.08	0.02
Peak1	FWHM	0.19	0.05	0.16	0.03	0.19	0.05
Peak1	Height	58.52	15.88	67.06	11.38	131.06	39.71
Peak2	y0	0	0	0	0	0	0
Peak2	Xc	0.1	0	0.1		0.1	0
Peak2	W	0.2	0	0.2	0	0.2	0
Peak2	A	3.86	1.25	5.51	1.34	5.5	0
Peak2	sigma	0.1	0	0.1	0	0.1	0
Peak2	FWHM	0.24	0	0.24	0	0.24	0
Peak2	Height	15.39	4.99	22.0003	5.337	21.94	0
Peak3	y0	0	0	0	0	0	0
Peak3	Xc	0.65	0.06	0.64	0.03	0.66	0.07
Peak3	W	0.45	0.10	0.47	0.06	0.39	0.10
Peak3	A	28.64	7.34	40.89	5.42	50.33	15.75
Peak3	sigma	0.22	0.05	0.24	0.03	0.20	0.05
Peak3	FWHM	0.53	0.12	0.56	0.07	0.46	0.12
Peak3	Height	50.80	4.39	68.83	3.66	102.10	11.16

Table A.20: CaM construct was measured in 25 mM Tris, 100 mM KCl, pH 7.5 buffer.

S-CaM-C	FRET position	Mean value	STDEV
+10 mM EGTA	0.08/0.45 0.06/0.45 0.13/0.44	0.09/0.44	0.035/0.01
+1mM Ca^{2+}	0.1/0.6/0.9 0.1/0.56/0.87 0.1/0.61/0.93	0.1/0.6, 0.88	0.00/0.03/0.02
+1 mM Ca^{2+} +10 μM M13	0.1/0.65/0.92 0.1/0.64/0.93 0.1/0.66/0.92	0.1/0.65/0.92	0.00/0.01/0.004
S-CaM-C	Width (σ)	Mean value	STDEV
+10 mM EGTA	0.01/0.75 0.076/0.18 0.07/0.14	0.05/0.16	0.03/0.02
+1mM Ca^{2+}	0.08/0.23/0.06 0.056/0.5/0.12 0.1/0.24/0.1	0.08/0.3/0.9	0.02/0.15/0.03
+1 mM Ca^{2+} +10 μM M13	0.1/0.22/0.08 0.1/0.24/0.07 0.1/0.2/0.08	0.1/0.2/0.076	0.00/0.015/0.005

Table A.21: FRET positions and its mean values of directly labeled CaM protein by Kim *et al.* [78]. The measurements were done in 25 mM Tris, 100 mM KCl, pH 7.5 buffer.

S-Cam-C	FRET position	Width (σ)
+10 mM EGTA	0.76	0.12
+1mM Ca^{2+}	0.71	0.2
+1 mM Ca^{2+} +10 μM M13	0.85	0.09

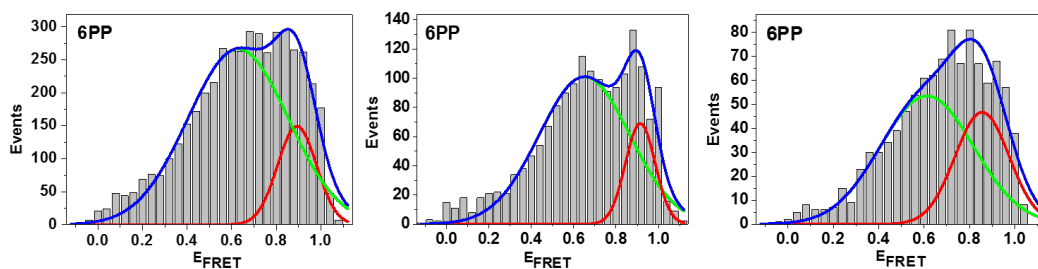


Figure A.15: 6PP construct in 20 mM Tris-HCl, 300 mM NaCl, pH 7.4 buffer.

Table A.22: Goodness of Fit for Gaussian fitting results of FRET histograms for 6PP construct in 20 mM Tris-HCl, 300 mM NaCl, pH 7.4 buffer.

Model	Gauss
Equation	$y=y_0 + (A/(w*\sqrt{PI/2}))*\exp(-2*((x-xc)/w)^2)$
Reduced Chi-Sqr 1	487.69
Adj.R-Square1	0.96
Reduced Chi-Sqr 2	134.17
Adj.R-Square 2	0.92
Reduced Chi-Sqr 3	45.73
Adj.R-Square 3	0.94

Table A.23: Gaussian fitting results of FRET histograms for 6PP construct in 20 mM Tris-HCl, 300 mM NaCl, pH 7.4 buffer.

	Value	Standard 1	error 1	Standard 2	error 2	Standard 3	error 3
Peak1	y0	0	0	0	0	0	0
Peak1	xc	0.89	0.01	0.65	0.03	0.61	0.02
Peak1	w	0.17	0.04	0.43	0.05	0.41	0.14
Peak1	A	32.57	15.91	54.10	6.52	27.57	1.94
Peak1	sigma	0.09	0.02	0.21	0.02	0.21	0.07
Peak1	FWHM	0.21	0.05	0.50	0.05	0.48	0.17
Peak1	Height	149.08	41.88	101.001	5.313	53.50	19.45
Peak2	y0	0	0	0	0	0	0
Peak2	xc	0.63	0.03	0.91	0.01	0.86	0.03
Peak2	w	0.45	0.04	0.14	0.03	0.24	0.10
Peak2	A	150.12	18.99	12.10	5.03	13.97	18.62
Peak2	sigma	0.22	0.02	0.07	0.02	0.12	0.05

continued ...

Table A.23 Continued from previous page

	Value	Standard 1	error 1	Standard 2	error 2	Standard 3	error 3
Peak2	FWHM	0.53	51	0.16	0.04	0.28	0.11
Peak2	Height	266.32	13.63	68.95	15.86	46.69	45.01

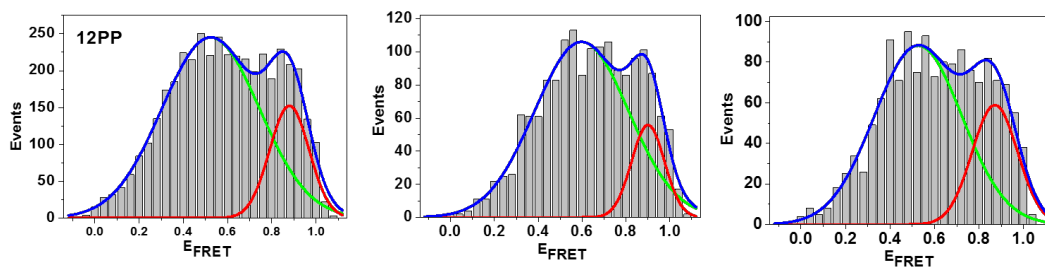


Figure A.16: 12PP construct in 20 mM Tris-HCl, 300 mM NaCl, pH 7.4 buffer.

Table A.24: Goodness of Fit for Gaussian fitting results of FRET histograms for 12PP construct in 20 mM Tris-HCl, 300 mM NaCl, pH 7.4 buffer.

Model	Gauss
Equation	$y=y_0 + (A/(w*\sqrt{PI/2}))*\exp(-2*((x-xc)/w)^2)$
Reduced Chi-Sqr 1	178.99
Adj.R-Square1	0.98
Reduced Chi-Sqr 2	61.61
Adj.R-Square 2	0.96
Reduced Chi-Sqr 3	68.51
Adj.R-Square 3	0.94

Table A.25: Gaussian fitting results of FRET histograms for 12PP construct in 20 mM Tris-HCl, 300 mM NaCl, pH 7.4 buffer.

	Value	Standard 1	error 1	Standard 2	error 2	Standard 3	error 3
Peak1	y0	0	0	0	0	0	0
Peak1	xc	0.52	0.01	0.60	0.02	0.53	0.02
Peak1	w	0.44	0.02	0.43	0.03	0.39	0.04
Peak1	A	135.56	6.72	56.91	4.14	43.48	4.65
Peak1	sigma	0.22	0.01	0.21	0.02	0.20	0.02
Peak1	FWHM	0.52	0.03	0.50	0.04	0.46	0.05

continued ...

Table A.25 Continued from previous page

	Value	Standard 1	error 1	Standard 2	error 2	Standard 3	error 3
Peak1	Height	245.19	5.47	105.98	3.31	88.19	3.73
Peak2	y0	0	0	0	0	0	0
Peak2	xc	0.88	7	0.900	0.009	0.87	0.02
Peak2	w	0.18	0.02	0.15	0.03	0.20	0.03
Peak2	A	34.11	5.66	10.5	3.3	15.09	4.25
Peak2	sigma	0.09	0.008	0.08	0.01	0.10	0.02
Peak2	FWHM	0.21	0.02	0.18	0.03	0.24	0.04
Peak2	Height	152.11	14.93	55.78	9.98	58.84	10.14

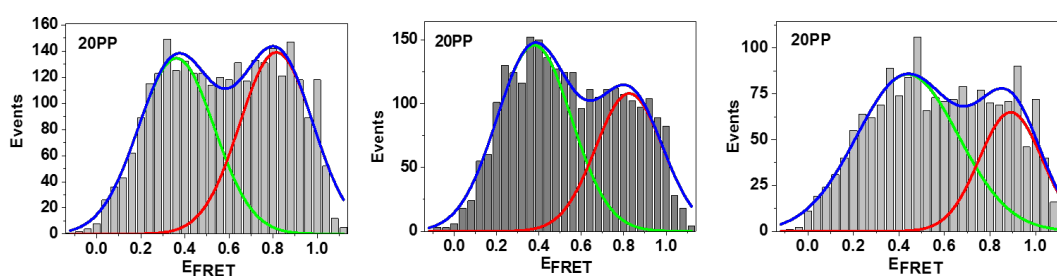


Figure A.17: 20PP construct in 20 mM Tris-HCl, 300 mM NaCl, pH 7.4 buffer.

Table A.26: Goodness of Fit for Gaussian fitting results of FRET histograms for 20PP construct in 20 mM Tris-HCl, 300 mM NaCl, pH 7.4 buffer.

Model	Gauss
Equation	$y=y_0 + (A/(w*\sqrt{PI/2})) * \exp(-2*((x-xc)/w)^2)$
Reduced Chi-Sqr 1	194.35
Adj.R-Square1	0.92
Reduced Chi-Sqr 2	140.53
Adj.R-Square 2	0.94
Reduced Chi-Sqr 3	100.89
Adj.R-Square 3	0.88

Table A.27: Gaussian fitting results of FRET histograms for 20PP construct in 20 mM Tris-HCl, 300 mM NaCl, pH 7.4 buffer.

	Value	Standard 1	error 1	Standard 2	error 2	Standard 3	error 3
Peak1	y0	0	0	0	0	0	0
Peak1	xc	0.36	0.02	0.38	0.02	0.44	0.03
Peak1	w	0.34	0.04	0.35	0.03	0.45	0.05
Peak1	A	57.99	7.06	64331	5.94	48.10	5.62
Peak1	sigma	0.17	0.02	0.18	0.01	0.22	0.03
Peak1	FWHM	0.41	0.04	0.42	0.03	0.53	0.06
Peak1	Height	134.49	7.15	145.52	5799	85.65	4.19
Peak2	y0	0	0	0	0	0	0
Peak2	xc	0.82	0.021	0.83	0.02	0.89	0.02
Peak2	w	0.33	0.04	0.31	0.04	0.28	0.04
Peak2	A	58.02	7.20	42.95	5.97	22.55	5.37
Peak2	sigma	0.17	0.02	0.16	0.02	0.14	0.02
Peak2	FWHM	0.39	0.04	0.37	0.04	0.33	0.05

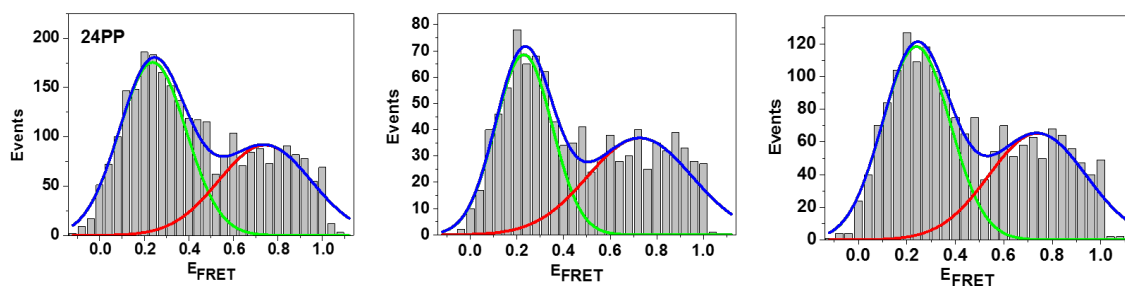


Figure A.18: 24PP construct in 20 mM Tris-HCl, 300 mM NaCl, pH 7.4 buffer.

Table A.28: Goodness of Fit for Gaussian fitting results of FRET histograms for 6PP construct in 24 mM Tris-HCl, 300 mM NaCl, pH 7.4 buffer.

Model	Gauss
Equation	$y=y_0 + (A/(w*\sqrt{PI/2}))*\exp(-2*((x-xc)/w)^2)$
Reduced Chi-Sqr 1	224.33
Adj.R-Square1	0.92
Reduced Chi-Sqr 2	52.47
Adj.R-Square 2	0.88
Reduced Chi-Sqr 3	114.11
Adj.R-Square 3	0.91

Table A.29: Gaussian fitting results of FRET histograms for 6PP construct in 24 mM Tris-HCl, 300 mM NaCl, pH 7.4 buffer.

	Value	Standard 1	error 1	Standard 2	error 2	Standard 3	error 3
Peak1	y0	0	0	0	0	0	0
Peak1	xc	0.24	0.01	0.23	0.01	0.24	0.01
Peak1	w	0.30	0.02	0.24	0.02	0.28	0.02
Peak1	A	66.0	5.8	20.9	2.2	41.4	3.4
Peak1	sigma	0.15	0.01	0.12	0.01	0.14	0.01
Peak1	FWHM	0.35	0.03	0.29	0.02	0.33	0.02
Peak1	Height	175.44	8.40	68.54	4.49	118.35	5.75
Peak2	y0	0	0	0	0	0	0
Peak2	xc	0.74	0.03	0.73	0.03	0.74	0.02
Peak2	w	0.41	0.06	0.45	0.07	0.40	0.06
Peak2	A	47.63	6.47	20.62	2.71	32.82	3.87
Peak2	sigma	0.21	0.03	0.22	0.04	0.20	0.03
Peak2	FWHM	0.49	0.07	0.53	0.08	0.47	0.06
Peak2	Height	91.59	6.36	36.83	3.03	65.29	4.61

Table A.30: FRET positions and mean values of PP constructs in 20 mM Tris-HCl, 300 mM NaCl, pH 7.4 buffer.

S-PP-C	FRET position	Mean value
6PP-1	0.63/0.89	$0.63 \pm 0.02, 0.88 \pm 0.03$
6PP-2	0.65/0.91	
6PP-3	0.61/0.86	
continued ...		

Table A.30 Continued from previous page

S-PP-C	FRET position	Mean value
12PP-1	0.52/0.88	$0.55 \pm 0.04, 0.88 \pm 0.02$
12PP-2	0.60/0.90	
12PP-3	0.65/0.87	
20PP-1	0.36/0.82	$0.38 \pm 0.04, 0.84 \pm 0.04$
20PP-2	0.38/0.83	
20PP-3	0.44/0.89	
24PP-1	0.24/0.74	$0.23 \pm 0.006, 0.73 \pm 0.01$
24PP-2	0.23/0.73	
24PP-3	0.24/0.74	
S-PP-C	Width (σ)	Mean value
6PP-1	0.22/0.09	$0.2 \pm 0.01, 0.09 \pm 0.025$
6PP-2	0.21/0.07	
6PP-3	0.21/0.12	
12PP-1	0.22/0.09	$0.2 \pm 0.01, 0.09 \pm 0.01$
12PP-2	0.21/0.08	
12PP-3	0.2/0.1	
20PP-1	0.17/0.17	$0.2 \pm 0.03, 0.15 \pm 0.01$
20PP-2	0.18/0.16	
20PP-3	0.22/0.14	
24PP-1	0.15/0.2	$0.14 \pm 0.015, 0.88 \pm 0.02$
24PP-2	0.12/0.22	
24PP-3	0.14/0.2	

Table A.31: FRET positions of directly labeled 20 polyproline oligomer [74].

	FRET position 1	FRET position 2
20 polyproline oligomer	0.53	0.725

Table A.32: Summary of fit results of polarized decays from free SNAP-Surface Alexa Fluor 546 and Alexa Fluor 546 conjugated to the SNAP-tag.

	$\tau_1(ns)$	$A_1(\%)$	$\tau_2(ns)$	$A_2(\%)$	χ_2	$\tau_r(ns)$
A546	3.39 ± 0.01	70	0.46 ± 0.03	30	1.20 ± 0.01	0.6 ± 0.02
SNAP-A546	3.53 ± 0.04	63	0.79 ± 0.02	37	1.65 ± 0.03	13 ± 1

Acknowledgements

For all those who have contributed to the success of this work, I have an opportunity to thank you cordially.

First, I would like to express my gratitude to **Prof. Dr. G. Ulrich Nienhaus** who has given an opportunity in his department to prepare my dissertation. His constant encouragement, support, and invaluable suggestions made this work successful.

A big thank you is addressed to **Dr. Yuji Ishitsuka** has supervised at all times and listen to my questions and for the thousand time correcting without comment - almost. The discussions with his have been very constructive and I have always been very motivated, even when they have turned a hundred times in a circle. His interest in my work has inspired me further.

My sincere thanks go to **Dr. Karin Nienhaus** and **Dr. Andrey Kobitski** for providing me valuable insights on project and for correction of my English texts, respectively.

I would like to thank **Prof. Nils Johnsson** group and **Baden-Württemberg Stiftung** for funding the projects, which I was involved in during four years.

I particularly thank all **my colleagues**, current and former for their help in numerous aspects, for creating a friendly atmosphere and for the good times shared in and outside the laboratory.

I would like to thank all my **Iranian friends** for their help and moral support during these years.

I am deeply and forever indebted to **my husband** and **my parents** for their love, support and encouragement throughout my entire life.

List of Publications

- Yuji Ishitsuka[‡], Naghmeh Azadfar[‡], Andrei Yu. Kobitski, Karin Nienhaus, Nils Johnsson, and G. Ulrich Nienhaus. (2015) Evaluation of Genetically Encoded Chemical Tags as Orthogonal Fluorophore Labeling Tools for Single-Molecule FRET Applications. *J. Phys. Chem. B*, 2015, 119 (22), pp 6611–6619. [‡]Y.I. and N.A. contributed equally.
- Shang, L., Stockmar, F., Azadfar, N., Nienhaus, G. U. (2013) Intracellular Thermometry by Using Fluorescent Gold Nanoclusters, *Angew. Chem. Int. Ed.*, 52, 1-5.
- Shang, L., Dörlich, R. M., Brandholt, S., Azadfar, N., Nienhaus, G. U. (2012) Facile Synthesis of Fluorescent Gold Nanoclusters and Their Application in Cellular Imaging, *Proc. SPIE 8232*, 82321J.
- Shang, L., Azadfar, N., Stockmar, F., Send, W., Trouillet, V., Bruns, M., Gerthsen, D., Nienhaus, G. U. (2011) One-Pot Synthesis of Near-Infrared Fluorescent Gold Clusters for Cellular Fluorescence Lifetime Imaging, *Small*, 7, 2614-2620.

List of Posters

- Azadfar, N., Ishitsuka, Y. and Nienhaus, G.U. (2013) Applications and Assessments of Self-Labeling Protein for Single Molecule FRET-based Protein Conformation Assay, Karlsruhe Days of Optics and Photonics, Karlsruhe, Germany.
- Azadfar, N., Ishitsuka, Y. and Nienhaus, G.U. (2013) FRET rulers: From polyproline to double-stranded DNA (ds-DNA), Joint Meeting of the British and German Biophysical Society, Hünfeld Monastery, Germany.
- Azadfar, N., Ishitsuka, Y. and Nienhaus, G.U. (2012) Improved Genetically Encoded Biosensors with SNAP-tag and CLIP-tag Inside Yeast Cells, Annual Meeting of the German Biophysical Society (DGfB), Göttingen, Germany.
- Azadfar, N. and Nienhaus, G.U. (2011) Experimental techniques for monitoring intracellular protein-protein interactions, Joint Meeting of the Swedish and German Biophysical Societies, Hünfeld Monastery, Germany.
- The Research Day of the Baden-Württemberg Stiftung, Heidelberg, Germany, June 2011.